Coordination Chemistry Reviews 449 (2021) 214168

Contents lists available at ScienceDirect

Coordination Chemistry Reviews

journal homepage: www.elsevier.com/locate/ccr

Review

Ubiquity of cubanes in bioinorganic relevant compounds

Alec Bigness [a,1], Shivaiah Vaddypally [b,1], Michael J. Zdilla [b,*], Jose L. Mendoza-Cortes [c,*]

[a] University of South Florida Morsani College of Medicine, 560 Channelside Dr, Tampa, FL 33602, United States
[b] Department of Chemistry, Temple University, 1901 N. 13th Street, Philadelphia, PA 19122, United States
[c] Department of Chemical Engineering & Materials Science, Michigan State University, East Lansing, MI 48824, United States

ARTICLE INFO

Article history:
Received 8 February 2021
Accepted 15 August 2021
Available online 11 October 2021

Dedication. In memory of Larry Dahl: A founding father of synthetic heterocubane cluster chemistry.

Keywords:
Cubane
Bioinorganic chemistry
Clusters
Metalloenzymes
Iron-sulfur proteins
Bioinorganic model compounds

ABSTRACT

The heterocubane (commonly referred to as the cubane cluster, a molecular species comprising a cube-shaped core with different atom types at opposite corners) is a conserved general structure found in some of nature's most crucial enzymes. Nature owes some of its most important reactions—like catalytic water splitting, nitrogen fixation, and the citric acid cycle—to the reactive versatility of the cubane structure. Few reviews have comprehensively highlighted the importance of this naturally occurring structure outside of (and prior to) the biological context, or have explicitly focused on the role of the cluster's global coordination environment on reactivity and electronic structure across multiple core metal and core ligand identities. In this review we summarize the scope of existing synthetic chemistry in context of coordination environment and geometry. Connections are drawn between these systems and the natural systems to offer insights into the properties of heterocubane clusters and their relation to biology. With biological uses ranging from simple one-electron transfer to some of the most challenging chemistries such as water oxidation and nitrogen fixation, the cubane cluster is ubiquitous and requires a more general elaboration than has been previously provided; thus, we aim to provide a summary of the history and the current research climate regarding heterocubanes, hoping that it will inspire future endeavors and discoveries.

Contents

* Corresponding authors.
E-mail addresses: mzdilla@temple.edu (M.J. Zdilla), jmendoza@msu.edu (J.L. Mendoza-Cortes).
[1] These authors contributed equally.

https://doi.org/10.1016/j.ccr.2021.214168
0010-8545/

1. Introduction

Cubane clusters have become a pervasive topic in the field of inorganic chemistry in the past few decades, largely due to their prevalence as metallocofactors in biology.[1,2] However, their functions as synthetic catalysts[2,3] and magnetic materials[4] have made them of interest to a broader community of chemists as well. A cubane cluster is an inorganic cluster containing an 8-membered cube-shaped core, where each atom is placed in a corner. The most common motif is the heterocubane cluster, typically made of 4 metal atoms and 4 non-metal atoms arranged as concentric opposing tetrahedra (Fig. 1).

Although diagramed as having square faces in Fig. 1, the faces of cubane clusters can be rhombs resulting in a 3D structure more accurately described as a rhombohedron. The degree to which these facial rhombs are distorted from 90° in this manner is dependent upon the coordination environment about the metals and has implications for the reactivity and electronic structure of the resulting cluster. Cubane cluster chemistry has been reviewed on a number of occasions, usually with a focus on their relationship to specific biological cofactors[1,5–11] or focusing on specific core atom compositions.[12–21] However, a comprehensive review of synthetic heterocubane cluster chemistry outside the context of direct biomimetics, and one exploring the role of global coordination environment (core and terminal ligand identity, cluster geometry, and metal coordination number) on reactivity and electronic structure has not been undertaken. Such a broad-scope examination of older systems, and systems that have not been explicitly linked to biology, reveals links to the biological systems and can offer insights. This review will highlight the importance of coordination environment and geometry in understanding the properties of heterocubane clusters as they relate to biological and biomimetic chemistry, reactivity, and electronic structure.

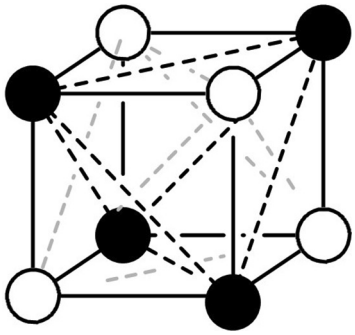

Fig. 1. Diagram of a simple heterocubane cluster constructed from an intervening tetrahedron of metal atoms (black) and one of non-metal atoms (white). Terminal ligands not shown.

2. A Brief Early History

To our knowledge, the first known reports of a heterocubane cluster structure came in 1936 from Mann and Wells[22,23] of a copper iodide heterocubane (though this word was not yet coined) with terminal trimethylarsine ligands. The structure was described as having "four cuprous atoms. . .arranged at the apices of a regular tetrahedron: the four iodine atoms lie each at the centre, but above the plane of, one face of the tetrahedron. . ." The structural figures from this report are shown in Fig. 2.

A second structure of such a cluster was not seen again for twenty-four years, until 1960, when a cube cluster structure was proposed as one of several possibilities for $Cr_4O_4Cp_4$ (Fig. 3),[25] a proposal that turned out to be correct.[26] Prior to this confirmation of the structure of $Co_4O_4Cp_4$, the crystal structure of analogous $Fe_4S_4Cp_4$ cubane systems were determined almost simultaneously in 1966 by Schunn et al at Dupont [27] and by the group of Dahl. [28]

3. An overview of synthetic cubanes in the literature

Since reports on synthetic heterocubane clusters precede the discovery of their biological counterparts by a significant margin, they were not connected to biology until much later in the 1970s. For structurally characterized compounds alone, the Cambridge Structural Database suggests >4000 clusters; far too many

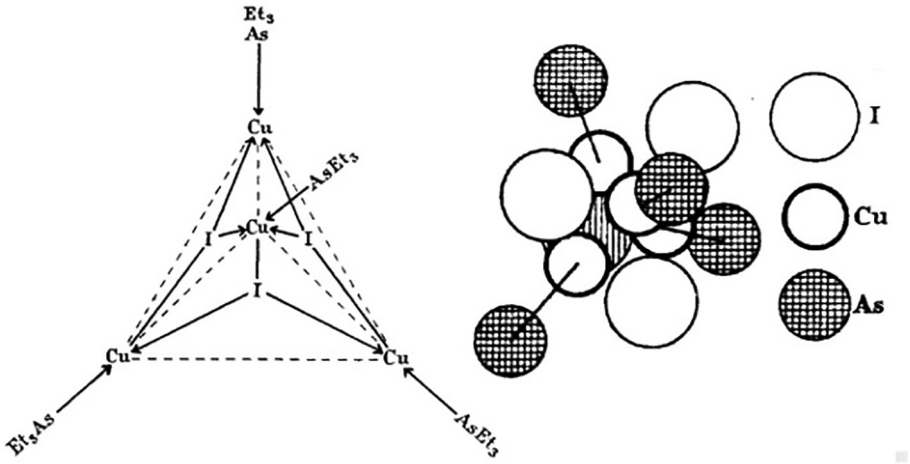

Fig. 2. Reproduction of structural figures from the original report of the Cu_4I_4 cubane cluster, reproduced with permission from the Royal Society of Chemistry. Left: "The broken lines represent the edges of the tetrahedron formed by the four copper atoms, the apex occupied by the central copper atom being tilted forward to show all the four bonds joined to this atom. The iodine atoms are depicted on the faces of the tetrahedron in order to show their linkage to the neighbouring copper atoms: actually they lie well above the plane of the tetrahedral faces, as shown [at right]. The iodine atom on the rear face of the tetrahedron is not shown." Right: "the relative positions of the atomic centre. . .the rear iodine atom is vertically shaded for identification." [24]

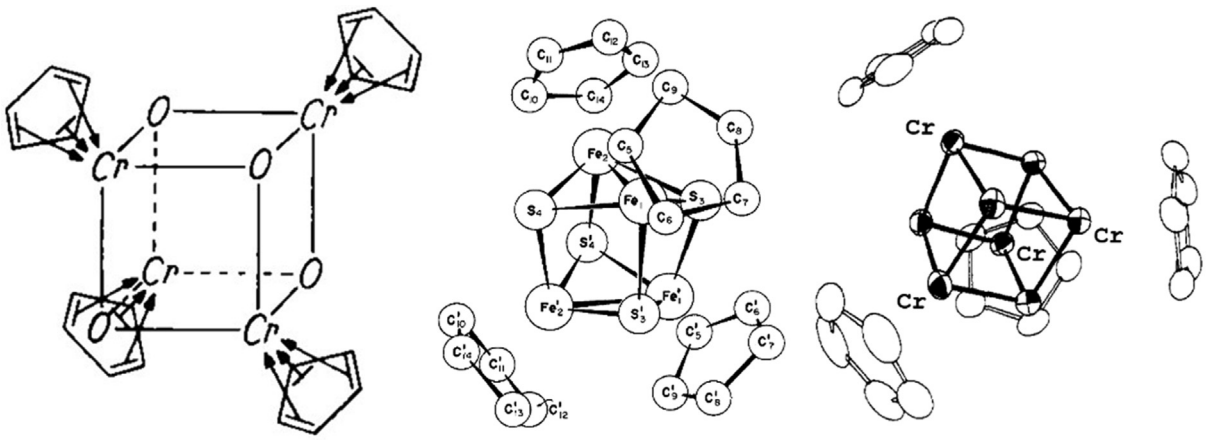

Fig. 3. Left: Proposed structure of $Cr_4O_4Cp_4$ from Fischer in 1960 [25], center: crystal structure of $Fe_4S_4Cp_4$ from Dahl in 1966, [28] and right: confirmed structure of $Cr_4O_4Cp_4$ from Bottomley in 1981[29]. Reproduced with permission from ACS and Wiley.

to review here. Instead, this review seeks to offer a reasonable sampling to illustrate the synthetic permutations achieved on the heterocubane synthon, and to select representative and noteworthy examples of particular specimens with structural, magnetic, and reactivity features relevant to the more famous biological systems. Since the discovery of cubanes in biology, reports of biomimetic synthetic cubane motifs have garnered additional interest, while their synthetic ancestors have largely been ignored. By a systematic and well-sampled review of this chemistry, it is hoped that forgotten but equally relevant compounds may awake new interest and attention.

3.1. Cyclopentadienyl-ligated systems

While the cyclopentadienyl ligand is not to be found in biology and is electronically and structurally dissimilar from any biological ligand, these systems laid the groundwork for understanding of the electronic structure of cubane type clusters relevant to biology. The study of the magnetic properties of the cyclopentadienyl systems led to molecular orbital descriptions explaining coupling through covalent interactions between transition metals ions, and forms the foundation for much of modern understanding of metal–metal coupling in biological cubane clusters discussed throughout this review.

The cyclopentadienyl-ligated cubane clusters typically display an η_5-cyclopentadienyl type ligand at the four metal-based corners of the cubane, as illustrated in Fig. 3, which shows the first examples of such systems. The reports on metal-oxo cubanes with Cp-type ligands are almost exclusively limited to chromium systems [29,30,31], with the sole exceptions being Rh and Ir heterometallic systems where the cubane is part of a larger molybdenum or tungsten oxide cluster.[32–35] Magnetic properties of these cubane systems find typically that Cr centers are antiferromagnetically coupled, giving rise to an S = 0 magnetic ground state with a characteristic S-shaped temperature dependent magnetic susceptibility curve (Fig. 4).[30] In this system, the default expectation is a T_d symmetric 60-electron, diamagnetic spin system, which is presumed the case at low temperature. However, the covalent interactions between metal ions are weak, leading to thermal population of asymmetric states, leading to geometric distortion and nonzero magnetic states at room temperature.

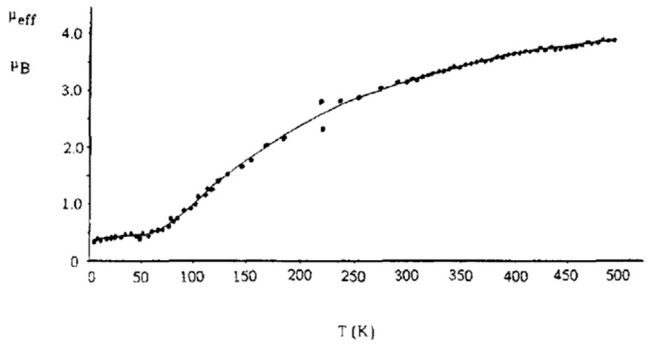

Fig. 4. Original plot of temperature-dependent effective magnetic moment of $Cr_4O_4Cp_4$, reproduced with permission from The American Chemical Society.[30]

The weak bonding, and thermally accessible magnetic excited states in the Cr_4O_4 systems is in contrast to the behavior in heavier-chalcogenide systems with terminal cyclopentadienyl type ligands. S-bridged cubanes are more common than the oxo-bridged systems[27,28,36–48] and are augmented by a few reports of analogous heavier chalcogenide-based cubanes containing metal ions bridged by Se[43,44,46,48–51] and Te[47,49,52] atoms. Many of these reports were specifically focused on the M-M bonding character in the cubane clusters. While weaker interactions in metal-oxo clusters gives thermally accessible paramagnetic states [36,37,39], systems with stronger covalent bonds in the clusters of heavier chalcogenides such as S[44,45,48,50,52] lead to strong antiferromagnetic coupling. For the Cr systems, whereas the Cr-O cubane cluster possesses a weak antiferromagnetic coupling between metal centers due to weak bonding interactions, the S- and Se-bridged systems exhibit temperature-independent diamagnetic behavior resulting from the formation of stronger M-M bonds, despite similar M-M distances for the sulfur system[37], and longer distances for the selenium system.[53] Based on magnetic data, extended Hückel calculations, and comparative photoelectron spectra of the O and S systems, the argument was made that a similar electronic structure description applies to the chromium chalcogenide systems, but that the more narrow range of O-based orbital energies gives a narrower range of resulting molecular orbital energies, resulting in thermally accessible paramagnetic states for the O-bridged systems, but not for the S or Se bridged systems.[30,53]

Many of the studies of 2nd and 3rd row transition metal analogues of the heavier chacogenide-bridged clusters focused on a common theme: the variation in bond order in the internal M-M tetrahedron as a function of electron count, wherein a 60-electron system (i.e., a tetrahedron of four 15-electron metal centers, each of which with 3 d-electrons available for bonding) would contain six covalent bonds within the M_4 tetrahedron (Fig. 5). This

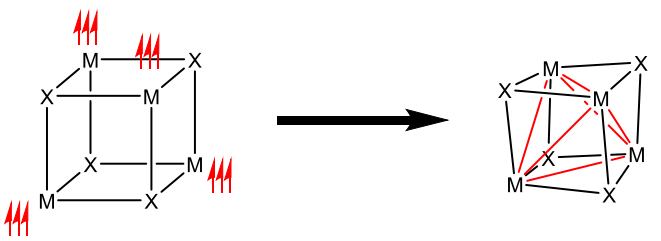

Fig. 5. Illustration of a 60-electron cubane cluster consisting of four 15-electron metal centers. The pairing of metal d-electrons (3 per metal center, red arrows) across the cubane provides a tetrahedron of six covalent M-M bonding interactions (red lines).

is the case in the Cr(III) systems discussed above. Every addition (or removal) of 2 more electrons effectively decreases the bond order by 1, giving systems with a partially covalently bonded central metal tetrahedron (Fig. 6).[36,39,44,45,48] The effects of this covalent bonding is apparent in asymmetric distortions in clusters with an incompletely bonded M-M tetrahedron. Rauchfuss showed that such systems can have "mobile" M-M bonds, demonstrated in a thoroughly characterized Ir-S system, where the geometric distortion is localized, but equilibrates across all the M-M faces based upon temperature-dependent NMR studies.[48]

The distortion of the heterocubane structure from the idealized 90° angles is thus highly dependent upon the electronic structure and does not obey a general set of rules. Systems with extensive M-M covalent bonding (e.g., Fig. 5) tend to have obtuse internal X-M-X bond angles due to the metal atoms being attracted toward one another, with concomitant acute M-X-M bond angles. In contrast, where M-M bonding is absent, and the M-M distances are increased, the rhombs of the cubane are distorted such that X-M-X angles are acute, and M-X-M angles obtuse. This is well illustrated in the crystal structure of the mixed-valent, formally $[Fe^{III}_2Fe^{IV}_2S_4Cp_4]^{2+}$ cluster[39], a 66 e^- system which shows Fe-Fe bonding interactions across four faces of the cubane, and two faces without Fe-Fe bonds. The result is a distorted cubane with acute-S-Fe-S angles across the two non-bonded faces, and obtuse S-Fe-S angles across the four bonded faces. In Fig. 7, this is contrasted with an analogous 60-electron Cr_4S_4 cluster with covalent interactions across all faces of the cubane.

Examples of cyclopentadienyl-terminated cubane clusters with hydroxide[54–57] ligands are less common and associated only with synthetic and crystallographic studies. CO-[58–62], imide [62], and hydride [60,62] bridging ligands in Cp-ligated clusters have also been reported. The few examples of structurally characterized μ_3-phosphide-bridged heterocubane clusters are all at Cp-terminated clusters.[63–65]

Carbon-based bridging organic ligands are much less common than those bearing nitrogen, oxygen, or sulfur, though these types of ligands are of particular interest to the iron molybdenum cofactor of the nitrogenase enzyme (section 3.7), and its central carbide atom. An example is methyl, which has been reported at structurally characterized Cp-type cubane clusters in a few instances [60,61,66–70], with iron-based examples iron being particularly relevant to nitrogenase (see section 3.7.4).[61,63,71,72] Some of these C-based ligands will be discussed further in section 3.7.4.

The most closely spaced metal–metal contacts in heterocubane clusters occur in boride (BH) systems. This is because the bridging boron atoms provide few electrons to the total electron count, leading to unpaired d-electrons for M-M bonding, and is due to the small size of B, which allows the metal ions closer to one another. For example, the $Ni_4(BH)_4Cp_4$ cluster of Grimes[73] featured a *closo* structure with two Ni-Ni covalent bonds at a remarkably short 2.35 Å, while the other unbonded Ni-Ni contacts were longer at 3.56–3.59 Å (Fig. 8). Though Grimes argued this structure was unexpected based on Wade's rules[74] for borane clusters, a full electron count including the Ni, Cp, and BH ligands indicates this structure is a 68-electron cluster, consistent (see Fig. 6) with the observed two Ni-Ni bonds.

Surprisingly, the analogous cobalt cluster from the same group, $Co_4(BH)_4Cp_4$ exhibited the same *closo* structure with two apparent Co-Co bonds based on two crystallographically independent molecules, one on a general position, and one on a special position. This violates the expected M-M bond order for such a 70-electron cluster, which should have only one Co-Co bond. The authors also note [75] that the structure does not obey Wade's rules either. This anomaly may be explainable by the presence of two 0.5-bond-order contacts across the two bonded pairs of cobalt atoms. This half bond order is consistent with the rather longer (2.47–2.48 Å)

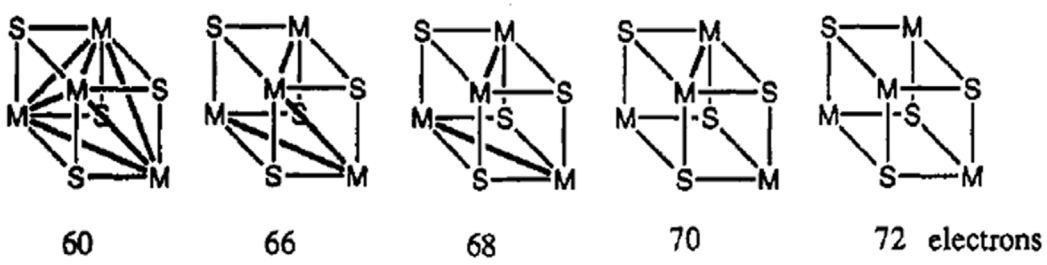

Fig. 6. Reproduced figure from Venturelli et al[48] showing idealized structures of $M_4S_4Cp_4$ cluster cores showing patterns of localized M-M bonding as a function of electron count. Reproduced with permission from The American Chemical Society. Terminal ligands are not shown but their donated electrons are included in the total electron count.

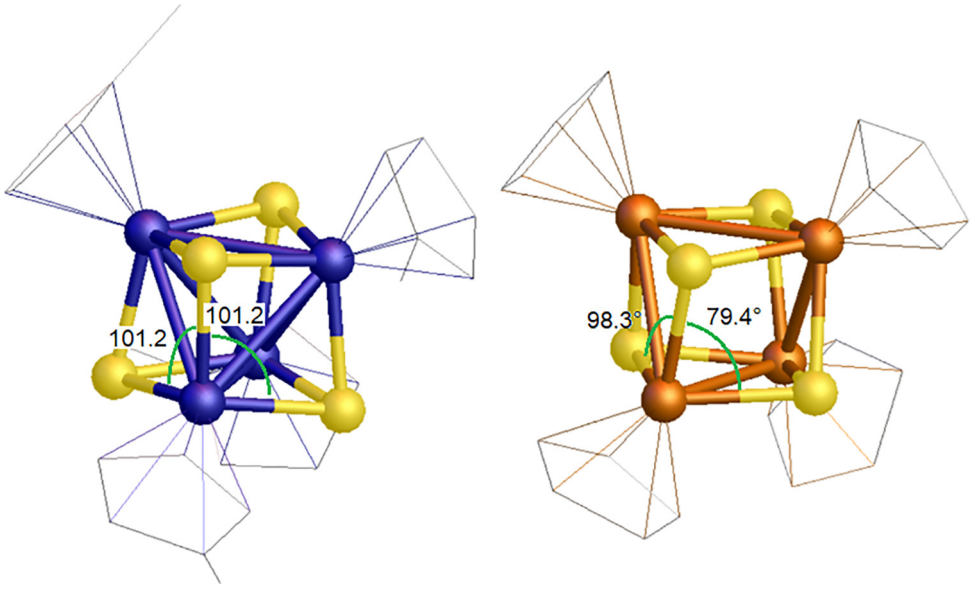

Fig. 7. X-ray crystallographic structures of $[Cr_4S_4(MeCp)_4]^{2+}$(left) and$[Fe_4S_4Cp_4]^{2+}$ (right) illustrating distortions resulting from covalent interactions. In the fully-bonded Cr system, all S-Cr-S bonds are obtuse, while in the partially-bonded Fe system, widening of S−M−S bond angles is observed where M-M bonding occurs, and compression of S−M−S angles is observed where M-M bonding is absent.[37,39] Cp ligands shown in wireframe mode and hydrogens omitted for clarity. Coloring: Cr: blue, Fe: orange, S: yellow.

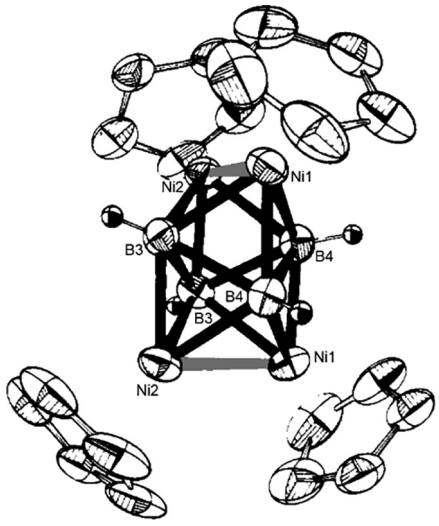

Fig. 8. X-ray crystal structure of $Ni_4(BH)_4Cp_4$ cubane cluster with two Ni-Ni covalent bonds shown in gray.[73] Reproduced, recolored, and relabeled with permission from the American Chemical Society.

Co-Co bonds in comparison to the 68-electron nickel system (2.35 Å).[73] Alternatively, some uncertainty in the composition of the crystalline phase is evidenced by the refinement of a spurious 1/5-occupancy chloride atom as part of the structure, whose origin and effect on electronic structure was not fully explained in this report.

3.2. Strong-field-ligated cubane clusters

Metal carbonyl cluster systems constitute perhaps the most extensive general class of cluster compounds. With the exception of the all-ferrous CN-ligated Fe_4S_4 cluster of Holm,[76] strong-field-ligand-ligated cubanes are not frequently discussed in the context of biological systems. However, these systems provide an important illustration of the biologically relevant bonding in cubane clusters by illustrating the stark contrast in M-M bonding effects in high-electron-count vs low-electron-count clusters. An overview of the M-M bonding in these systems is thus presented here using a few selected examples to provide completeness in the discussion of these biologically relevant bonding descriptions.

In synthetic heterocubane clusters, CO[71,77–88], CN^-[76,89–95], and NO[96–100] are frequently found as terminal ligands. Due to their π-acidic nature and neutral charge, CO terminal

ligands typically support low-valent (electron-rich), low-spin, octahedral metal centers. Due to the low metallic charge, these systems most often achieve charge balance by featuring monovalent bridging ligands such as OH[77–85,101], OR[82,83], and SR [86–88] ligands. These systems have metal centers that tend toward ideal octahedral geometry with approximate 90° terminal X-M-X angles, but unlike the Cp-ligated systems, the core rhombs are usually distorted such that the X-M-X angles are slightly acute, and the M-C-M angles slightly obtuse (Fig. 9). NO ligands almost exclusively feature S^{2-} bridging ligands,[97,99,100] with the exceptions being examples of imide (NR^{2-}) bridging ligands,[96] or mixtures of imide and sulfide.[97,98]

In addition to its π-acidity, CN is also negatively charged, and a stronger σ-donor than CO, and supports metals in the oxidation states (II-V), and usually with dianionic bridging ligands such as S^{2-} [76,81,89,90,94,95,101,102], Se^{2-} [91,92], and Te^{2-} [93] for charge balance. Cubane clusters terminally ligated by CN can have either six-[91–94] or four-coordination.[76,89,95,101,103,104] Six-coordinate clusters are almost exclusively $Re^{IV/V}$-based clusters[91–94], with Mo- and W-based clusters constituting the second most common class.[105–111] There have been a few classes of four-coordinate clusters terminally ligated by CN: 1) Fe_4S_4 model clusters of the nitrogenase iron protein cluster (more in Section 3.7),[76,89,95] 2) Fe-S clusters with corner substitution by Mo [112] or V[113] analogous to the heterometallic nitrogenases (more in section 3.7), or 3) a class of Cu-S cubane clusters with corner-substituted Mo[114,115] or W[116–118]. This latter class of Cu clusters is of interest in light of the sulfide-bridged Mo-Cu active site of the molybdopterin-based carbon monoxide dehydrogenase enzyme discovered in the early 2000s (Section 3.6).[119–122]

The facial rhombs of terminally CN-ligated clusters distort in a manner opposite that of the CO- based clusters, with M-M contacts shortening, resulting in obtuse X-M-X angles and acute M-X-M angles. Unlike in the case of predictably bonded Cp-ligated clusters, there is very little variation in these structural trends, which hold for 1st, 2nd, and 3rd row, and for both early and late transition metals. These structural features occur because octahedral CO clusters tend to have high total electron count due to having six donor ligands per metal, and lower oxidation state (higher d-electron count) bringing them closer to the fully M-M antibonding 72 e^- scenario, whereas the other geometries tend to have lower electron counts toward the fully bonding, 60 e^- scenario. Though isolelectronic to CO, CN-ligated clusters show this tendency toward covalent metal–metal interactions because the negatively charged ligand encourages higher concomitant oxidation states for charge balance, reducing the electron count. And in the case of the four-coordinate clusters, the decreased number of ligands further lowers the total electron count. In one example, the synthetic replacement of four NO ligands on tetrahedral $Fe_4Q_4(NO)_4$ clusters (Q = S, Se) by twelve CO ligands resulted in a geometry change whereby the short 2.65 Å Fe···Fe contacts in the 60-electron nitrosyl (NO^+-Fe^I) cluster expand substantially to 3.47 Å. This may be attributed to the conversion of the 60-electron cluster to the fully Fe-Fe antibonding 72 e^- cluster[123].

A thorough computational study for the idealized 60-electron case in $[Re_4S_4(CN)_{12}]^{4-}$ was predicted [124] to have the full complement of a tetrahedron of 6 M-M bonds based on electron localization function (ELF) analysis.[125] ELF is a useful analysis for the visualization of bonding and non-bonding electron pair locations, which provides a computationally rigorous analogy to Lewis theory. The ELF takes advantage of the Pauli exclusion principle to assign basins with high probability of paired electrons, which correspond to the locations of bonds, non-bonding "lone pairs", or paired core electrons. This analysis uncovered disynaptic basins (bonds) centered between all six Re-Re vectors. (Fig. 10). The analysis is consistent with the atoms in molecules (AIM) analysis[126] which also identifies six bond-critical points between all six of the Re-Re contacts. The terminal ligation by CN in these systems results in a cubane core distortion that moves the Re atoms toward one another and into bonding range (i.e., Fig. 9, center).

An example of a non-60-electron case, $[Mo_4S_4(CN)_8(NO)_4]^{8-}$, [127] (Fig. 11) may be described as a formally Mo(I) anionic cluster, a 68-electron system, four electrons short of the fully antibonding 72 e^- case and providing the opportunity for the formation of two Mo-Mo bonds. Crystallographic evidence for these two Mo-Mo bonds is observed, and the cluster geometry is described as "two linked Mo_2S_2 quadrilaterals with metal–metal bonds (Mo-Mo = 2.99(3))".

As an example of a system lacking M-M bonds, the neutral $Co_4Sb_4(CO)_{12}$ system represents the fully antibonding 72 e^- system, and exhibits a cluster distortion that moves the metal atoms away from one another due to M-M antibonding (as in Fig. 9, left), with a > 4 Å separation between the metals, and thus possessing no evidence of Co-Co bonding interactions.[128]

The terminally cyano-ligated tetrahedral iron-sulfur cluster, $[Fe_4S_4(CN)_4]^{4-}$ was biologically inspired and represented the first example of a fully ferrous iron sulfur heterocubane cluster[76], inspired by the iron protein of nitrogenase (discussed further in section 3.7).[76,89,95] This cluster features a heterocubane with the expected distortion for a low-electron-count cluster, moving the iron atoms nearer the center of the cluster (Fig. 9-right), but outside of covalent bonding distance (2.68–2.69 Å), and despite structural similarity to the biological cluster, and to later synthetic models, the cyano-ligated cluster appears somewhat electronically distinct from the biological systems; it exhibits four equivalent iron centers based on Mössbauer spectroscopy, whereas the comparative biological[129] and more accurate synthetic model systems[130,131] show an electronic distortion evidenced by a 3:1 Mössbauer signal.

One particularly unusual iron heterocubane cluster, which bridges the discussion of cyclopentadienyl- and strong-field-

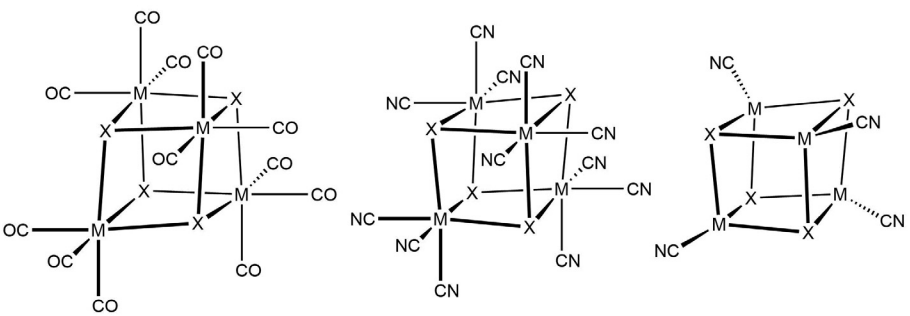

Fig. 9. Typical distortions of the cubane core with the metal six-coordinated with (left) CO, (middle) CN, and (right) four-coordinate CN (or NO).

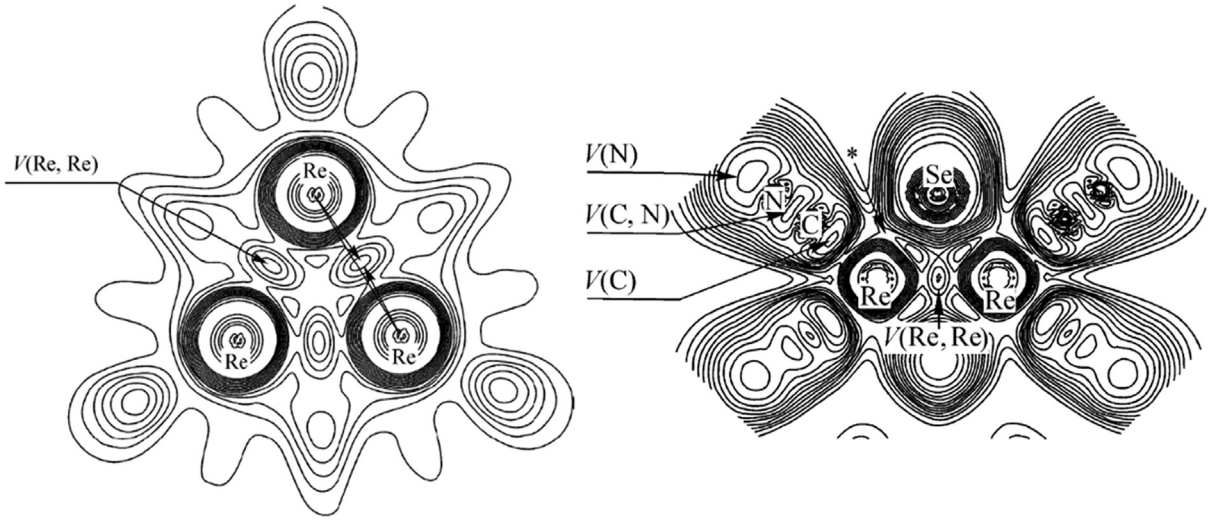

Fig. 10. (Left) ELF secant plane through three Re atoms in $[Re_4Se_4F_{12}]^{4-}$, essentially identical to the bonding motif in $[Re_4Se_4(CN)_{12}]^{4-}$. *V*(Re, Re) is the center of the disynaptic basin. (Right) ELF secant plane through two Re atoms and the Se atom in $[Re_4Se_4(CN)_{12}]^{4-}$ illustrating disynaptic basins (bonds) for the C≡N (*V*(C, N)), Re-Se (*), and Re-Re (*V*(Re, Re)) covalent bonds. Monosynaptic basins (lone pairs) are shown for the CN^-nitrogen lone pair (*V*(N)) and for the CN^- donor pair *V*(C), which suggests the Re-C bond is predominantly an ionic interaction. Figures reproduced and modified with permission from Springer-Nature.[124]

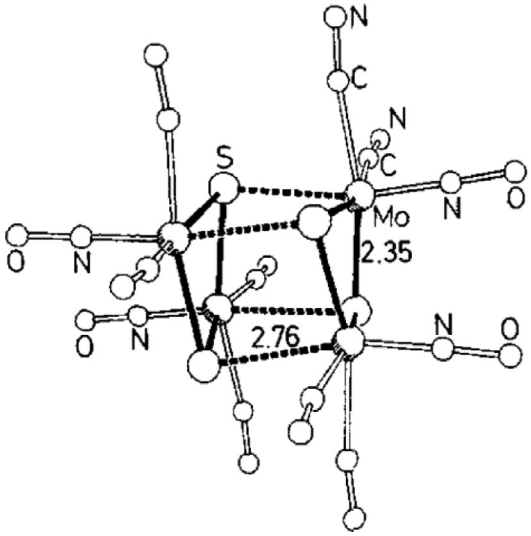

Fig. 11. X-ray crystallographic structure and selected bond lengths in the distorted cubane cluster $K_8[Mo_4S_4(CN)_8(NO)_4]$. [127] The bond metrics suggest Mo-Mo bonds between the two pairs of metals in each of the left and right Mo_2S_2 rhombs (individually), but no Mo-Mo bonding contacts across the cluster between the left- and right-hand rhombs. Image reproduced with permission from Wiley.

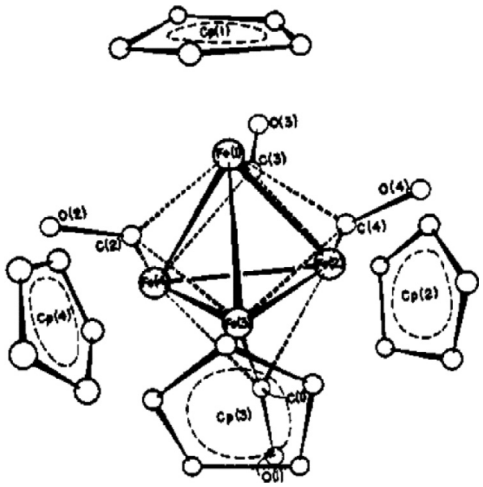

Fig. 12. X-ray crystallographic structure of $Fe_4(CO)_4(Cp)_4$ from Neuman et. al[58] illustrating an inscribed tetrahedron of covalent Fe-Fe bonds.

ligated clusters, is the carbonyl-bridged, Cp-terminated iron cubane cluster of King[132] whose structure was determined by the group of Dahl (Fig. 12).[58] Unlike the iron-sulfur clusters, this system is described as having a central tetrahedron of fully-covalently-bonded Fe^I ions with internuclear Fe···Fe separations from 2.50 to 2.53 Å. This arrangement of Fe(I) and CO makes this system a tetrameric 1:1 CO:Cp analogue of the cyclopentadienyliron dicarbonyl (Fp) dimer, $[(Cp)(CO)(\mu\text{-}CO)Fe]_2$ for which the existence of an Fe-Fe bond is controversial. While the Fp dimer possesses an Fe···Fe interatomic vector of 2.46 Å, well within the range for possible covalent bonding, most careful analyses have concluded that there is no formal Fe-Fe bond in the Fp dimer, and that the Fe-Fe interaction is actually an antibonding one. [133] In the heterocubane cluster, however, the four Cp ligands and the d^7 electron count of each tetrahedral Fe(I) ion implies a 60 e^- cluster, and suggests the possibility of a full set of six Fe-Fe covalent bonds, and the pairing of all available d-electrons. This electronic structure is supported by the compound's diamagnetic ^1H NMR spectrum, which shows only a single, sharp Cp-based resonance.[132]

3.3. Weak-field metal oxide/imide heterocubane systems

The oxo ligand, being a strong σ- and π-donor, tends to favor high-oxidation states at early-to mid-transition metals (so-called "oxophillic" metals). As such, the class of mid- to high-valent metal-oxo clusters with cubane motifs constitute a large class of reported molecules. While a large proportion of these are of interest as small molecule magnets (SMMs), the manganese-oxo systems are of interest as biological mimics of the Oxygen Evolving Complex (OEC: a Mn-Ca-O cluster coenzyme responsible for the oxidation of water to dioxygen, Section 4). Due to the high-spin, d_5 nature of Mn(II) ions (S = 5/2 per Mn) and their propensity for ferromagnetic coupling in octahedrally ligated clusters, their SMM behavior is of interest and has been reviewed.[134,135] A

number of parent Mn_4O_4 cubane systems are worthy of note[136–143] as model compounds of the OEC of photosystem II (PSII, see Section 4).

Among the most explored examples is the Mn_{12} cluster containing a Mn_4O_4 heterocubane core with an equatorial ring of 8 carboxylate-bridged manganese atoms.[134] This motif was made famous by the group of Christou for having remarkably large magnetic moments: as high as S = 19/2 and S = 10 (Fig. 13), and has been the subject of extensive study.[144–163] Additional examples of Mn-O cubane clusters are shown in Fig. 14. Additional manganese cubane clusters with greater biological relevance are discussed in Section 4.

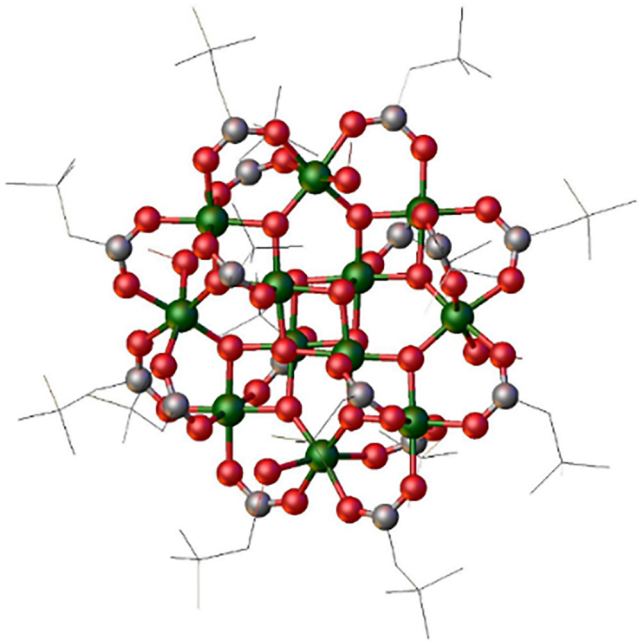

Fig. 13. Crystal structure of the Mn_{12} SMM motif[150] showing central heterocubane with 8 equatorial, pendant, carboxylate-bridged Mn centers. Neopentyl and methyl groups shown in wireframe mode and hydrogens omitted for clarity.

Reactivity studies on MnO cubane clusters are rare, usually limited to ligand exchange reactions[163], and a few examples of geometric rearrangements[167,168], which will be further discussed in the context of the biological OEC in Section 4. Structurally characterized manganese oxo clusters with coordination number less than 6 are rare, though cubane clusters with other bridging ligands, such as organic oxide[169,170], phosphine nitride[171,172], and imide[173–175] are known.

Cubane clusters of other metals with oxide are not as extensively reported, but include examples with cobalt[176–182], chromium[26,29,30,31,53,183–185], iron[186–188], copper[189], zinc[190,191], ruthenium[192], and mixed-metal systems[32–39,193–196]. Reactivity in metal-oxo cubane systems frequently involves oxidation chemistry, suggesting possible parallels to the powerful cubane oxidant in the OEC—the biological water oxidation catalyst—since the cubane cluster systems of redox-active transition metal ions can act as a reservoir of electron density, and serve as a template for cooperative catalysis between multiple metal centers. Noteworthy examples include a cobalt heterocubane catalyst for oxidation of benzylic alcohols to the corresponding benzaldehyde at low (0.2%) catalyst loading[176]. A zinc-oxo cubane system[190] exhibits unique O_2 activation chemistry (Fig. 15), succeeding in dioxygenation of a methyl ligand to a methyl peroxo ligand, detectable at low temperature. Upon warming, this system converts to the well-established[197–203] corner-fused methylzinc-alkoxo double-cubane motif. It is worthwhile to note that Zn is putatively redox innocent, and the reducing equivalents that activate O_2 are stored—not in the metals—but in the methyl ligands, which are formally oxidized to methylperoxo ligands. An iron-oxo heterocubane cluster with four additional pendant iron atoms was shown to exhibit water oxidation electrocatalysis, and act as a possible iron-based mimic of the Oxygen Evolving Complex of Photosystem II (Fig. 16).[204]

An important class of metal oxo cubanes are the cobalt oxide cubane clusters that have been implicated as water oxidation catalysts or precatalyts. Cobalt is often explored as an alternative metal to manganese in models of the oxygen evolving complex of photosystem II (see section 4) due to the abundance of cobalt in the earth's crust.[205] Molecular cubane clusters act as homogenous analogs to the water-oxidizing cobalt oxide/hydroxide amor-

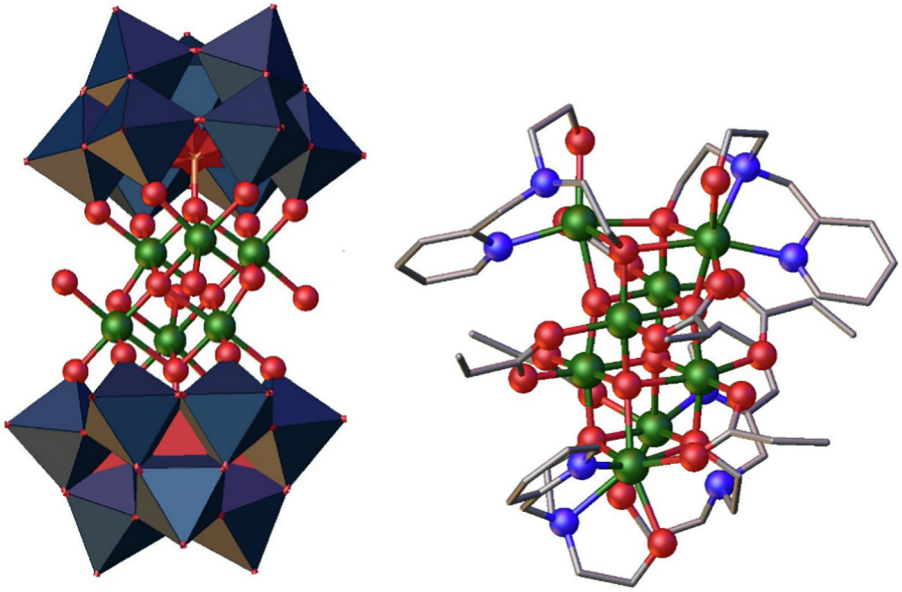

Fig. 14. Face-fused dicubane-[165] and tricubane-[166] based SMMs. Polyoxometalate frameworks are shown in polyhedron mode. Carbon atoms shown in stick mode and hydrogen atoms omitted for clarity.

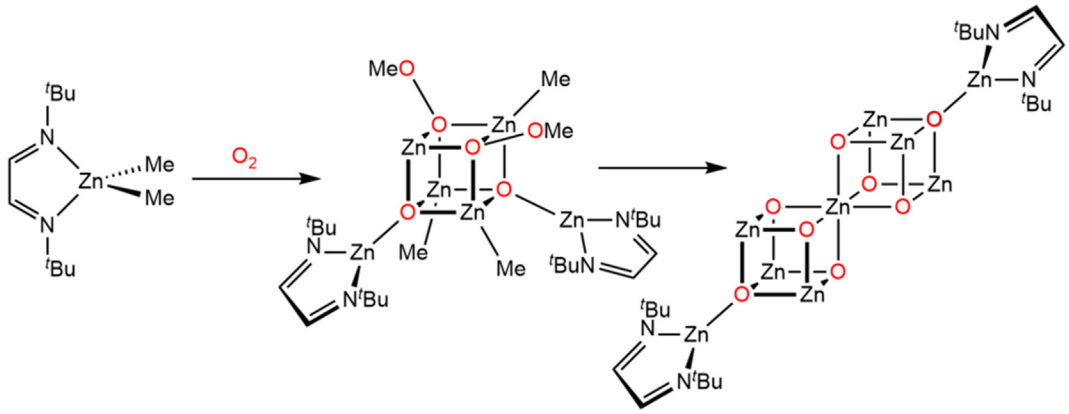

Fig. 15. O_2 activation by a methylzinc diamine system to give cubane clusters concomitant with oxidation of methyl ligand to methylperoxo and methoxo ligands.

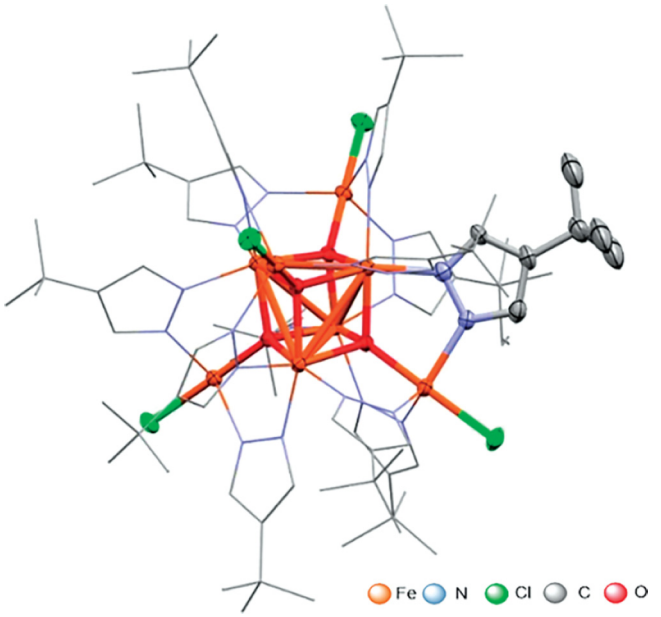

Fig. 16. X-ray crystallographic structure of the octanuclear water-oxidizing cubane cluster of Deutscher et al. Most carbon and nitrogen atoms shown as wireframe and hydrogen atoms omitted for clarity. Reproduced with permission from Wiley.[204]

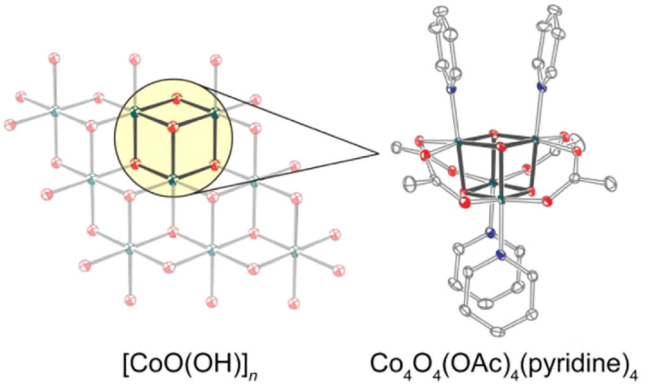

Fig. 17. Comparison of the structure of the $Co_4O_4(OAc)_4Py_4$ cubane cluster of Tilley with the hemicubane-containing structure of cobalt oxyhydroxide. Reproduced with permission from the American Chemical Society.[205]

phous films of Nocera, which are proposed to contain Co-O cubane motifs.[206] The cubane structure is also implicated in other cobalt catalysts as well; the group of Dismukes showed that incomplete (voided) cubane catalysts did not oxidize water in high pH environments (pH $\geq$ 7) that favor water oxidation, but the completed Co_4O_4 cubane cluster did catalyze the reaction.[207] Thus, a class of Co_4O_4 clusters for water oxidation have emerged,[208,209] with various ligands aimed towards optimizing the catalysis. Studies using oxygen isotopic labeling of a homogenous $Co_4O_4(OAc)_4py_4$ (py = pyridine, OAc = acetate) revealed that the core stays intact during the reaction, hinting that the terminal oxo ligands are accountable for forming O_2.[205] However, combined EPR, ^{31}P NMR, and EDTA titrations determined that a Co(II) impurity may be responsible for most of the water oxidizing activity in the $Co_4O_4(OAc)_4(Py-X)_4$ class of cobalt cubanes (Fig. 17).[210]

In addition to the abundance of reported metal oxo cubane systems, the isolobal imido ligand has a propensity to form the analogous cubane systems (see Fig. 18), with iron and manganese systems representing the largest portion of reported structures. Also worthy of note are the cobalt imido structures of Fenske. [211] These clusters have been related to the nitrogenase and photosystem II clusters, and will be discussed further in Sections 3.7 and 4.1.4. Like the Cp-ligated systems, metal imido cubane clusters tend to exhibit antiferromagnetic coupling, resulting in systems with minimized quantum spin. An all-Fe(III)-imido cluster from Lee, $Fe_4(\mu_3\text{-NTol})_4(SMes)_4$ (Mes = 2,4,6-trimethylphenyl)[212] exhibits the S = 0 shaped magnetic susceptibility curve,[213] analogous to that for $Cr_4O_4Cp_4$ (see Fig. 4),[31] and is suggestive of weak antiferromagnetic coupling. A one-electron-reduced analogue, $[Fe_4(\mu_3\text{-NTol})_4(SMes)_3(N(SiMe_3)_2)]^-$, a formally 3-$Fe^{III}$:1-$Fe^{II}$ cluster, exhibited an S = ½ ground spin state based on electron paramagnetic resonance (EPR) spectroscopy, also indicative of antiferromagnetic coupling.[213] In a related paper, the all-ferric $Fe_4(\mu_3\text{-N}^t\text{Bu})_4Cl_4$ cluster was EPR silent, but a cluster with a one electron oxidized core, $Fe_4(\mu_3\text{-N}^t\text{Bu})_4N^t\text{BuCl}_3$ possessed a S = ½ ground state also based on EPR spectroscopy, consistent with the expected antiferromagnetically coupled 3-Fe^{III}-1Fe^{IV} core. This cluster represented the first example of a terminal imido ligand on iron, which had previously been claimed an impossibility.[214] The antiferromagnetic coupling behavior is analogous to that observed in biological Fe_4S_4 cubanes and their analogues (Section 3).

In a related, but higher-oxidation-state Mn-based system, the all-Mn^{IV} cluster, $Mn_4(\mu_3\text{-N}^t\text{Bu})_4(N^t\text{Bu})$ possesses remarkably close Mn-Mn contacts in the range of 2.54–2.56 Å.[174] With triply-bonded terminal imido ligands (M–N distance = 1.64 to 1.65 Å) donating 6 electrons to each manganese atom, this cluster represents an idealized fully M-M bonded 60-electron system (see

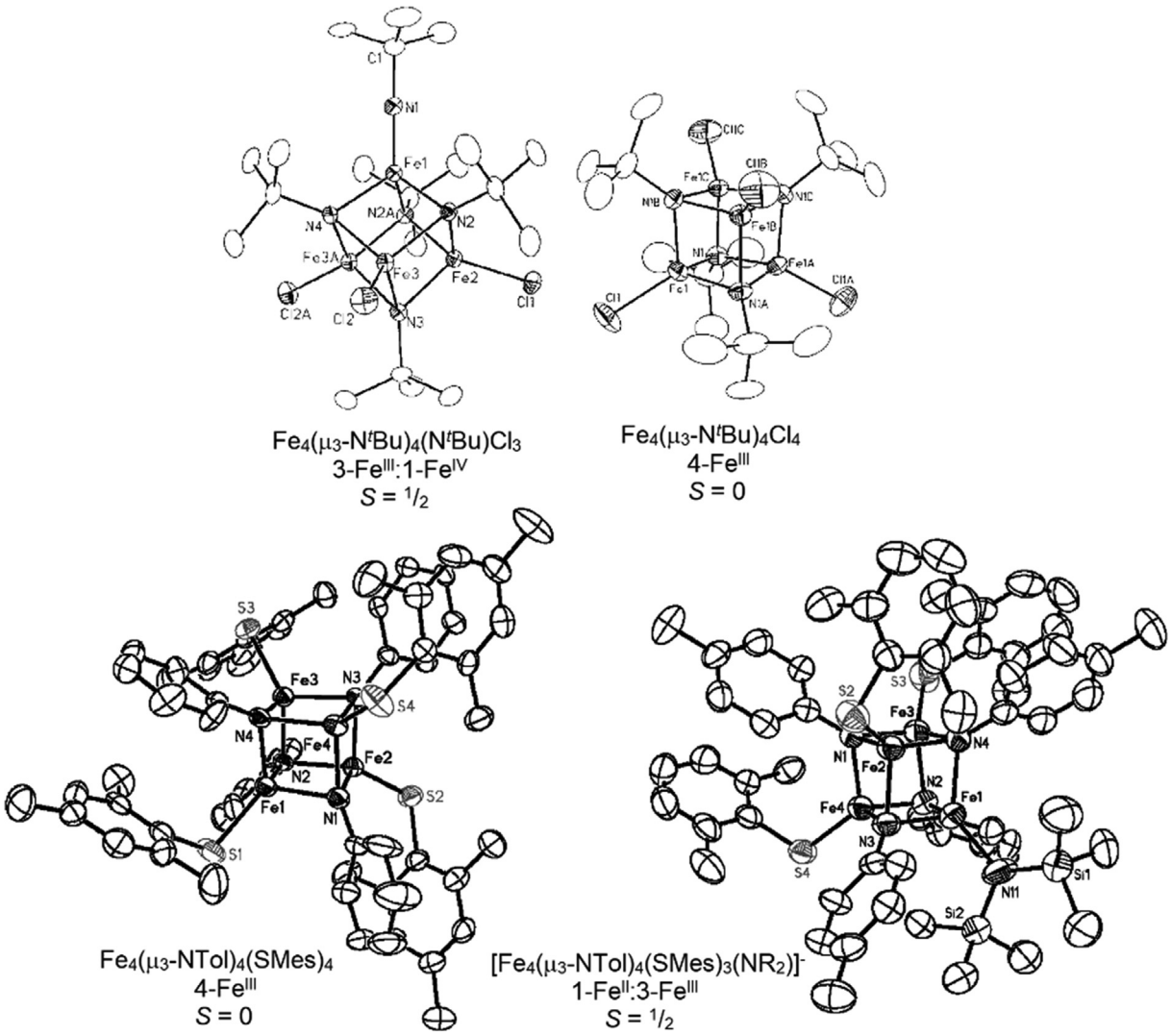

Fig. 18. Iron-imido cubane clusters from the group of Lee. Odd-d-electron systems exhibit S = ½ quantum spin, while even-electron systems exhibit S = 0 spin, consistent with antiferromagnetic coupling of high-spin metal centers in all cases. Reproduced with permission from the American Chemical Society. [213,214]

Figs. 5, 6). Unlike typical weak antiferromagnetic coupling in heterocubanes of four-coordinate first-row transition metals, this system exhibits temperature-independent diamagnetism suggestive of full M-M bonding similar to 2nd and 3rd row transition metal chalcogenide cubane clusters with terminal Cp ligation. [44,45,48,50,52] In the Mn-N system, M-M bonding orbitals were described using MO theory and DFT, and these models suggested bonding combinations through the expected frontier orbital combinations (dx^2-y^2 d_{xy}, and dz^2) described by Peters [215] for four-coordinate metals with one multiply bonded terminal imido ligand (Fig. 19).

A few additional examples of simple metal imido structures exist, such as yttrium-[203] and iridium-imido[216,217] analogues of the cyclopentadienyl structures, a zinc-titanium system with parent imido (NH) bridging ligands and Cp* and terminal acetylene organometallic ligands,[218] and a series of halide-ligated cadmium cubane systems. Outside of imido clusters, most N-bridged cubane cluster systems are bridged by the nitrogen atom of phosphine nitride. [171,172,213,218–224] While only a small percentage of metal-oxo cubane clusters feature reactivity (with exceptions highlighted in various sections of this review), the relatively fewer reports of metal imido cubane cluster reports feature extensive reaction chemistry with potential relevance to several cubane-cluster containing enzymes such as nitrogenase and carbon monoxide dehydrogenase. Specific reactions include catalytic disproportionation chemistry[212], N-N bond cleavage [212,213,225], N=N bond formation[174], C–N bond cleavage [226–228], hydrogen atom transfer, and alkene oxygenation.[175]

Cubane complexes of metals with bridging monoanionic oxygen ligands such as hydroxo[54–60,77–86,229–237] and alkoxo [82,83,169,170,198–206,237–266] are the most common type of structurally characterized M_4O_4 clusters, especially with regard to non-manganese transition metals. Many of these have already been covered in sections 2.1 and 2.2 on cyclopentadienyl and CO-ligated systems, but the set of OR bridged metal clusters also includes carboxylate-terminated systems[169,229,230,232, 235,240,249–255,265,267] conceptually related to the extensive class of MnO molecular magnets and to the oxygen evolving complex of Photosystem II. Acetonylacetate and related terminal ligands also make up a significant fraction of the reported structures.[238–244,244,253]

3.4. Weak-field, low-valent metal chalcogenide clusters.

Heavier chalcogenide (Q) bridging ligands such as S, Se, and Te are of interest in comparisons and labelling experiments in biological Fe_4S_4 clusters and model systems. These chalcogenides are "softer" ligands according to the Pearson hard-soft acid-base the-

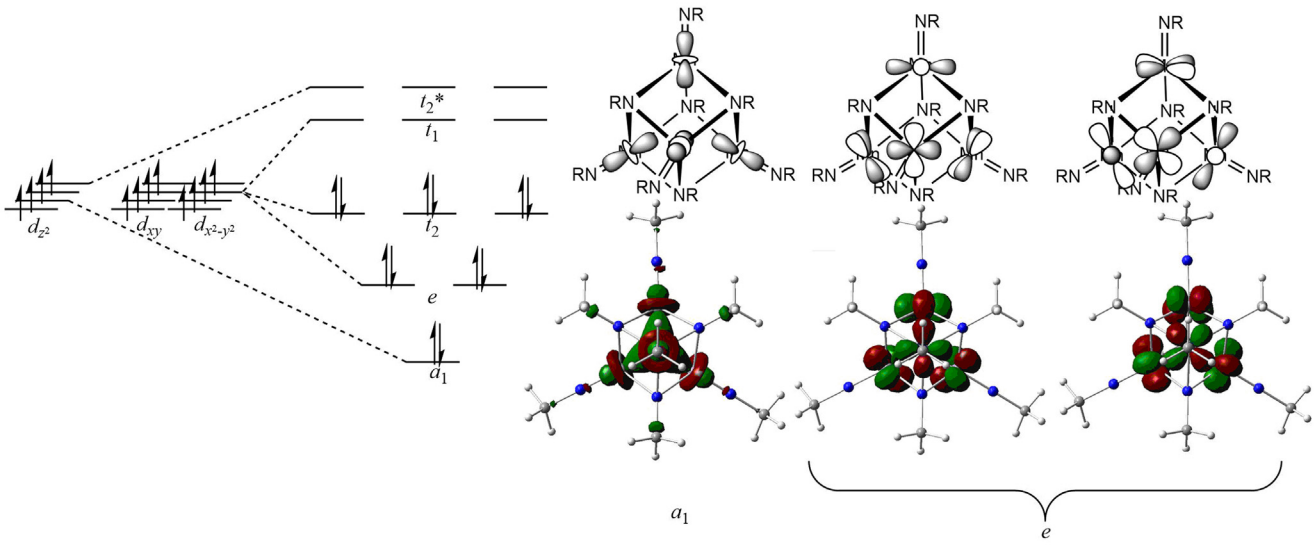

Fig. 19. (Left) Orbital interaction diagram between the basis dx^2-y^2 d_{xy}, and dz^2 orbitals of the four Mn atoms, in T_d symmetry, showing formation of six bonds. (Top) molecular orbital cartoon of the a_1 and e symmetry Mn-Mn orbitals, and (Bottom) Kohn-Sham molecular orbitals of the a_1 and e symmetry Mn-Mn orbitals. t_2 bonding orbitals are not shown.

ory[268], and as such, tend to promote lower oxidation states in metals they bridge. Due to their ability to form good $p\pi$-$d\pi$ overlap with metals, 2nd-row nonmetal atoms (O, N) tend to have different ligation properties than their 3rd-and-higher-row counterparts (S, P), which do not form good π-bonds. For example, while terminal oxo and nitrido compounds are common, terminal sulfo and phosphido compounds are not for these reasons. In cubane clusters however, *p*-orbitals are unavailable for π bonding, but are ideally suited for σ-bonding in all-μ_3-binding modes of bridging ligands, and therefore, analogous geometries are accessible down the columns of nonmetals due to similar σ-only bonding properties of these bridging atoms. A surge of interest in the cubane structural motif occurred after the discovery of the Fe_4S_4 cubane cluster in biology (discussed further in section 3.1), and since then, extensive synthetic exploration has shown that these cubane motifs are widely accessible using different metals and different bridging ligand atoms. The biologically relevant chemistry of biomimetic synthetic metal chalcogenide clusters, especially that of Fe-S clusters, will be discussed further in section 4.

Reported synthetic metal chalcogenide clusters are predominantly of the Fe_4S_4 type, containing four-coordinate iron, most often with a biomimetic terminal thiolate ligand, as observed in biological iron-sulfur proteins.[1,269] There has been interest in the degree to which core ligand substitution alters the electronic structure of such systems. The electronic structure of Fe_4S_4, Fe_4Se_4, Fe_4Te_4 are all remarkably similar considering the differences in basicity, polarizability, and ionization potential of these chalcogenides. For instance, the three homologous iron chalcogenide clusters: $[Fe_4Q_4(SPh)_4]^{3-}$ (Q = S, Se, Te) all have an analogous cubane structure, with the Fe-Fe distances increasing slightly down the Q series due to increasing size of the chalcogenide ligand.[270] These clusters all have a ground spin state of 3/2, attributed by these authors to strong zero-field splitting, but magnetic behavior at elevated temperature is more simple, described as antiferromagnetic coupling of three high-spin Fe(II) ions and one high-spin Fe(III) ion, with the value of the antiferromagnetic coupling, *J*, decreasing down the Q series due to increasing intermetallic distance: J = -114.7, −65.3 cm^{-1} and −30.5 cm^{-1} for Q = S, Se, and Te, respectively (Fig. 20). Magnetic ordering in Fe_4Se_4 clusters was also thoroughly investigated by Holm[270] and showed the same antiferromagnetic coupling with a ground spin state of 3/2. No analogous four-coordinate Fe-O cubane clusters have been reported to our knowledge. This is presumably due to the influence of the hard oxide donors, which favor higher oxidation state and octahedral iron centers instead of the low-valent tetrahedral sites of Fe_4Q_4 clusters. The extensive chemistry of Fe_4S_4 cubanes will be discussed in more detail in the next section.

4. FeS cubanes

4.1. Discovery

The chemistry of iron-sulfur clusters has been extensively reviewed,[1] and the present discussion is therefore limited to a short historical development of Fe-S cubane chemistry, with an emphasis on the electronic effect of core and terminal ligand identities where appropriate. In 1971, a structure of the long-sought "non-heme" iron center of the high-potential iron protein (HiPIP) was determined.[271] This structure showed the cofactor to be a heterocubane cluster of iron and sulfur atoms ligated to the protein by four cysteine residues (Fig. 21).

A few examples of Fe-S heterocubanes had already been synthesized at this time using cyclopentadienyl terminal ligands.[272,273] However, with the discovery of the iron sulfur cubane cluster came a new effort to synthesize model compounds. The first report of a Fe-S heterocubane model complex came in 1972, close on the heels of the HiPIP crystal structure, and featured a Fe_4S_4 cubane core, with benzylthiolato terminal ligands accurately modeling the tetrahedral cysteine ligand environment of the protein (vide infra, section 3.2.2).[274] Since this discovery, the ubiquitous use of iron-sulfur clusters in electron transfer reactions has become apparent, not only in HiPIP, but also in ferredoxins, and other specialized electron transfer proteins.

The discovery of Fe-S cubane clusters as catalytic cofactors widened the scope of the chemistry of these systems. Aconitase [275–277] is a hydrolytic enzyme responsible for isomerization of citrate to isocitrate in the Krebs cycle. The consensus mechanism of aconitase is a dehydration-rearrangement-hydration reaction with an unsaturated aconitate intermediate.[278] It is curious that nature has evolved the use of an iron-sulfur cluster (an archetypal redox cofactor) to act as a redox-innocent Lewis acid catalyst to mediate a non-redox reaction, and a number of other hydrolases are based upon a similar motif exist as well.[279] In addition to

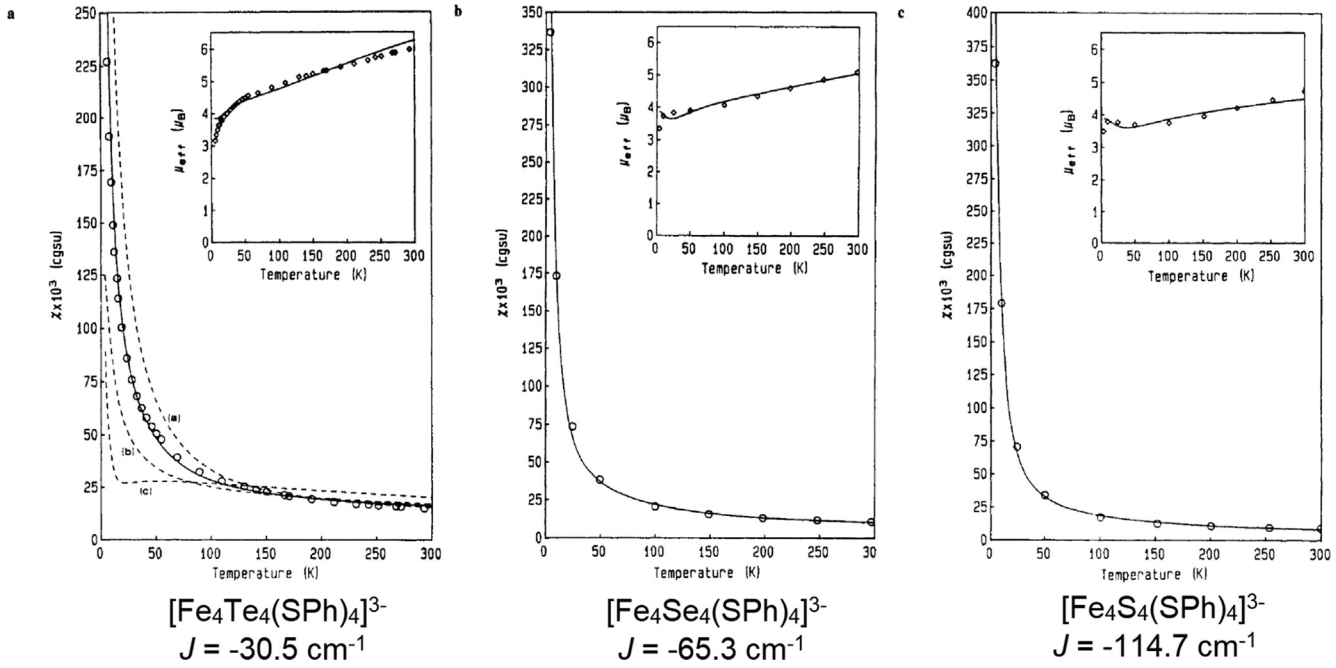

Fig. 20. Magnetic susceptibility for a series of Fe_4Q_4 cubanes (Q = Te, Se, S) and their corresponding values of magnetic coupling constant. Figures reproduced with permission from the American Chemical Society. [269]

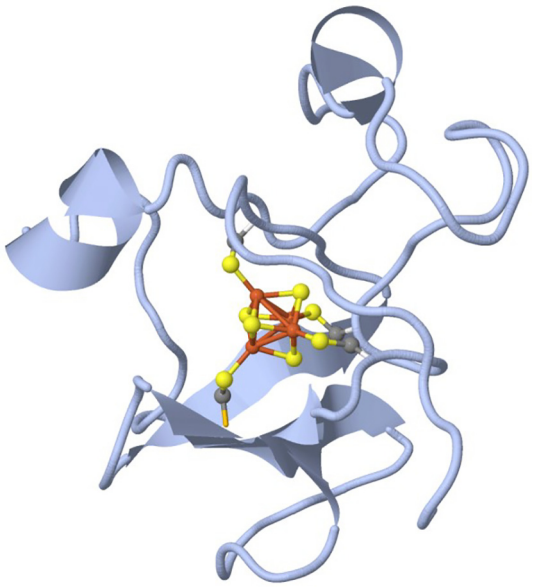

Fig. 21. 3D crystal structure of the HiPIP of Chromatium, displaying the central Fe_4S_4 heterocubane cluster.[274]

serving as electron reservoirs or Lewis acid catalysts, Fe-S cubane systems can serve as redox catalysts, acting as a substrate binding site, but also as storage for redox equivalents for catalysis, as in nitrogenase, CO dehydrogenase, and hydrogenase. The highly variable functionality of these motifs will be described further in the following sections.

4.2. Electron transfer

4.2.1. Fe-S cubane electron transfer proteins.

The chemistry and biology of electron transfer proteins has been reviewed in a comprehensive book chapter accessible to a wide range of readers.[280,281] The general purpose of iron-sulfur cubane clusters is electron transfer, for which they serve roles in bacterial HiPIP, as well as in the ferredoxins (Fdx). The cofactor also appears in numerous redox enzymes such as nitrogenase[282–285], hydrogenase[286], and multi-cofactor electron transfer proteins in the electron transport chain. [280,281]

Ferredoxins[280,281] are found in all life forms, and several different versions are known. The archetypal 4-Fe Fdx has a single Fe-S cubane cluster ligated by four cysteine thiolates. There also exists a rarer 3-Fe Fdx with a "voided" Fe_3S_4 cubane structure (See Fig. 23). The 7- and 8-Fe Fdxs each have two iron-sulfur clusters; the 7-Fe ferredoxin possesses both a Fe_4S_4 heterocubane cluster, and a Fe_3S_4 voided cubane cluster, while the 8-Fe Fdx has two Fe_4S_4 cubane clusters. These are attached to the protein via ligation of each iron by cysteine thiolate ligands. Despite having as many as eight potentially redox active metal centers, iron-sulfur electron transfer proteins carry only one redox equivalent per protein. The four-iron ferredoxins, for example, use only the 2-Fe^{II}:2Fe^{III}/3-Fe^{II}:1Fe^{III} redox couple (abbreviated Fdx^{ox}/Fdx^{red} respectively).

Although some other members of the Fe-S protein families do not possess cubane structure, it is worthwhile to briefly mention them in the interest of completeness.[280,281] These include the 2-Fe Fdxs, whose active sites contain a dimeric Fe_2S_2 rhomb, also held into the protein via four cysteine thiolates. A similar cofactor in the Reiske protein family possesses the same Fe_2S_2 rhomb but it is ligated by two cysteine and two histidine residues. Finally, the 1-Fe rubredoxin (Rdx), despite the absence of sulfide ligands, is considered among the Fe-S proteins due to its sole iron center being ligated by four cysteine thiolate residues.

Despite their apparent structural and compositional similarity, iron-sulfur cubane clusters have a remarkable versatility in their range of reduction potentials, spanning >1 V! These reduction potentials (vs. NHE) range from less than −600 mV for the 7-Fe ferredoxin to greater than + 400 mV for the HiPIP (though there is a gap in the middle between −150 and + 100 mV vs. NHE that is spanned by other Rdx, Reiske, and cytochrome *c* proteins). [280,281] Biology tunes the potentials of Fe-S proteins via a num-

ber of means. Proximity of the cofactor to nearby amino acid dipoles or full charges (such as other Fe-S cofactors, as in the 7- and 8-Fe Fdx) will alter the reduction potentials. Additionally, the sign of the charged surface amino acids, which solubilize the protein, can alter the reduction potential over a range of 400 mV, with negatively charged residues (carboxylates) lowering the reduction potential while positively charged (ammonium) residues raise the reduction potential. Reduction potentials can also be tuned by the degree of solvent accessibility of the Fe_4S_4 cluster; an Fe_4S_4 cubane cluster near the surface of the protein will experience an increased reduction potential since the buildup of negative charge upon reduction can be shielded by nearby solvent water molecular dipoles. Similarly, poorly-solvent accessible (deeply buried) iron-sulfur cofactors will have a decreased reduction potential since the buildup of negative charge upon one-electron reduction is poorly masked by the hydrophobic protein interior. The HiPIP system (Fig. 21) exemplifies the alteration of redox potentials by deeply burying the cofactor in the low-dielectric interior of a protein. This deeply-buried cofactor has its reduction potential lowered by such a large degree that under physiological conditions it operates one entire oxidation number higher in comparison to Fdx. In other words, to avoid the buildup of a large negative charge in a low-dielectric protein pocket, while ferredoxins use the Fdx^{2-}/Fdx^{3-} couple ($2Fe^{II}$:$2Fe^{III}$/3-Fe^{II}:$1Fe^{III}$), the high-potential iron protein instead uses the $HiPIP^{1-}$/$HiPIP^{2-}$ couple (1-Fe^{II}:$3Fe^{III}$/2-Fe^{II}:$2Fe^{III}$). Being an entire electron more oxidized, this protein has a higher reduction potential than the more reduced Fdxs, hence the name: high-potential iron protein. The combination of all these redox tuning approaches permits biology to alter the redox potential of this simple cubane motif over a range of about 1.1 V. The tactics by which biological systems tune the potentials of Fe-S proteins are illustrated in Fig. 22. Illustrations of the structures of ferrodoxins are shown in Fig. 23. The exquisite tuning of redox potentials is prerequisite for effective electron transfer processes essential to life; precise redox tuning controls not only the thermodynamics, but the kinetics of electron transfer to selectively and precisely direct the flow of redox equivalents between proteins in the cell.[281]

4.2.2. Model chemistry.

While a few examples of Fe_4S_4 cubane clusters existed prior to the discovery of the cubane structure of the HiPIP, these clusters were terminally ligated by Cp, making them electronically distinct from the thiolate-ligated clusters of biology. A number of thorough reviews from Holm and collaborators have summarized progress in this area.[1,5,6,268,287] We focus therefore on a subset of historically important results, starting with the report from Herskovitz, et al, representing the first synthetic model of the iron-sulfur cubane in 1972, the year after the discovery of the Fe-S cubane of HiPIP.[274] The compound was prepared using an anion

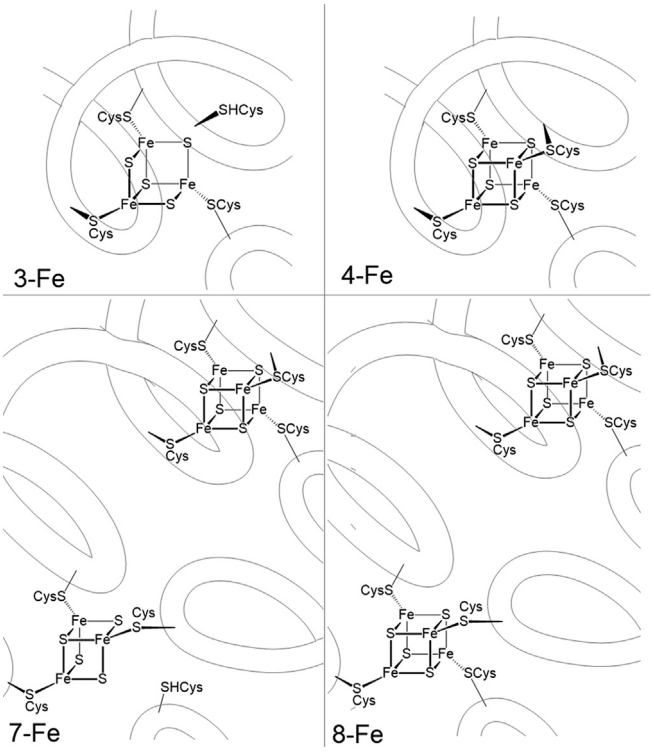

Fig. 23. Cartoon diagram of the structures of the 3-, 4-, 7-, and 8-Fe ferredoxins.

metathesis approach that became standard for such cluster types: the reaction of the metal chloride with a hydrosulfide source and a base. The iron centers are partially reduced to the ferrous state by oxidation of hydrosulfide (and/or thiolate), and the compound is crystalized as the tetraethylammonium salt by the introduction of Et_4NCl:

$$4FeCl_3 + 5\,NaSH + 4\,BzSH + 9\,NaOMe + 2\,Et_4NCl \rightarrow [Et_4N]_2[Fe_4S_4(SBz)_4] + 14NaCl + 9MeOH + S$$

The compound, shown in Fig. 24, is the redox analogue of $HiPIP^{red}$ (or Fdx^{ox}), and features remarkable geometric similarity to the biological system. The Fe-Fe spacing of ~ 2.73–2.78 Å and the obtuse angles at Fe in the Fe_2S_2 rhombs (104-117°) faithfully reproduce the metrics of the biological crystal structure. The reported structure features an axial distortion from the idealized regular rhombohedron that results in two types of S-Fe-S bond angles (more acute 104°, and more obtuse 112 and 117°). The authors attributed this distortion to crystal packing, not to an asymmetric electronic structure, even though this mixed diferrous/diferric system possesses a total electron count of 54 e^-, which

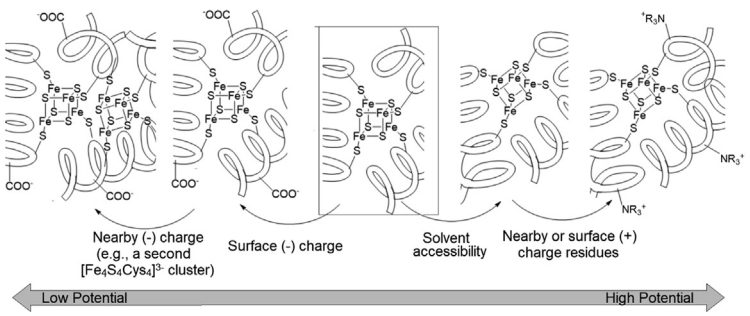

Fig. 22. Cartoon illustration of a generic Fe_4S_4 protein (center) and modifications used by biology to tune reduction potential from low to high. The diagrams are not meant to represent specific biological proteins, but to illustrate the concepts relevant to potential tuning.

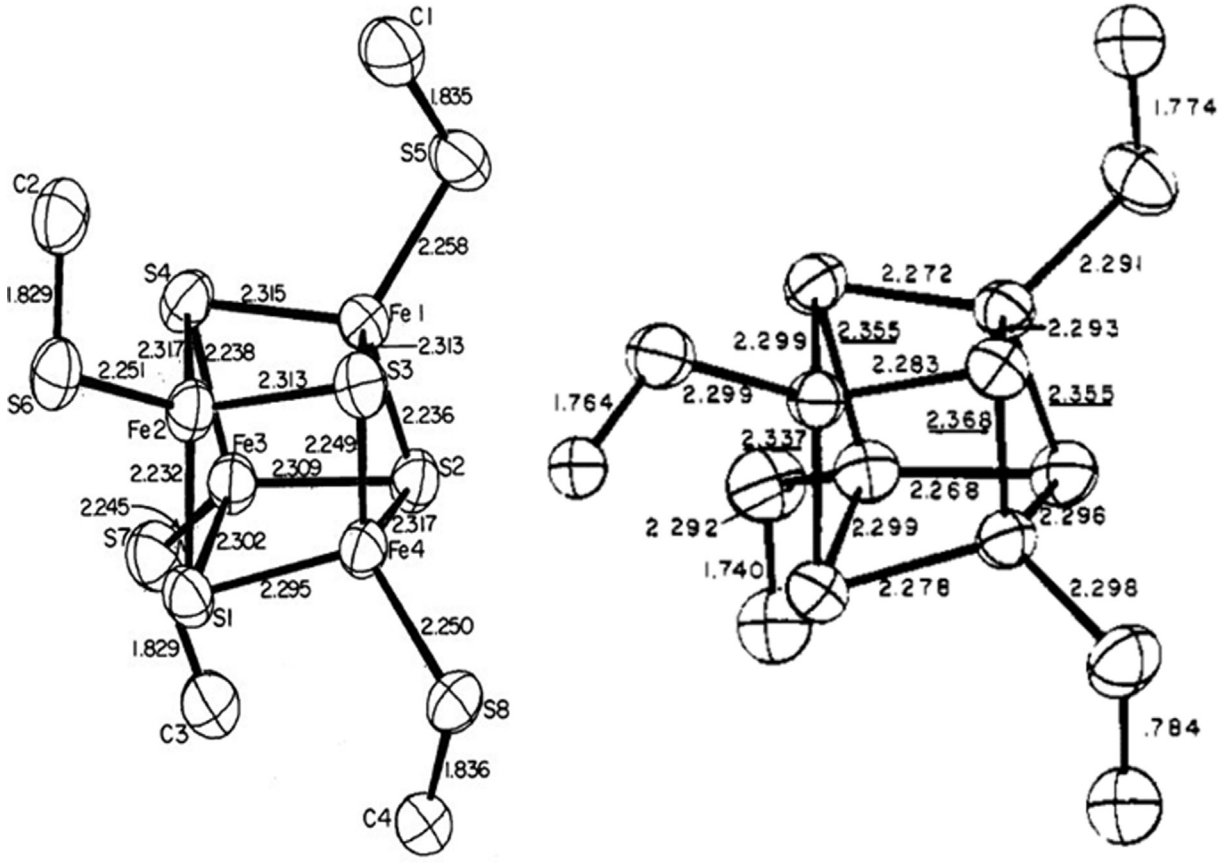

Fig. 24. (left) Crystal structure of $[Fe_4(\mu_3\text{-}S)_4(SBz)_4]^{2-}$ and (right) $[Fe_4(\mu_3\text{-}S)_4(SPh)_4]^{3-}$. Figures reproduced with permission from the National Academy of Science of the USA and the American Chemical Society). [274,290] Ellipsoids are set at 50 percent probability level. Hydrogen atoms and phenyl rings are omitted for clarity.

would lead to asymmetric Fe-Fe covalent interactions (see Fig. 6); the Fe-Fe separation of > 2.7 Å may be too large for meaningful metal–metal covalent bonding. The electronic structure of the synthetic cluster indicates a ground state singlet, S = 0 spin state based on the S-shaped magnetic susceptibility curve (Fig. 25), suggesting antiferromagnetic pairing between the two ferrous sites, and between the two ferric sites as the simplest electronic description. It should be noted that detailed electronic coupling descriptions of

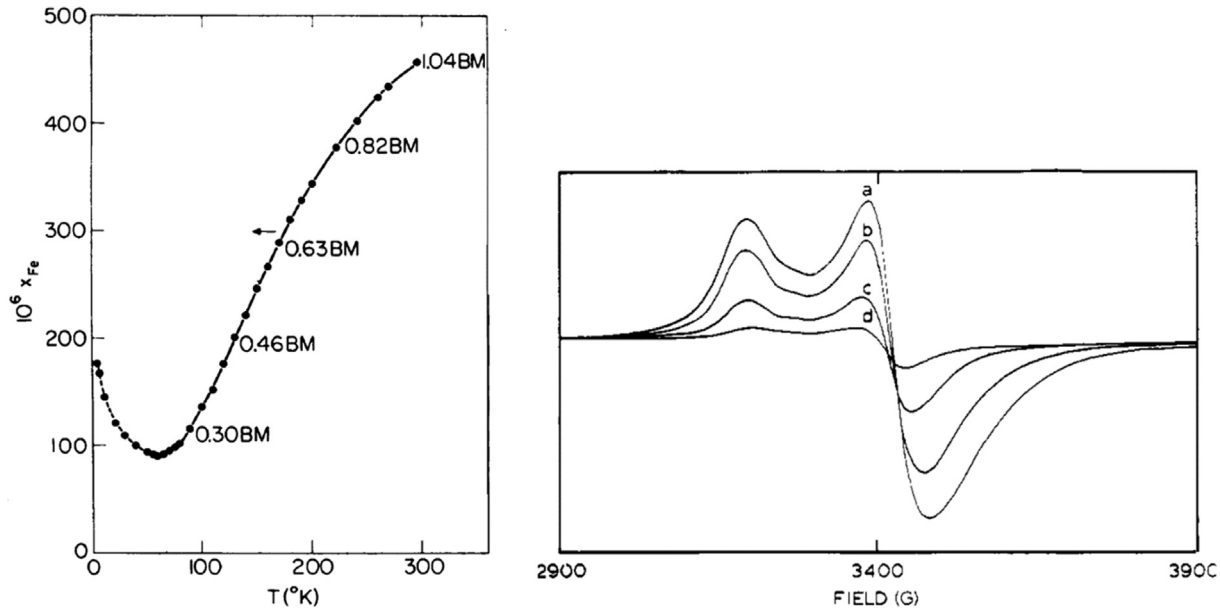

Fig. 25. (Left) Magnetic susceptibility of $[Fe_4S_4(SBz)_4]^{2-}$ given as magnetic moment per iron showing S = 0 antiferromagnetically coupled S-shape profile. (Right) EPR spectra of $[Fe_4S_4(SPh)_4]^{3-}$ at (a) 4, (b), 14, (c) 24, and (d) 35 K, showing a rhombically distorted axial $g \sim 2$ signal consistent with an S = ½ system. Figures reproduced with permission from the National Academy of Science of the USA and the American Chemical Society.[274,290]

Fe-S systems are more complicated than simple whole-ion coupling, and can involve, for example, antiferromagnetic coupling of two ferromagnetically coupled S = 9/2 Fe^{II}/Fe^{III} pairs,[288] which also gives an apparent antiferromagnetically coupled S = 0 result, behavior more consistent with a system containing covalent metal–metal interactions across some but not all faces of the cubane. The S = 0 spin state of this model compound is also a match to the behavior of the equivalent valence state in $HiPIP^{red}$ and 4-Fe Fdx^{ox}, which are both S = 0 clusters. Further, the Mössbauer spectral parameters for the compound are described by a simple quadrupole doublet that matches closely to the isomer shift and quadrupole splitting of the HiPIP and Fdx clusters, suggesting delocalization of the Fe^{II} and Fe^{III} centers across the cluster.[289]

About five years later, the first structures of synthetic analogues of the reduced 4-Fe ferredoxins were published also by the Holm group.[290] The reduced form of the cluster, $[Fe_4S_4(SPh)_4]^{3-}$ is also distorted from an idealized regular rhombohedron, but with slightly elongated bonds consistent with overall reduction by one electron (Fig. 24). This cluster exhibits an EPR signature (Fig. 25) consistent with an S = ½ spin system, most simply described by an antiferromagnetically coupled system of three high-spin Fe^{II} ions and one high-spin Fe^{III} ion. Further, the Mössbauer spectra show two overlapping quadrupole doublets, suggesting two types of iron centers in this complex. This suggests a description in Fe_4S_4 clusters of two pairs of antiferromagnetically coupled iron centers, where the Fe^{II} and Fe^{III} sites comprise a single spin system and share the extra electron more rapidly than the timescale of the Mössbauer experiment (Fig. 26). Thus, for the oxidized 2-Fe^{II}:2-Fe^{III} cluster, (Fdx^{ox}) antiferromagnetic coupling and rapid exchange of Fe^{II} and Fe^{III} character gives a S = 0 with one apparent type of metal center, while the reduced 3-Fe^{II}:1-Fe^{III} cluster (Fdx^{red}) exhibits a S = ½ state, and two types of iron signals on the Mössbauer timescale: a Fe^{II}:Fe^{III} pair (analogous to the Fdx^{ox} irons) and a Fe^{II}:Fe^{II} pair, with a different signal shape. This behavior is all analogous to the spectral and magnetic properties in the protein system, suggesting these clusters represent reliable synthetic structural and electronic analogues.[1]

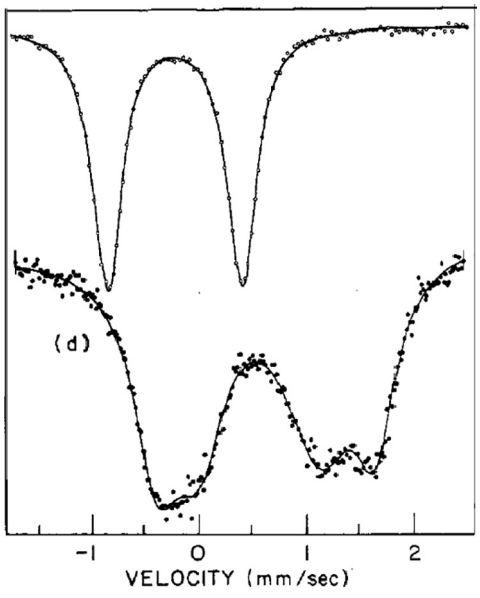

Fig. 26. Mössbauer spectra of synthetic models of Fdx. Top: 1.5 K spectrum of $[Fe_4S_4(SBz)_4]^{2-}$ showing single quadrupole doublet suggesting all iron atoms are equivalent on the Mössbauer timescale. Bottom: 4.2 K spectrum of $Fe_4S_4(SPh)_4]^{3-}$ showing two sets of overlapping quadrupole doublets, suggesting two types of distinct iron atoms on the Mössbauer timescale. Figure reconstructed with permission from the American Chemical Society.[289,290]

In the intervening years, extensive examples of Fe_4S_4 clusters have been published, pushing the boundaries of the redox capabilities of these systems. Almost 10 years later, a synthetic model of the oxidized form of the high-potential iron protein, $HiPIP^{ox}$, a 1-Fe^{II}:3-Fe^{III} cluster, was prepared by Millar; the compound $[Fe_4S_4(SC_6H_2{}^iPr_3)_4]^-$ was crystallized as a tetrabutylammonium salt.[291] The isolation of this unstable structure was made possible by the use of sterically encumbered diisopropylaryl groups on the thiolate capping ligand, which serve as electron donors to stabilize the oxidized core, and as steric protectors against decomposition. This synthetic system also mirrored biology by virtue of an overall antiferromagnetically coupled S = ½ description based on EPR spectroscopy, and a delocalized Fe^{II} ion based upon the observation of a single Mössbauer quadrupole doublet.[292] Other synthetic achievements worthy of note are the realization of the all ferrous Fe_4S_4 cubanes stabilized by π-electron withdrawing terminal CN^-[76] or n-heterocyclic carbene ligands[293], which bear potential analogy to the Fe_4S_4 cubane cluster of the iron protein of nitrogenase (more in section 3.7). At the other extreme is the realization of the all-ferric Fe_4S_4 cubane by the use of strongly σ-donating and sterically encumbered bis(trimethylsilylamido) terminal ligand.[294,295]

4.3. Aconitase

4.3.1. Biological cofactor.

Aconitase is a key enzyme in the Krebs (or citric acid) cycle of heterotrophic organisms. It is a hydrolytic isomerase responsible for the interconversion of citrate and isocitrate, which it achieves via the dehydrated intermediate aconitate (Scheme 1).

Generally, hydrolases act via Lewis acid catalysis, as inductive stabilization of transition states through coordination chemistry is sufficient to achieve most hydrolysis reactions. It is therefore curious that aconitase evolved to use an Fe_4S_4 heterocubane cluster motif—an active site usually associated with electron transfer reactions—for a redox-innocent Lewis acid catalyst. Unlike the HiPIP and Fdx systems, aconitase possesses only three ligating cysteine residues. The fourth iron center binds and activates the substrate water molecule used in the hydrolysis/hydration reactions, and aconitase, in its active form, does not change its oxidation state, remaining in the ferric/triferrous 1-Fe^{III}:3-Fe^{II} state throughout catalysis.

Nature's selection of this 3-Cys coordination environment has implications for the chemical behavior of the aconitase cofactor. While redox chemistry is not inherent in the operation of the enzyme, exposure to air results in oxidation of the cluster active site. In this inactive form, due to the lack of a 4th cysteine templating ligand, an iron ion is lost, giving the Fe_3S_4 "corner-voided cubane" cluster at the active site[277,296,297] (Fig. 27). This cluster is an all-Fe^{III} species based upon a single quadrupole doublet observed by Mössbauer spectroscopy consistent with an all-ferric system.[298] Reduction of this all-ferrous cluster by one electron using sodium dithionite gives a new Mössbauer spectrum nearly identical to that of the oxidized 3-Fe Fdx, indicating 2-Fe^{III}:1-Fe^{II} systems that are highly analogous. Both these systems exhibit two Mössbauer quadrupole doublets in a 1:2 ratio. However, the intensities of the two signals are opposite of that expected for a 1-Fe^{II}/2-Fe^{III} cluster. The low δ, low ΔE_Q doublet—corresponding to more oxidized iron—is half the intensity of the larger δ, larger ΔE_Q doublet corresponding to more reduced iron. This suggests again that simple whole-ion coupling models are not applicable, and that the more oxidized ferric iron is delocalized with one ferrous iron ion such that the 2:1 signal ratio represents an Fe^{III}/Fe^{II} pair and a single Fe^{III} respectively (Fig. 28).[278,299]

The EPR spectrum of the all-ferric oxidized aconitase exhibits a S = ½ EPR signal [276] (Fig. 29). The fact that an all-ferric Fe-S clus-

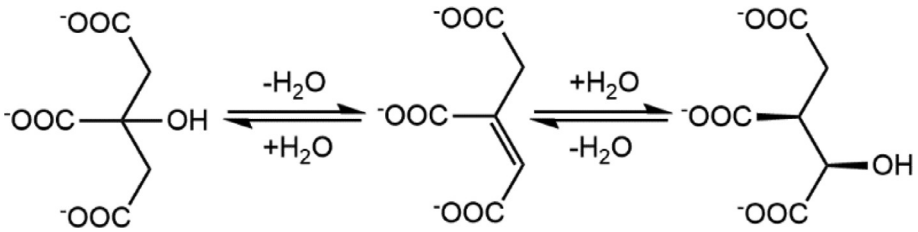

Scheme 1. Catalysis by aconitase: Reversible dehydration of citrate to aconitate, followed by reversible asymmetric hydration of aconitate to isocitrate.

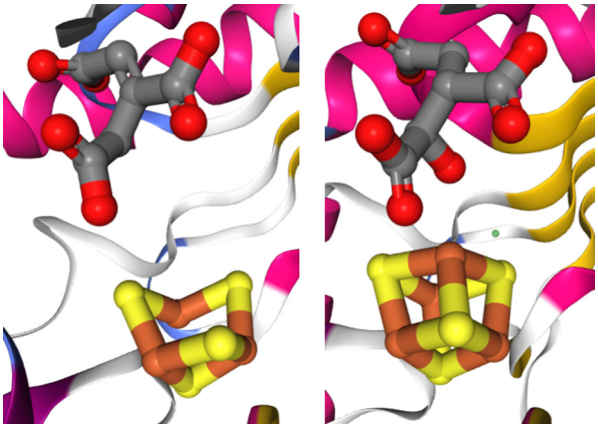

Fig. 27. X-ray crystal structures of aconitase crystalized with isocitrate. (Left) Inactive, oxidized form, showing the Fe_3S_4 voided cubane cluster (PDB: 1ACO).[300] (Right) Active, reduced form showing the catalytic Fe_4S_4 cluster (PDB: 1B0J).[301]

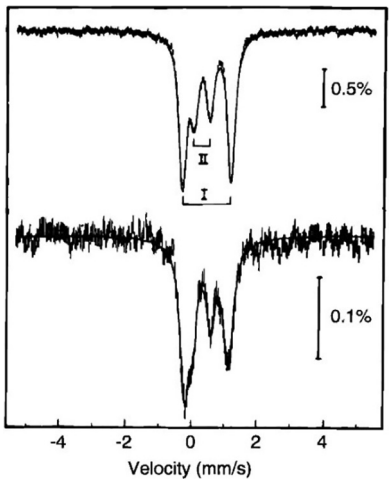

Fig. 28. Mössbauer spectra of the three-iron center of oxidized aconitase reduced by 1 e^- (bottom spectrum), compared to the 3-Fe bacterial Fdx (top spectrum) for comparison. Both spectra fit well to two doublets (I and II) in an integral ratio of 2:1 respectively, consistent with a Fe^{II}/Fe^{III} pair and another Fe^{III} center. Reproduced with permission of the American Chemical Society.[278,299]

ter could give rise to a S = ½ signal serves as another clear example of the failure of whole-ion ferro- or antiferromagnetic coupling models to describe electronic structure in cubane cluster systems. With a simple antiferromagnetic description for an all-ferrous Fe_3S_4 cluster, the smallest quantum spin that could be arrived at would be S = $^5/_2$. The experimental S = ½ spin illustrates that more complex coupling structures are frequently in place in Fe-S cubanes and may be relevant even when a more simplistic coupling model can explain the spin state. More sophisticated descriptions of magnetic coupling are informed by the Dahl bonding model (Section 2.1), which permits non-Hund electron configurations via Fe-Fe covalent interactions. Such a scenario will be further invoked in the section on nitrogenase, Section 3.7.

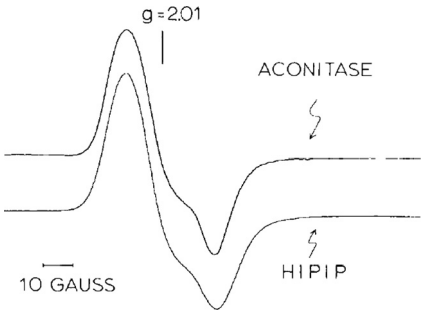

Fig. 29. EPR spectrum of fully oxidized S = ½ all-ferric $[Fe_3S_4]^+$ cluster in pig heart aconitase in comparison to the spectrum of oxidized S = ½ 3-Fe^{III}:1Fe^{II} $[Fe_4S_4]^{3+}$ cluster in $HiPIP^{ox}$, both exhibiting a rhombic S = ½ EPR signature.[276] Image reproduced with permission from the American Society for Biochemistry and Molecular Biology.

The inactive voided-cubane structure of aconitase may be reactivated by the addition of reducing agents and additional iron. The resulting reconstituted catalyst regains the 4th iron center and the substrate water-hydroxide ligand on the removable iron. Several Mössbauer and EPR studies have examined the reconstituted cluster using ^{57}Fe.[276,298,302] Unlike the isoelectronic Fdx^{ox} or $HiPIP^{red}$ clusters, which exhibit Fe^{II} and Fe^{III} centers in analogous all-sulfur ligation fields, the active site of aconitase exhibits different Mössbauer signatures for the apical iron than for the three cysteine-ligated iron atoms. This difference in behavior is partially explainable by the asymmetric coordination environment. The presence of a hard hydroxide (or carboxylate) donor at the apical iron results in a localized electronic structure that is different from the three iron ions with all soft sulfur donors. These differences may be observed in light of substrate binding, which causes drastic changes to the Mössbauer peaks corresponding to the ^{57}Fe axial iron even as the three remaining sulfide-ligated Fe centers are comparatively unperturbed.[302]

4.3.2. Synthetic model compounds

Along with the existence of 3-Fe ferredoxins in bacteria, [272,273,303–305] the Fe_3S_4 motif in aconitase resulted in synthetic modeling efforts for the Fe_3S_4 cluster.[7,306] This was achieved by a wide-bite tridentate hexakis(arylthio)benzenetri thiol, $L(SH)_3$ (Fig. 30). The resulting synthetic cluster, $[Fe_3S_4(LS_3)]^{3-}$ exhibits remarkable spectroscopic similarity to the protein based Fe_3S_4 centers. Fig. 31 shows the comparative Mössbauer and parallel mode EPR spectra of the 1-Fe^{II}:2-Fe^{III} clusters of one-electron reduced inactive aconitase and the synthetic model compound, illustrating that both possess 1:2 Mössbauer doublets with similar isomer shifts and quadrupole splitting, and similar EPR spectra

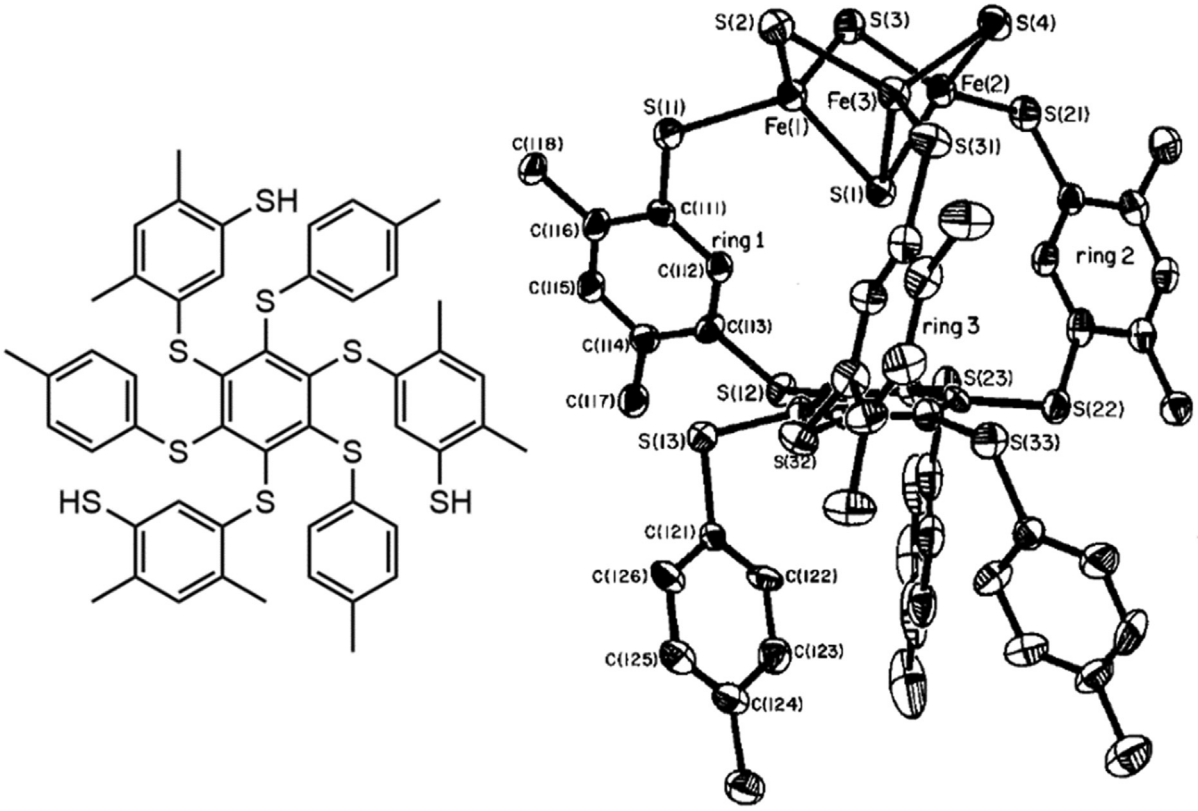

Fig. 30. Left: structure of hexakis(arylthio)benzenetrithiol ligand ($L(SH)_3$) template used in the preparation of stable Fe_3S_4 clusters. Right: X-ray crystal structure of $[Fe_3S_4LS_3]^{3-}$ cluster. Reproduced with permission from the American Chemical Society.[7]

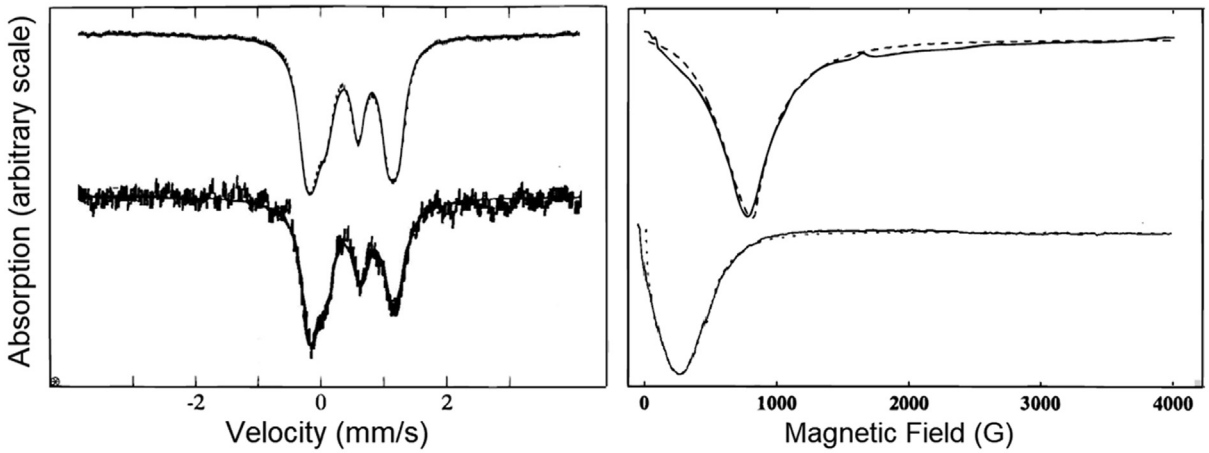

Fig. 31. Comparative spectra of synthetic $[Fe_3S_4LS_3]^{3-}$ cluster (top) and isoelectronic reduced $[Fe_3S_4(CysS)_3]^{3-}$ cluster of inactive aconitase. (Left) Mössbauer spectra[7,299] (figure reconstructed with permission from The American Chemical Society and The Federation of American Societies for Experimental Biology). (Right) Parallel mode X-band EPR spectroscopy[7,307] (figure reconstructed with permission from The American Chemical Society and Elsevier.)

assigned to an S = 2 quantum spin state for the reduced trinuclear cluster.

4.4. Radical SAM enzymes.

In addition to aconitase, the role of catalytic Fe_4S_4 clusters is now broadly recognized, as these clusters serve as redox cofactors (or components-thereof) for several catalytic metalloenzymes. These enzymes may feature direct connection of Fe_4S_4 clusters to the catalytic active site, or binding of the activated molecule directly at the Fe_4S_4 cluster catalyst. The radical S-adenosyl methionine (radical SAM) class of enzymes is an example of the latter.[308,309] Like aconitase, the Fe_4S_4 binding site has only three cysteine donors, with the fourth iron atom ligating to the SAM cofactor, and activating it for catalysis of one-electron processes. Correspondingly, this protein-unbound iron center is also dissociable under oxidizing conditions to form an all-ferric voided $[Fe_3S_4]^+$cubane analogous to that of aconitase,[310] which has

facilitated insertion of isotopically labeled ^{57}Fe into the active site for Mössbauer spectroscopic studies.[311] These studies, along with EPR[311,312], showed that adenosyl methionine (AdoMet) binds directly to this iron atom. This direct binding of AdoMet was also later supported by ^{2}H and ^{13}C isotopic labelling[313], electron-nuclear double resonance (ENDOR)[314] and by several solutions of the single-crystal X-ray crystallographic structure of the enzyme.[313,315,316]

The normal role of radical SAM enzymes is to facilitate mechanistically challenging, synthetically powerful, one-electron chemistry. The development of such one-electron chemistry by living systems has been essential to the evolution of complex life. The carbon cycle especially is dependent upon one-electron chemistry carried out through radical intermediates and processes. Adenosyl cobalamin (AdoCbl) is normally considered as the quintessential radical enzyme cofactor, and forms a transient adenosyl radical by the homolytic cleavage of an organometallic Co-C bond to form a cobalt(II) metalloradical and adenosyl radical (Ado·), the latter of which acts as a spatially confined reactive radical, giving controlled, one-electron transformations at the active site (Scheme 2).[281] However, radical SAM enzymes, being more recently discovered, yet more ancient than AdoCbl, can serve a similar purpose via the reductive cleavage of a weak S-C bond in adenosylmethionine (AdoMet) to form methionine and Ado· radical. This is achieved via an electron transfer from an iron-sulfur cubane cluster (Scheme 2).

As illustrated in Scheme 2, the mechanistic approach taken by radical SAM enzymes is the direct binding of the active cationic AdoMet cofactor to an iron center of a 3-Fe^{II}:1Fe^{III} $Fe_4S_4(SCys)_3$ cluster. The formation of the Ado· radical is achieved by an electron transfer from the cluster to the AdoMet cofactor, giving the 2-Fe^{II}:2Fe^{III} cluster, and effecting the homolytic cleavage of the C-S bond to give methionine and the neutral Ado· radical. Analogous to its role in AdoCbl, this radical can effect catalytic one-electron reactions on substrates bound in the nearby active site pocket before recombining with the metallocofactor. One of the most well characterized examples is pyruvate formate-lyase activating enzyme (PFL-AE), which uses a radical-SAM-based Ado· to activate the pyruvate formate-lyase enzyme by abstracting a hydrogen atom from a glycine residue, which forms a glycyl radical. This glycyl radical is used in turn for homolytic bond cleavage in pyruvate to form Acetyl CoA and formate.[317–319]

In addition to radical-based carbon chemistry, radical SAM enzymes also play a number of other roles, including sulfur insertion,[320,321] molybdopterin synthesis,[322–325] synthesis of CO and CN^- ligands in maturation of the hydrogenase cofactor (next section),[326–328] and in the insertion of the central carbide during maturation of the iron molybdenum cofactor of nitrogenase (see section 3.7).[329]

4.5. Fe-Fe hydrogenase

There are three known classes of hydrogenase enzymes, responsible for catalyzing the interconversion between protons and H_2: The mono-Fe hydrogenase (which does not feature a Fe_4S_4 cluster, but instead uses a methenyltetrahydromethanopterin as a redox cofactor), the Ni-Fe hydrogenase, which features a number of Fe_4S_4 clusters, including one nearby but unattached to the active site, and the Fe-Fe hydrogenase (Fig. 32), which features the direct connection of the cofactor to an electron reservoir.[330]

A distinguishing feature of the Fe-Fe and the Ni-Fe hydrogenases is the presence of strong field CO and CN^- ligands, which ligate the iron ions of the binuclear active sites. The presence of these ligands was viewed as somewhat surprising due to their high general toxicity to biological systems. The two iron atoms of Fe-Fe hydrogenase are bridged to one another via a dimethylaminedithiolate ligand. The identity of the amine nitrogen atom was positively identified relatively recently by the insertion of synthetic dimethylaminedithiolate to generate a fully active enzyme.[331] The iron binuclear cluster is tethered to a redox-active Fe_4S_4 cluster via a cysteine thiolate. While no model complex had been prepared containing all of these features, remarkably accurate models [332] tethering Fe-Fe binuclear complex models to redox active groups (like ferrocene, Fig. 33) have been achieved.[333,334] More

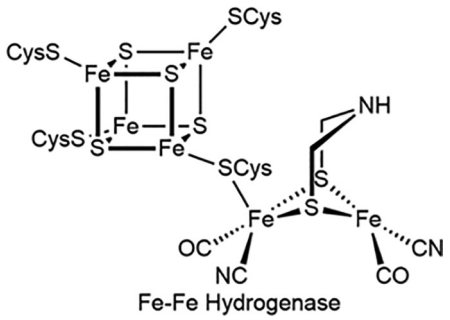

Fig. 32. Active site structure of the Fe-Fe hydrogenase.

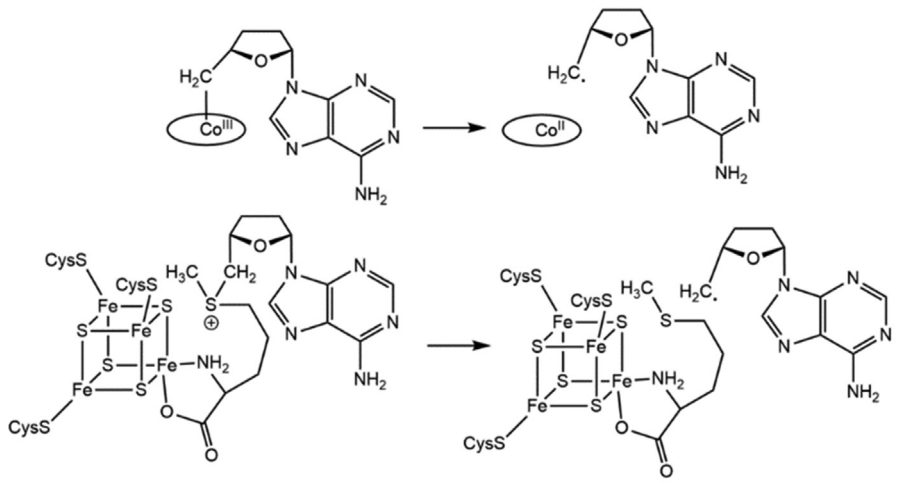

Scheme 2. Formation of Ado· radical from AdoCbl (top) by homolytic cleavage of the C-Co bond, and from AdoMet (bottom) by one electron reduction of the methionine ligand by electron transfer from the Fe_4S_4 cluster followed by homolytic cleavage of the S-C bond.

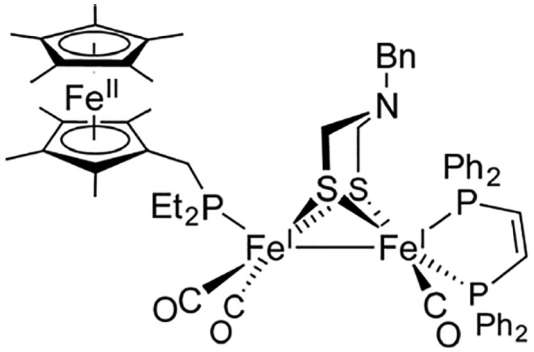

Fig. 33. Fe-Fe hydrogenase model compound from the laboratory of Rauchfuss, featuring CO ligation, a biologically realistic dithiodimethylamine, and a tethered redox-active ferrocene (instead of the Fe_4S_4 cluster). Figure reproduced with permission from the American Chemical Society.[332]

than just a structural model, this complex, along with many others in all hydrogenase classes,[332] catalyzes the redox interconversion of H^+ and H_2, making synthetic functional hydrogenase mimics one of the most successful subdisciplines of bioinorganic model complex chemistry.

4.6. CO dehydrogenase

CO dehydrogenase is a redox enzyme responsible for the biological reduction of carbon monoxide to CO_2 for energy production via the generation of reducing equivalents; formally:

$$CO + H_2O \rightarrow CO_2 + 2H^+ + 2\ e^-$$

In certain anaerobic bacteria, this process may be coupled to a hydrogenase to catalyze the formation of CO_2 and H_2, permitting organisms to metabolize CO as a source of metabolic energy.[335,336] It was later discovered that this enzyme class is central to the synthesis of acetyl coenzyme A (acetyl-CoA), and is thus sometimes termed Acetyl-CoA synthase when coupled to this enzyme.[337] As such, its role in the conversion of CO to acetate led to it, in one instance, being humorously referred to as "Nature's Monsanto acetic acid catalyst"[338] due to its role catalyzing the same reaction as the famous industrial process. The enzyme was long known to incorporate iron and nickel in its functional form. Several high-resolution crystal structures[339–342] revealed that there are two unique iron-sulfur cubane centers involved in catalysis: the A-cluster, and the C- cluster (Fig. 34), both involved in the catalytic mechanism.

The C-cluster is the initial site of binding and activation of carbon monoxide. Crystal structure solutions have indicated the Ni atom as the CO binding metal, with the adjacent Fe atom serving as a water binding site, leading to proposed mechanisms involving an activated nucleophilic hydroxide analogous to that in aconitase, but attacking the bound CO substrate and ultimately extruding CO_2 (Scheme 3).[343]

As the nickel site of the C cluster has been implicated as the active site, nickel substituted Fe-S cubanes have been the subject of some synthetic interest,[10] and particularly, the group of Holm has structurally characterized several model complexes where one iron site of the cubane cluster is substituted by Ni (Fig. 35).[344–348] The more recent examples[344,346] make use of the same hexakis(arylthio)benzenetrithiol ligated Fe_3S_4 cluster chemistry discussed previously in section 3.3.2 on voided cubane models of aconitase. The use of the stabilized 3-Fe voided cubane cluster simplifies the insertion of a heterometal into the cubane cluster. Model chemistry on the A-cluster has primarily focused on the nickel center, rather than on the cubane cluster.[338]

4.7. Nitrogenase

Nitrogenase is a bacterial enzyme responsible for the reduction of atmospheric nitrogen to ammonia, a reaction termed "nitrogen fixation." Despite the exothermicity of the overall reduction of nitrogen to ammonia by hydrogen, the large activation barrier to nitrogen fixation requires large levels of energy consumption, as evidenced by the hydrolysis of at least 16 equivalents of ATP per nitrogen molecule, and the "waste" of two reducing equivalents by the compulsory evolution of one molecule of hydrogen, according to the limiting stoichiometry (under optimal conditions):

$$N_2 + 8H^+ + 8\ e^- + 16\ ATP \rightarrow 2\ NH_3 + H_2 + 16\ ADP + 16P_i (P_i = \text{inorganic phosphate})$$

Molybdenum nitrogenases—the most efficient nitrogenase enzymes—possess two protein components: the Fe-protein, which contains an iron-based active site, and the MoFe protein, which possesses both iron and molybdenum atoms. Variants of the latter protein exist that use vanadium instead of molybdenum, and there are also variants with only iron that were identified.[349–353] These alternative versions of the enzyme are normally expressed under stressed conditions of limiting molybdenum. A recent surge of informative biological and model complex studies have improved our understanding rapidly in the past decade, including an explanation for the obligatory evolution of an equivalent of H_2. While these studies are not enumerated here, the reader is referred to recent work from Hoffman and Seefeldt on the biological system [284,285,354] and reactive (non-cubane) model complexes from Peters and Holland [355–360].

The set of unique Fe-S cubane cluster motifs in biology expanded when the original crystal structure of the Mo-Fe was solved in 1992.[361,362] This original crystal structure depicted the catalytic active site of the molybdenum iron (MoFe) protein (termed the iron-molybdenum cofactor or FeMoco), as a pair of voided cubanes—Fe_4S_3 and $MoFe_3S_3$—bridged at the corners by three μ_2-sulfide ligands (i.e., Fig. 36, bottom, *minus* the central carbide atom). In 2002, Rees and coworkers discovered the previously

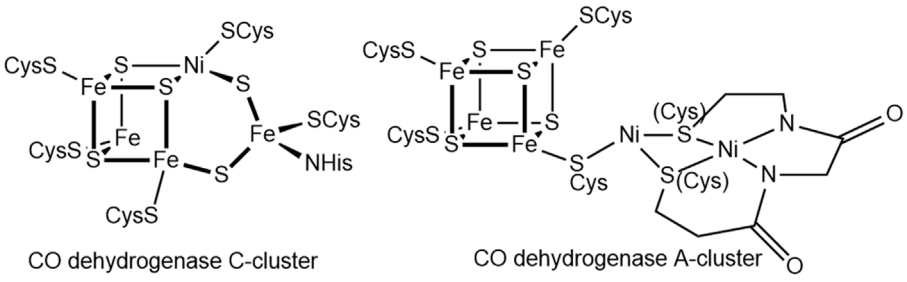

Fig. 34. Lewis structures of the C and A clusters of CODH.

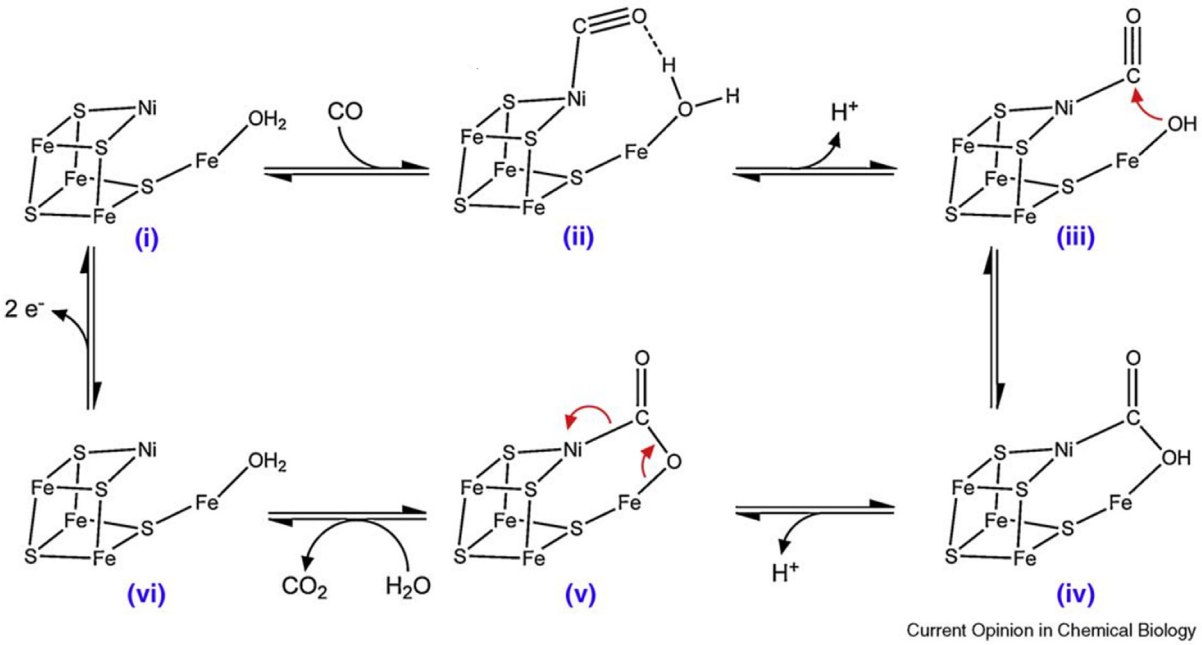

Scheme 3. Proposed catalytic mechanism for CO oxidation based upon protein X-ray crystallographic structures. Adapted with permission from Elsevier.[343]

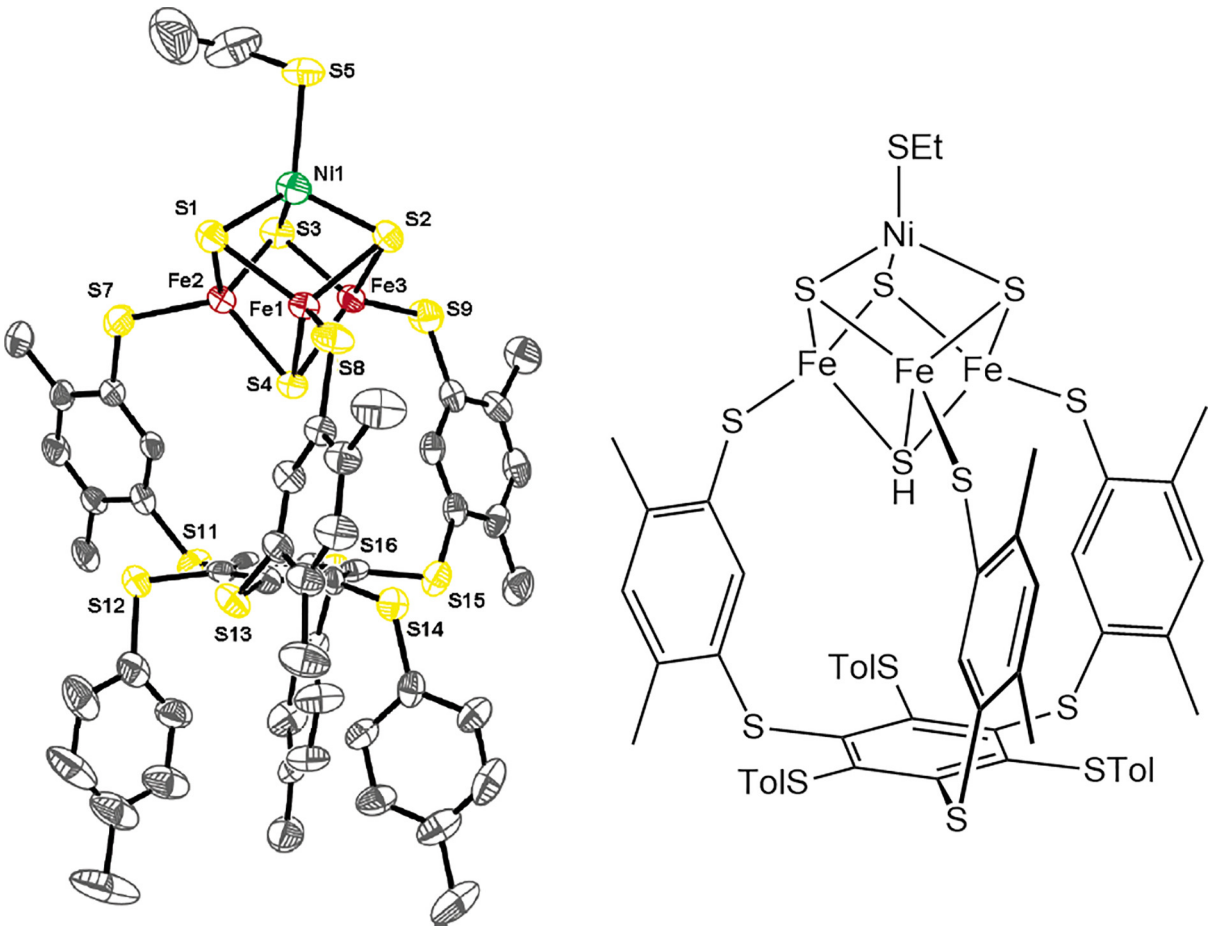

Fig. 35. Thermal ellipsoid plot and Lewis structure of Fe_3NiS_4 cubane cluster. Ellipsoids set at 50% probability level. Hydrogen atoms omitted for clarity. Reproduced with permission from the American Chemical Society.[346]

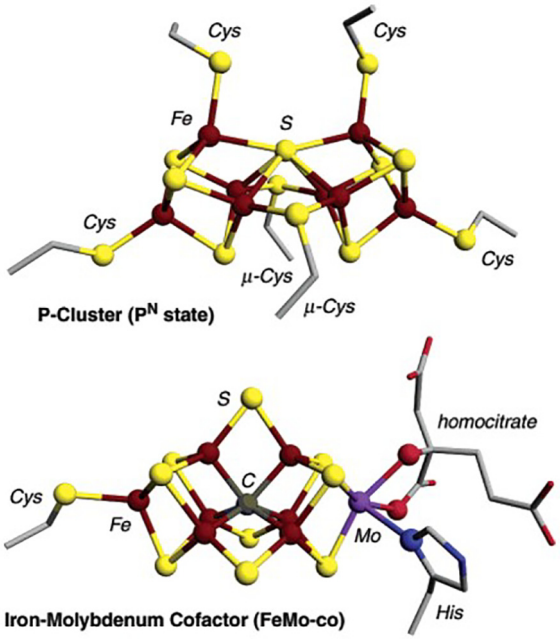

Fig. 36. The cofactors of the nitrogenase MoFe protein, adapted with permission from the American Chemical Society.[6] Top: the P-cluster (P^N state). Bottom: the iron molybdenum cofactor (FeMoco).

unnoticed light atom in the center of FeMoco of the molybdenum-dependent nitrogenase enzyme system, which had been invisible in the lower-resolution structures due its low electron density being obscured by Fourier series termination effects (i.e., Fourier "ripples") of the surrounding heavy atoms.[363] This central atom was originally presumed to be a substrate-derived N, leading to much discussion of the possibility, but was ultimately identified as carbide,[361,364,365] a unique ligand in biology. Recent crystallographic studies have revealed that the vanadium nitrogenase possesses an analogous cofactor, FeVco, with analogous geometry but for the replacement of Mo by V, and a μ_2-sulfide replaced by a carbonate anion.[366]

FeMoco is well established to be the binding and activation site of N_2. In addition to its native substrate, FeMoco can bind and activate isolobal substrates such as CO, CN, and acetylene. The structure of nitrogenase with bound CO shows that this substrate replaces an equatorial μ_2-sulfide ligand,[367] suggesting that this might be the binding site for N_2. Another recent crystal structure of nitrogenase at 1.83 Å described a bound N_2 substrate also at the μ_2-binding site,[368] though a recent report calls this result into question,[369] suggesting that the elongated electron density peak is better described by an anisotropically vibrating sulfide ligand.

A second unique corner-fused dicubane Fe-S cluster, the P-cluster (Fig. 36, top), was also uncovered by these crystallographic studies. This cluster acts as an intermediary in the electron transfer to FeMoco from the obligatory reductase of nitrogenase, the Fe protein. This soluble Fe protein contains a simple Fe_4S_4 cubane cluster, as well as an ATP-binding and hydrolysis active site.[370–372] Curiously, this Fe_4S_4 cubane uses a unique redox pair: the fully-reduced, all-ferrous cubane cluster ($[Fe_4S_4]^0$),[373,374] and its one electron oxidized analogue ($[Fe_4S_4]^+$), which has been modeled using synthetic compounds[76,293]. While the CN-ligated synthetic model cluster[76] shows a single Mössbauer quadrupole doublet, dissimilar from the biological spectrum, the carbene-terminated model[293] has spectroscopic features that match very well to the biological cluster, which has also been crystallographically characterized.[374] This lower-oxidation-state iron-sulfur protein has evolved commensurate with the low potentials and large energy requirement for nitrogen activation, and suggests that the MoFe protein has to be stocked with high-energy, reducing electrons via the use of both ATP hydrolysis and a very low-reduction-potential iron protein.

The nitrogenase enzyme is central to life on earth as we know it since reduced nitrogen is not geologically available in significant amounts. Thus, living systems (including both nitrogen fixing bacteria, and humans: via the industrial Haber-Bosch process) are almost exclusively responsible for reactions requiring the reductive cleavage of one of the strongest bonds in nature, the N-N triple bond, and ultimately forming ammonia for biosynthesis of nitrogen-containing biomolecules.

4.7.1. The Fe-S clusters of nitrogenase

FeMoco is the N_2 activation site and is a Mo-Fe-S cluster, previously thought to have an empty central cavity[361,362] until the discovery of the central light atom, "X."[363] This light atom, which has been positively identified as carbon,[361,364,365] redefined the geometry of FeMoco to that of a corner-fused dicubane cluster, joined at a central carbide (Fig. 36). In recent years, extensive details on the biosynthesis of FeMoco by the Nif proteins has emerged.[329] Fig. 37 describes the remarkable insertion of the carbide ligand during FeMoco maturation using an Fe-S cubane-dependent radical SAM enzyme (see section 3.4.3).

A second unique biological metallocluster, the P-cluster, exhibits a geometrically related corner-fused dicubane structure, but with a corner bridge at a sulfide ion rather than a carbide, and with two equatorial bridging cysteine ligands instead of FeMoco's three equatorial sulfides (Fig. 36). Crystallographic studies of the P-cluster of molybdenum-dependent nitrogenases demonstrate a redox-dependent geometric structure.[375] In the oxidized P-cluster, the corner-bridging sulfide associates more strongly with one end of the cluster, and two iron on the opposite side dissociate from the central sulfide, and are ligated instead by a serine oxide and an amide nitrogen of cysteine (Fig. 38). These structures have been modelled in synthetic clusters with some success but will not be discussed extensively in this review. The model compounds of Holm, Lenhert, and Tatsumi are worthy of note.[376–380] (Fig. 39).

Finally, the second protein component of nitrogenases, the Fe-protein, possesses a single Fe_4S_4 cubane cluster and is the sole reductase capable of passing reducing equivalents from an all-ferrous Fe_4S_4 cubane cluster to the catalytic active center. The Fe protein is the sole reductant for the MoFe protein due to the requirement for transferring electrons from significant distance (10 Å) to the FeMoco in the interior of the protein, which proceeds via the P-cluster. It has been established relatively recently that electron transfer precedes ATP hydrolysis, suggesting a tightly bound aggregate between the MoFe and the Fe proteins brings the Fe_4S_4 cluster into near proximity to the P-cluster to facilitate a single electron transfer, followed by hydrolysis of two ATP to mechanically dissociate the tightly bound Fe protein.[382] The transfer of 8 electrons to generate 2 NH_3 and H_2 therefore requires the hydrolysis of a minimum of 16 ATP in order for the enzyme to turn over. This energetically costly mechanism has most likely evolved to keep the highly reduced FeMoco at a large distance from the protein exterior to facilitate the storage of multiple high-energy reducing equivalents at a distance great enough to kinetically prevent back-electron-transfer.

Although the FeMoco cluster seems to exhibit a near threefold symmetry based on cluster geometry, data suggests electronic asymmetry and a complex electronic structure for a number of reasons, most simply, due to local polarity of the surrounding protein, which may influence localized electronic structure in the iron atoms.[356] Further, FeMoco has long been characterized by its

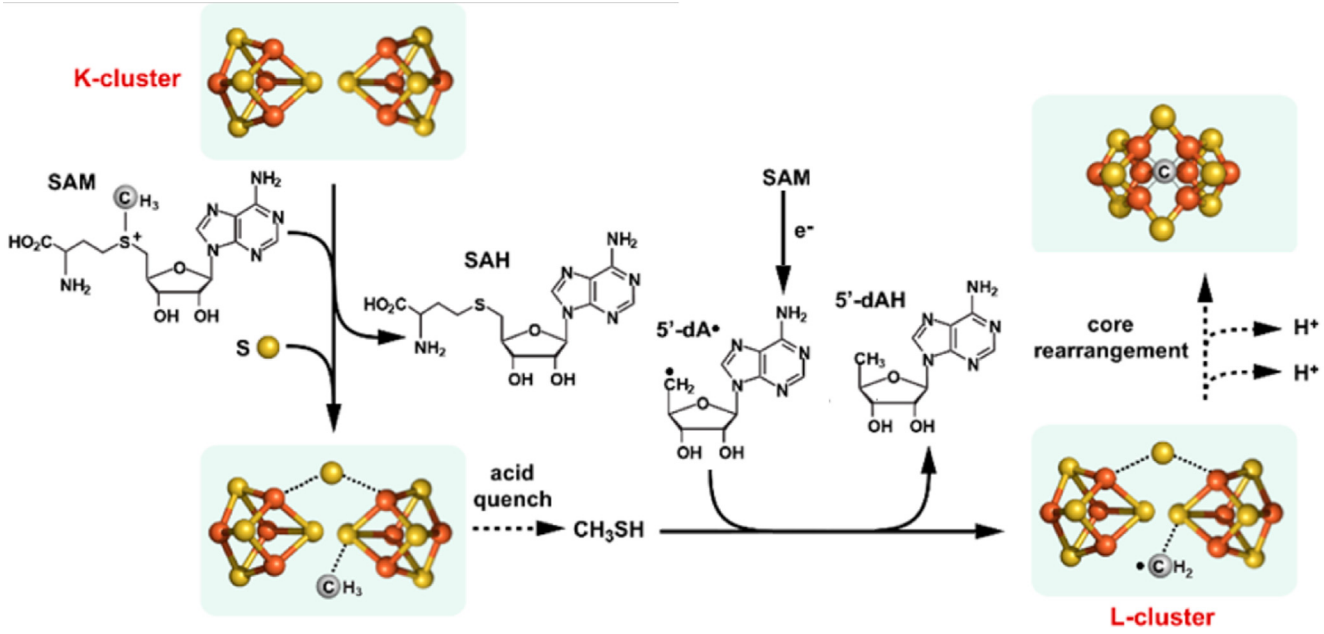

Fig. 37. Proposed mechanism of maturation of FeMoco, including carbide insertion using radical SAM. Figure adapted with permission from the American Chemical Society. [329]

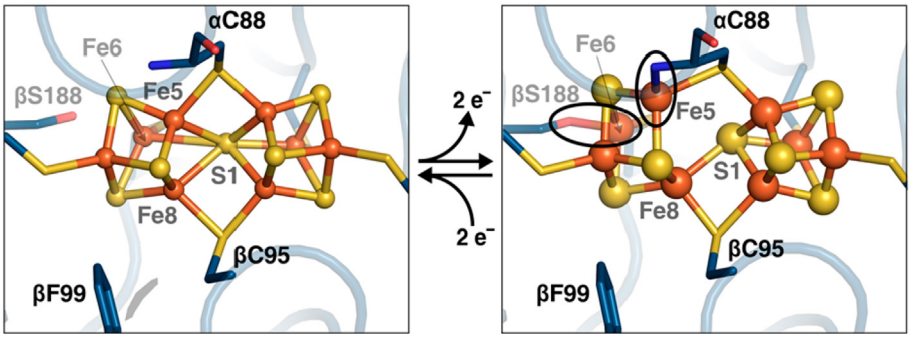

Fig. 38. Structures of the active (N-form) and oxidized forms P-cluster of molybdenum dependent nitrogenase. Circles denote formation of new bonds. Reproduced with permission from the American Chemical Society. [381]

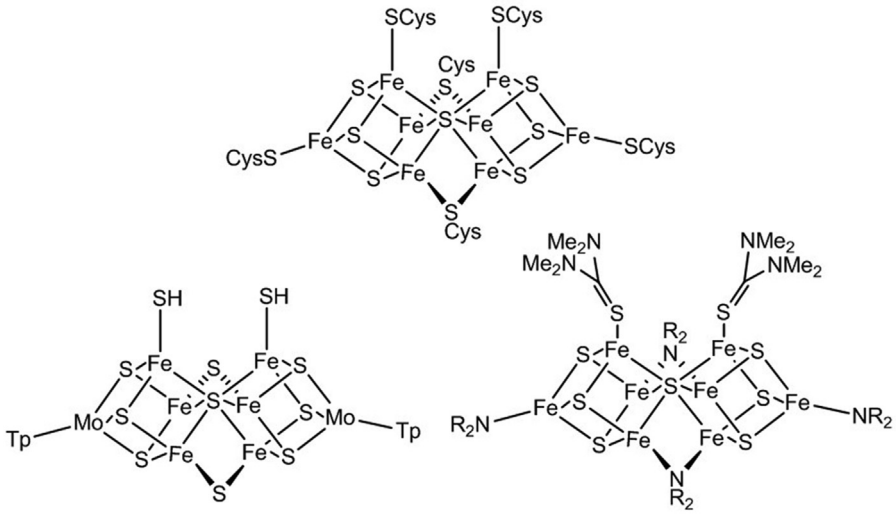

Fig. 39. Top: Structure of the P^N state of the nitrogenase P-cluster. Bottom: Synthetic models from Holm (left)[379,380] and Tatsumi (right).[376] Tp = trispyrazolylborate, R = trimethylsilyl.

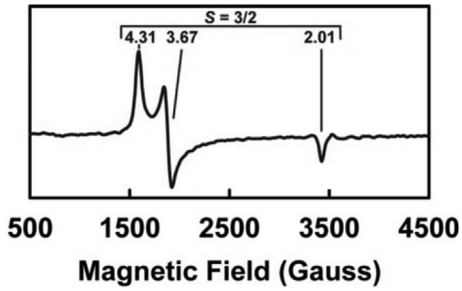

Fig. 40. S = 3/2 EPR signature from the resting state (E_0) of FeMoco. Reconstructed with permission from the National Academy of Science of the USA.[383]

distinctive S = 3/2 EPR signature in its resting state (Fig. 40), which serves as a linchpin for all other electronic structure considerations, and for all debate on FeMoco's electronic structure. Traditionally, (before the discovery of the central carbide) three oxidation state assignments were predominantly considered, each differing from its neighbors by exactly 2 e^- to preserve the odd *d*-electron count required for the S = 3/2 EPR signal: (1) 6-Fe^{II}:Fe^{III}:Mo^{IV}, (2) 4-Fe^{II}:3-Fe^{III}:Mo^{IV}, and (3) 2-Fe^{II}:5-Fe^{III}:Mo^{IV}. The experimental S = 3/2 state can (in *principle*) be explained with a simple antiferromagnetic coupling model. Taking for example, electron configuration (1), above, an antiferromagnetic model where four aligned high-spin Fe^{II} ions are antiferromagnetically coupled to two Fe^{II} and one Fe^{III} ion, this coupling description would result in an overall ground spin state of 3/2.

Yet, none of these descriptions of three-coordinate iron with these oxidation states are consistent with the Mössbauer spectra. [384,385] Further, it is worthwhile to note that in Fe-S cluster systems in general, while simple antiferromagnetic coupling models frequently can explain the ground spin state, more complicated electronic structure and magnetic coupling schemes are frequently extant, resulting in descriptions of coupling involving both ferro- and anti-ferromagnetic interactions between Hund or non-Hund metal ions, via M-M orbital interactions.[276,288]

The identification of a central carbide ligand[361,364,365] redefined the active site picture to that of a corner-bridged dicubane cluster of tetrahedral iron: unique in biology, but more akin to traditional cubane topologies than the previous empty-cavity proposal. This discovery of the central carbide, along with crucial roles played by spectroscopy and model complex chemistry led to reconsideration of previous electronic structure arguments, and a rapid resolution of several outstanding questions surrounding the electronic structure of FeMoco, which are discussed in the next section.

4.7.2. Electronic structure of FeMoco from spectroscopy, theory, and model chemistry.

Almost all of the traditional assignments of the metal ion oxidation states in FeMoco rigorously restricted the oxidation state of molybdenum to the IV state. Namely: (1) 6-Fe^{II}:Fe^{III}:Mo^{IV}, (2) 4-Fe^{II}:3-Fe^{III}:Mo^{IV}, and (3) 2-Fe^{II}:5-Fe^{III}:Mo^{IV}. As pointed out in a recent article, [402] the origin of these assignments appears to be more historical than strictly scientific, with the genesis of this assumption being from a number of early XAS and ^{95}Mo ENDOR studies that predated the first crystal structure, and which indicated a possibility of either Mo^{IV} *or* Mo^{III}, but with a *slight* interpretational preference for Mo^{IV} albeit without conclusive demonstration.[386–390] This appeared to build into a historical, but experimentally unverified consensus[391] that resulted in a lack of consideration of the possible role of an odd-spin Mo^{III} ion contributing to the spin description.

Over the same time period, immense success was achieved in the synthesis of Mo-Fe-S models by the groups of Holm, Garner, and Coucouvanis, which successfully introduced single molybdenum atoms into the corners of heterometallic cubanes (Fig. 41). [225,392–398] In direct contrast to the consistent assignment of a Mo^{IV} oxidation state in FeMoco, experimental investigation of the oxidation states of the model complex cubanes, *almost always* assign a Mo^{III} oxidation state based on the assignment of iron oxidation states using Mössbauer, and deduction of Mo oxidation state by charge balance. Further, redox reactions at these mixed Mo-Fe model complexes are normally iron-based,[1,391] and thus leave the oxidation state of Mo^{III} ion undisturbed. As such, model chemistry has always given every indication that Mo, in a weak-field Fe-S cubane framework, is most stable as Mo^{III}, even as the biophysical community rigorously held to a Mo^{IV} description.

Quantum chemical calculations on multi-metal clusters of magnetically coupled ions are necessarily challenging and complicated. Nevertheless, early computations on the electronic structure of FeMoco were performed in 1985 by Cook and Karplus,[400,401] and also indicated a probable Mo^{III} oxidation state. Further, in contrast to the expected S = 3/2 d^3 Mo^{III} ion, these broken-symmetry calculations predicted that the lowest energy description placed a non-Hund quantum spin of S = ½ at the molybdenum ion (↑↑↓), evidentiary of possible orbital–orbital covalent interactions between molybdenum and proximal iron atoms. Indeed, the Mo-Fe distance of 2.67 Å to the nearest iron atom[363] is well within the range at which one might expect electron pairing through a covalent Mo-Fe interaction.

Modern spectroscopic approaches combined with theoretical techniques and model complex chemistry have recently given new insights into the electronic structure of FeMoco.[402] In contrast to traditional X-ray absorption spectroscopy (XAS), which was unable to distinguish clearly between Mo(III) and Mo(IV), [386,390] high-energy resolution fluorescence detected X-ray absorption spectroscopy (HERFD-XAS), instead of traditional measurement of absorption, uses wavelength-sensitive detection of fluoresced X-rays as the absorption edge is scanned in order to improve the resolution of pre-edge features. This allows more precise theoretical fitting[403] of the absorption edge features to their respective electronic transitions, permitting electronic structure elucidation and oxidation state assignment. Using this approach, FeMoco was compared to Mo-Fe-S model complexes, with experimentally established Mo^{III} oxidation states, and with an analogous half-FeMoco structure,[6,404] as well as to Mo^{V} model complexes [405] for comparison. The pre-edge features of FeMoco (Fig. 42) match remarkably well to the Mo^{III} model compounds, and are not consistent with higher oxidation states of IV or V.[402]

While the experimental spectra (Fig. 42, top) are sufficiently compelling to argue a Mo(III) assignment, the use of quantum calculation permits an explanation of the spectroscopic features and the assignment of a more specific electronic structure. Simulation of the XAS spectra was best achieved by broken symmetry time-dependent density functional theoretical (TD-DFT) calculations that permit examination of the energies of unusual (non-Hund) spin descriptions.[402] These calculations uncovered that the lowest energy electronic description is that of a S = 3/2 cluster consistent with EPR measurements,[383] and with metal oxidation states of Mo^{III}–$Fe_2^{III}Fe^{II}$ for the Fe_3Mo half of the cluster. This description provides a good match to the Mössbauer parameters of nitrogenase[384,385] assuming a delocalized Fe^{II}/Fe^{III} pair common in Fe-S cubane clusters.[288] Most curiously, this electronic description with a non-hund d^3 configuration for the Mo(III) ion (↓↓↑) (Fig. 43) is analogous to that calculated by the broken symmetry approach of Cook and Karplus.[401] Importantly, the energy of electronic transitions predicted by TD-DFT for this model match well to the experimental HERFD-XAS spectra (Fig. 42, bottom).

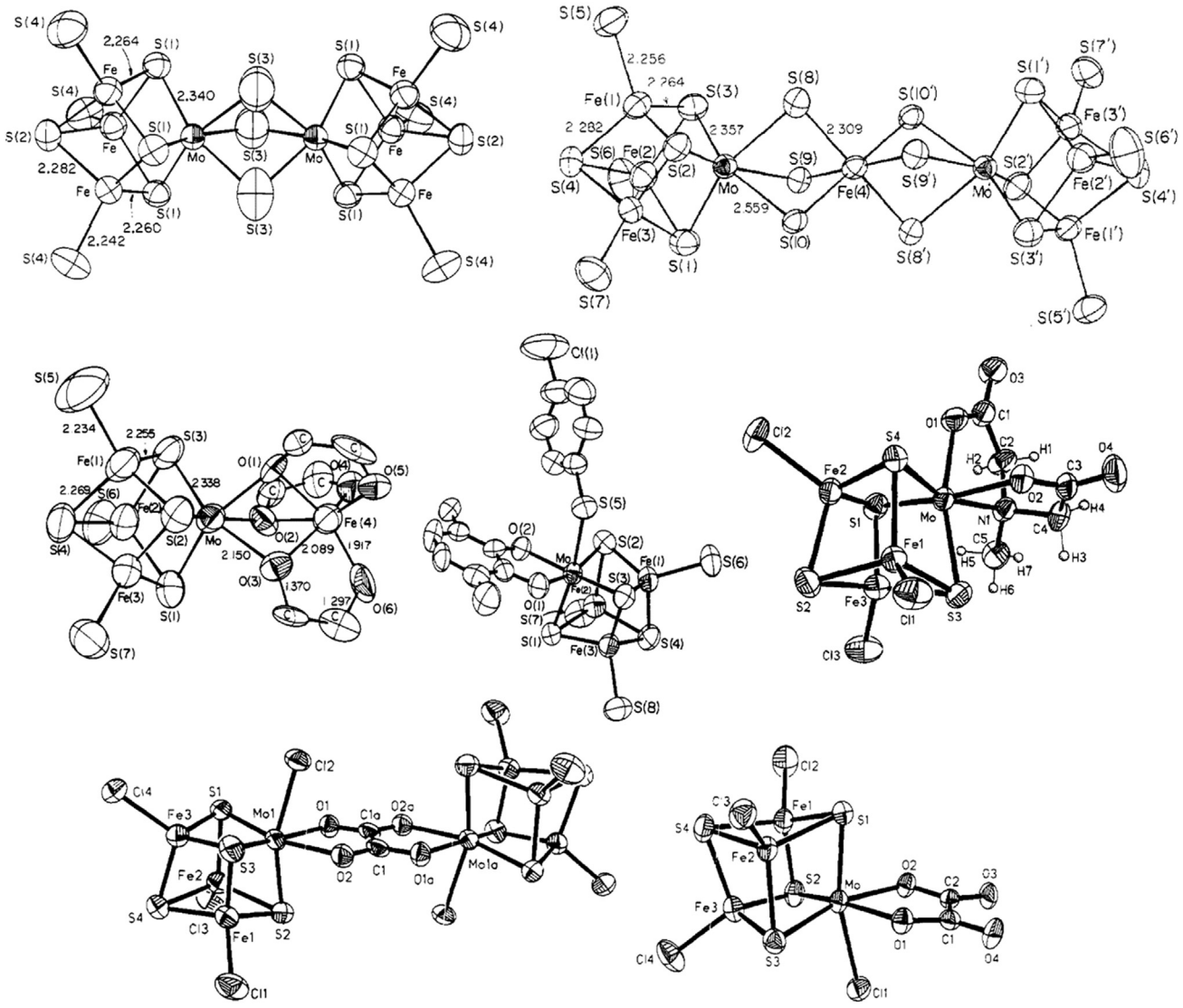

Fig. 41. X-ray crystallographic structures of selected Mo-Fe heterometallic heterocubane and dicubane clusters from the groups of Holm and Coucouvanis. [225,392,393,396,398,399]. From top, left–right: $[Mo_2Fe_6S_9(SEt)_8]^{3-}$, $[Mo_2Fe_7, S_8(SEt)_{12}]^{3-}$, $[MoFe_3S_4(SC_6H_4Cl)_4(Pr_2cat)]^{3-}$, $[MoFe_3S_4(S\text{-}p\text{-}C_6H_4Cl)_4((C_3H_5)_2cat)]^{3-}$, $[(MoFe_3S_4Cl_3)(mida)]^{2-}$, $[(MoFe_3S_4Cl_4)_2(\mu\text{-}C_2O_4)]^{4-}$, $[(MoFe_3S_4Cl_4)(C_2C)_4)]^{3-}$. Some organic R groups and some hydrogen atoms omitted for clarity. (cat = catecholate, mida = methyliminodiacetate).

The combination of similarity to model complexes, explanation of the Mössbauer, EPR, and XAS spectra, and its identity as the lowest-calculated-energy description by two independent groups [401,402] gives this assignment increased confidence and resolves longstanding ambiguity about the electronic structure of FeMoco. While these non-Hund descriptions of the molybdenum atom have been met with some surprise, these should not be viewed as improbable or even unusual. Such pairing of electron density across metal orbitals has been known since the earliest work in cyclopentadienyl-terminated cubane systems pioneered by Dahl (Section 2.1), and electron pairing in individual orbitals across clusters was described before the discovery of biological Fe-S clusters. Low-spin electronic configurations in voided cubane clusters of 3-Fe ferredoxins (Section 3.2), aconitase (Section 3.3), and radical SAM enzymes (Section 3.4) are explicable only by such non-Hund descriptions of electronic structure, involving coupling between specific electrons/orbitals, rather than via the simpler descriptions of antiferromagnetic coupling between whole ions that are more frequently invoked due to their (over)simplicity.

4.7.3. Synthetic whole-cluster models of FeMoco

Despite the spectroscopic insights gleaned from Mo-Fe-S cubane model complex chemistry, no atomically accurate model complex has been synthesized to date. We briefly detail reports of synthetic clusters with close compositional and geometrical analogy to the OEC to review progress in this area, and the current state of the field.

Prior to the discovery of the central light atom, the target cluster was believed to be an M_8X_9 cluster comprising two S-bridged voided cubane clusters with an empty central cavity (i.e., without the central μ_6 ligand in Fig. 36). Link and Fenske prepared the first example of such a cluster, a cobalt-imido cluster with formula $Co_8(NPh)_9(PPh_3)_2$, Fig. 44).[211] Five years later, a mixed Mo/Cu cluster, with the Mo atom occupying the ends of the cluster, and the six Cu ions occupying the belt atom positions, was reported by the group of Du (Fig. 45) [406]. This structure also featured a hollow cavity, plus bio-relevant bridging sulfide ligands, and molybdenum at the end cubane site. In the solid state, this cluster formed a dimer where one of the belt copper atoms was weakly

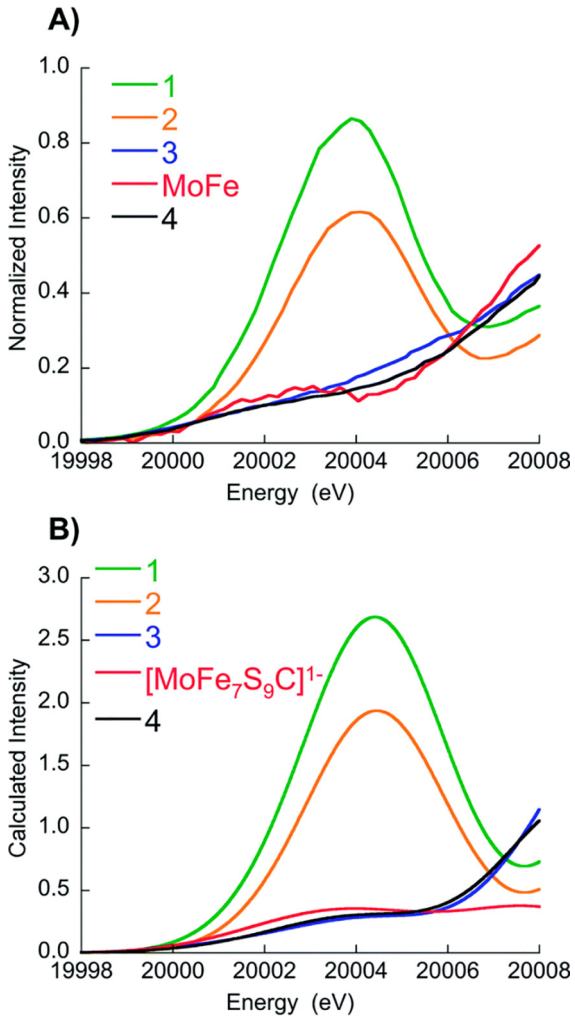

Fig. 42. HERFD-XAS spectra of FeMoco and Mo(V)-based (**1**, and **2**) and Mo(III)-based (**3**, **4**) model compounds.[402] A) Experimental spectrum. B) Theoretical spectra calculated from time-dependent DFT, and assuming a Mo(III) oxidation state assignment for FeMoco. Reproduced with permission from the Royal Society of Chemistry.

ligated by the molybdenum-capping terminal oxo ligand. Despite their relevance to the geometry of FeMoco, these reports did not call attention to the structural analogy (Fig. 45.).

Returning to models with a central atom, Tatsumi has prepared structural analogues with bridging μ_2-thiolate ligands, and a central μ_6-sulfide (instead of carbon), shown in Fig. 46.[407,409] While these represent topological analogues of FeMoco, the central bridging sulfide relates more to the P-cluster, which possesses a similar central sulfide, but with only two μ_2-bridging ligands connecting the two cubane halves.

Upon discovery of the light central atom, efforts have been underway in a number of groups to prepare analogs with central light atoms (C, N, O). Prior to the identification of the light atom as carbon, Tatsumi's group succeeded in the insertion of an oxo ligand into the center of a FeMoco-like cluster of two Fe_4S_3 cubane halves, bridged by two thiolates and one alkoxide ligand, and with an oxide inserted into the central void.[407] However, in this environment, the oxide did not arrange into the μ_6 bridging mode observed in the enzyme structure, but rather, associated more strongly with the three belt irons of one side of the cluster, and only one belt atom on the other side, breaking the symmetry of the cluster, and presenting an asymmetric μ_4 oxo (Fig. 47). Oxygen's preference for lower (four) coordination in this environment was suggestive that oxygen was not a probable assignment for the μ_6 light atom of FeMoco.

One of us reported the only other example of a cluster with related topology (to our knowledge) and which also contains a central light atom: nitride. The $Li_3Mn_5(\mu_6\text{-}N)(\mu_3\text{-}N^tBu)_6(\mu\text{-}N^tBu)_3(N^tBu)(N)$ cluster of Vaddypally et al (Fig. 48) possesses a structure analogous to FeMoco, but lacks biorelevant sulfide ligation, and features Lewis acidic $Mn^{IV/V}$ and Li^+ ions, dissimilar from the soft, low-valent, weak-field coordination environment in FeMoco.[173] One of the most substantial new contributions to synthetic model complexes of FeMoco is the N_2-bridged clusters of Suess, which features as a parent compound two Fe_3MoS_4 clusters bridged by dinitrogen, and several variants thereof. The approach involves the use of sterically encumbered isopropyl-substituted terminal carbene ligands terminating the iron centers, and pentamethylcyclopentadienyl ligands terminating molybdenum. The sterically protected pocket on the end of each cluster admits N_2 for binding when no alternative small ligands exists in solution. [408] $[CpMoFe_3S_4(IPr)_3]_2(N_2)$ is illustrated in Fig. 49 (IPr = 1,3-bis(2,6-diisopropylphenyl)imidazol-2-ylidene).

4.7.4. Synthetic inclusion of central light atoms in models of FeMoco

Exquisitely controlled kinetic conditions will be required to synthetically coordinate a weak-field Fe-S cluster with a strongly-donating, Lewis basic μ_6 carbide ligand. To date the synthesis of a carbide-coordinated weak-field iron cluster has not been achieved, much less a FeMoco structural analog. This difficulty of insertion of interstitial carbide ligands makes this reaction one of the most pursued aspects of synthetic biological cluster modelling.

Nitrogen has long been presumed to incorporate into FeMoco upon substrate activation, leading to a general interest in iron–nitrogen cluster chemistry. But upon the discovery of the light atom in nitrogenase in 2002, many initially favored the hypothesis that

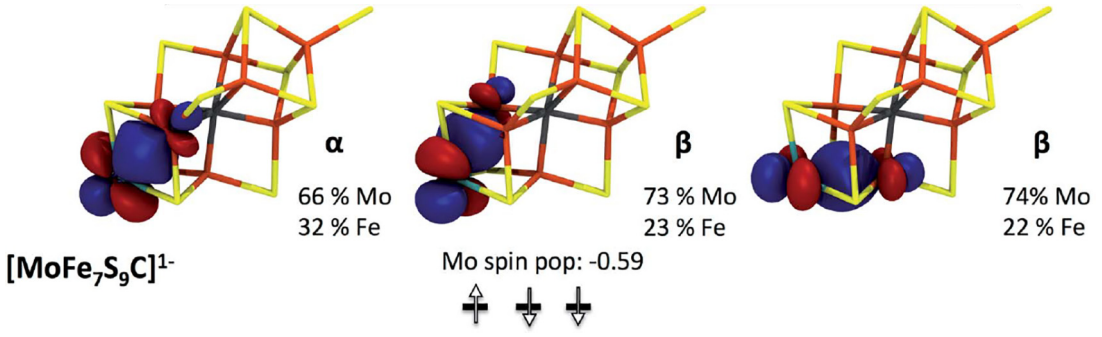

Fig. 43. Isosurfaces of molybdenum-based t_{2g} orbitals bonding with iron orbitals in resting state FeMoco. Orbital interaction with distinct Fe atoms results in a non-Hund electronic spin description rather than a simpler whole-ion coupling model. Reproduced with permission from the Royal Society of Chemistry[402]

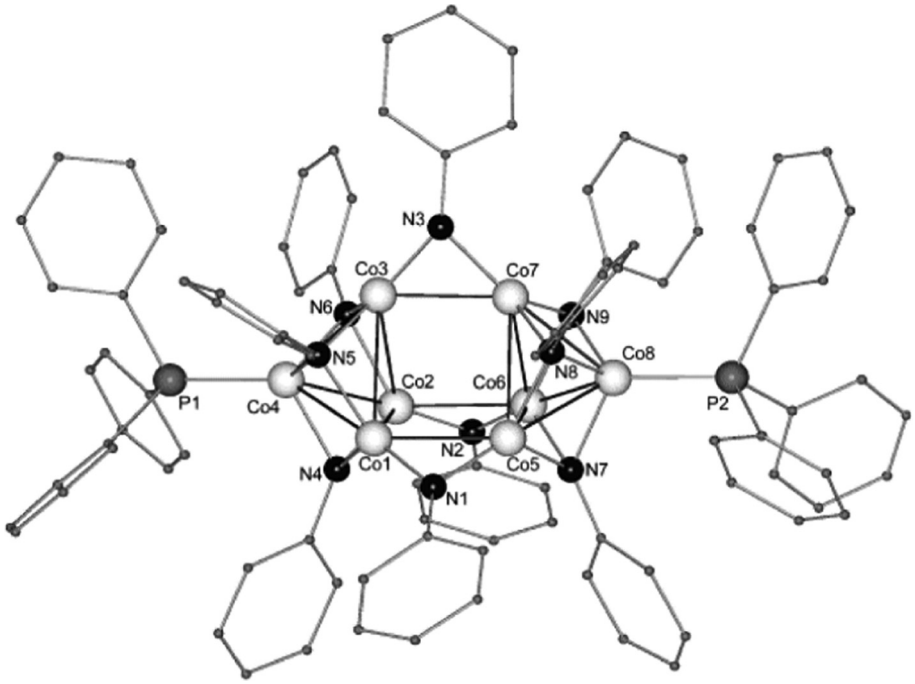

Fig. 44. Ball and Stick model of the X-ray crystallographic structure of the $Co_8(\mu_3\text{-}NPh)_6(\mu\text{-}NPh)_3(PPh_3)_2$ cluster of Link and Fenske, showing topological analogy to FeMoco minus the central light atom. Reproduced with permission from Wiley.[211]

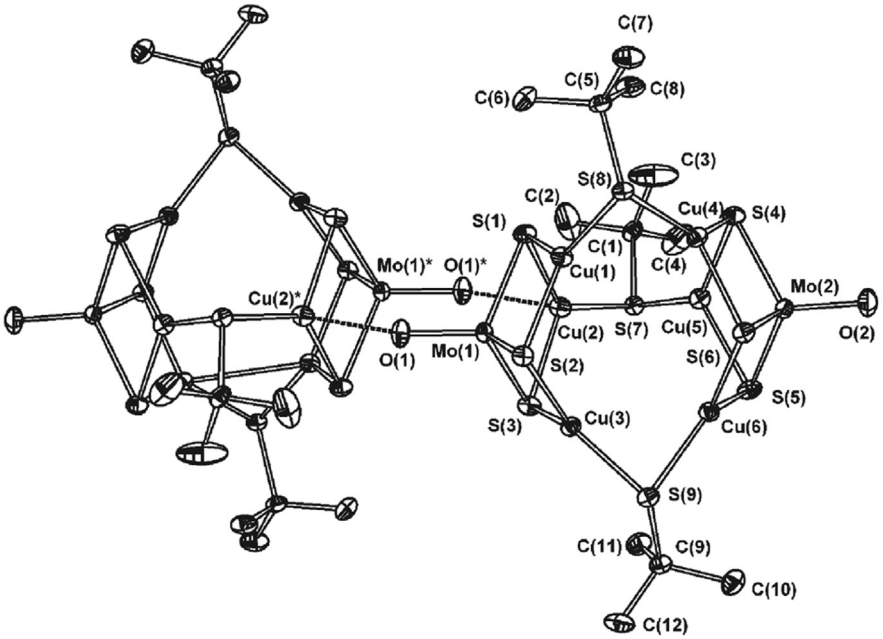

Fig. 45. X-ray crystallographic structure of the $Mo_2Cu_6(\mu_3\text{-}S)_6(\mu\text{-}S^tBu)_3(O)_2$ cluster of Li et al, showing topological analogy to FeMoco minus the central light atom. Reproduced with permission from the Royal Society for Chemistry.[406]

the central atom could be a substrate-derived nitride.[363,410–413] While nitride ligands had been known in iron carbonyl cluster chemistry for decades, these ligation environments are not biologically relevant, and this led to an intensified hunt for novel weak field iron–nitrogen (especially nitride) clusters.

Nitrogen incorporation into structurally characterized iron-sulfur heterocubane motifs were achieved by the 1970 s in the group of Dahl, long before the structure of nitrogenase was known. The first examples possessed *tert*-butyl imido ligands in place of two sulfides, and were terminally ligated by nitrosyl ligands.[98] The group of Lee achieved all three permutations of mixed S/NR cores in a series of iron heterocubane clusters with $[FeS_3(N^tBu)]^{2+}$, $[FeS_2(N^tBu)_2]^{2+}$, and $[FeS(N^tBu)_3]^{3+}$ cores.[414,415] In particular, the $[FeS_3(N^tBu)Cl_4]^{2-}$ cluster represents a close topological analogue of the Fe_4S_3C cubane half-core of nitrogenase (Fig. 50), but with the central carbide atom modelled by nitrogen[414]; the identity of the central light atom X had not yet been confidently assigned. Similarly, a recently reported $[WFe_3S_3(NSiMe_3)]^-$ cluster

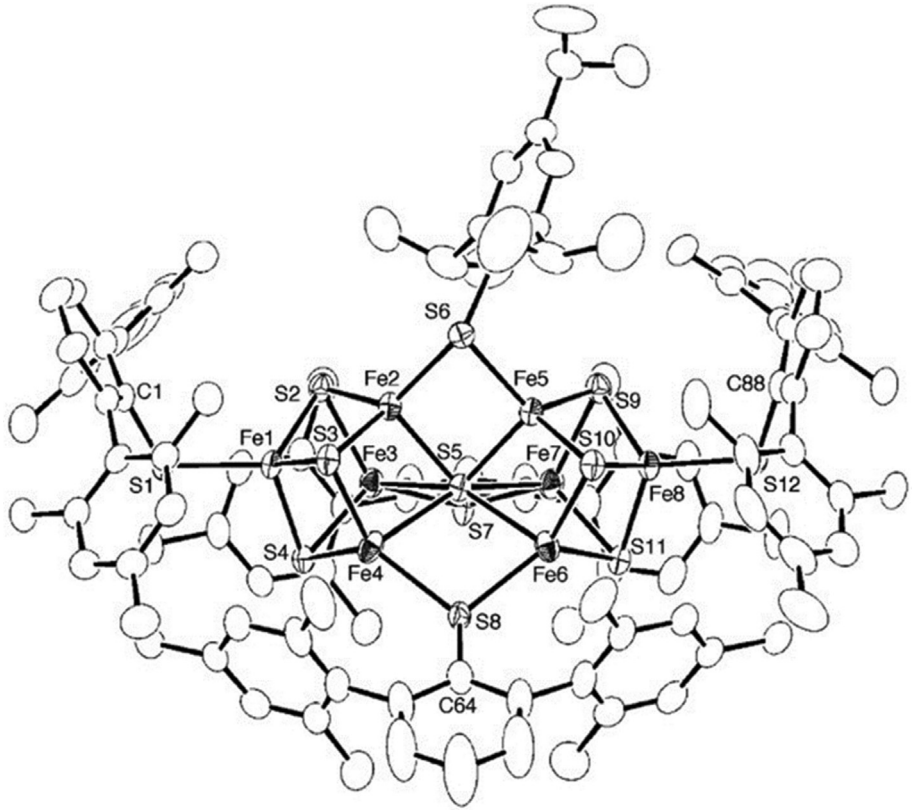

Fig. 46. Structure of FeMoco model complex from Tatsumi and coworkers with an atomically accurate core except for a central sulfide in place of the biological carbon atom. Ellipsoids set at 50 percent probability level. Carbon atoms shown as open ellipses. Hydrogen atoms omitted for clarity. Reproduced with permission from the American Chemical Society.[409]

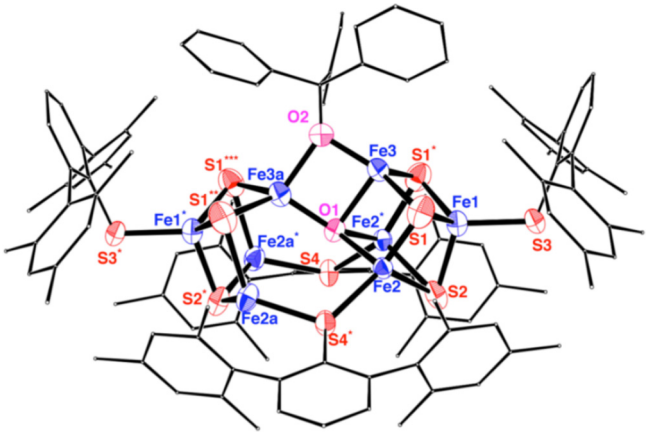

Fig. 47. $Fe_8(\mu_3\text{-}S)_6(\mu\text{-}SMes_2Ar)_2(SMes_2Ar)(\mu\text{-}OCPh_3)(\mu_4\text{-}O)$ cluster of Tatsumi, mimicking the structure of FeMoco with a central μ_4-oxide.[407] Reproduced with permission from the American Chemical Society.

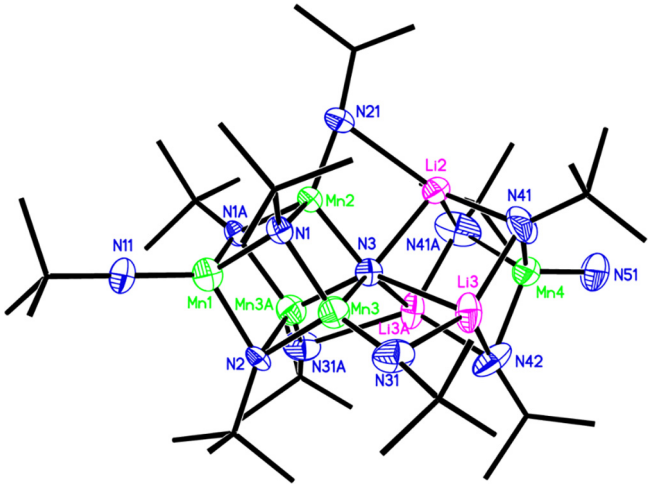

Fig. 48. Crystal structure of $Li_3Mn_5(\mu_6\text{-}N)(\mu_3\text{-}N^tBu)_6(\mu\text{-}N^tBu)_3(N^tBu)(N)$. Ellipses are set at the 50% probability level. Carbon atoms are displayed as stick models, and hydrogens are omitted for clarity. Reproduced with permission from the American Chemical Society.[173]

from Holm mimicked the geometry of the Mo-half of FeMoco with N in place of the central carbide, and with isoelectronic W in place of Mo (Fig. 50), which combined with the work of Lee,[414] accurately modeled the geometry of the two halves of FeMoco.

A number of multinuclear clusters feature nitride ligands.[417–420] A few noteworthy examples are cited here, the first, being from the lab of Holm, where non-cubane, higher nuclearity clusters were successfully prepared.[417,418] A nitride was inserted into a template triangle of iron atoms by the lab of Murray.[420] An example from the lab of Betley transferred the nitride as a nitrogen atom from azide to cap a triangle of iron atoms.[419] None to date have structures mimicking the complete FeMoco.

The insertion of biorelevant carbide into models of FeMoco has proved elusive to date as the tetraanionic carbide is a strong, hard donor, and the FeMoco target ligation environment is soft, with low-valent iron and polarizable, weak-field sulfide ligands. Presented in section 2.1, examples of cubane clusters ligated by

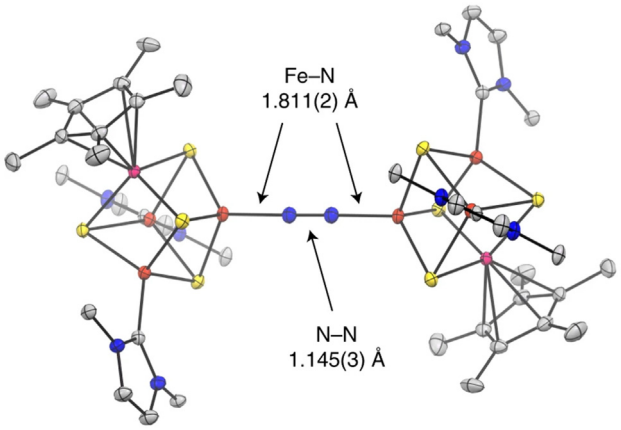

Fig. 49. X-ray crystal structure of N2-bridged dicubane cluster of Suess [408]. Figure reproduced with permission from Springer-Nature.

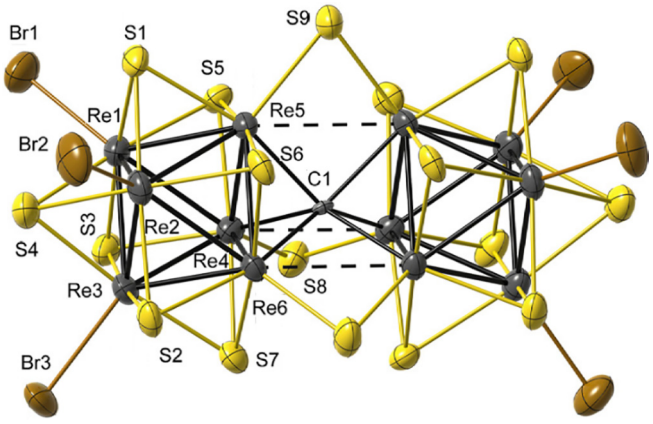

Fig. 52. X-ray crystal structure of $Re_{12}(\mu_3\text{-}S)_{14}(\mu\text{-}S)_3(\mu_6\text{-}C)Br_6$ with ellipsoids set at 30% probability level. Adapted with permission from Elsevier.[426]

carbon donor atoms are known, [61,63,71,72] but biomimetic iron cubane systems with a lone carbide have yet to be achieved. Carbide as a central ligand has long been known to form stable complexes as a central ligand atom in metal carbonyl clusters, however.[421] For example, the archetypal $Fe_5(\mu_5\text{-}C)(CO)_{15}$ cluster features a carbide ligand centered at the base of a square pyramid of five iron atoms (Fig. 51).

The vast array of carbide-containing metal-carbonyl clusters has included a $MoFe_5$ cluster characterized in 1980, featuring a central carbide encapsulated within an octahedral arrangement of the six metal atoms (Fig. 51).[422] This cluster has recently been reexamined by the group of Rose, and a potentially biomimetic reduction of acetylene (a nitrogenase alternative substrate) derivatives to *cis*-ethylene derivatives via a metal hydride intermediate was discovered.[423]

A curious class of little-recognized metal-sulfide-carbide clusters are the systems of Mironov[425–429], which feature a pair of sulfide-capped Re_6 octahedra bridged by three μ_2-sulfides and a central μ_6-carbide ligand (Fig. 52). Except for the identity of the metal, and that the two cluster halves are M_6S_7 clusters rather than M_4S_3, these structures show a central carbide with significant

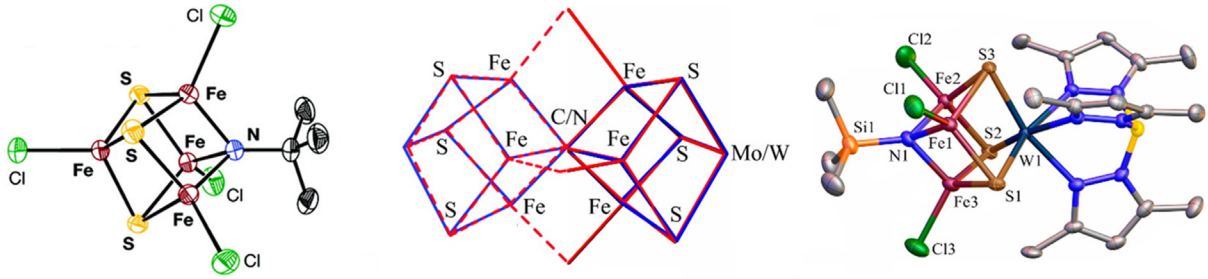

Fig. 50. (Left) Thermal Ellipsoid plot of $[Fe_4S_3(N^tBu)Cl_4]^{2-}$ with ellipsoids set at 50% probability and hydrogen atoms omitted for clarity. (Right) Thermal Ellipsoid plot of $[WFe_3S_3(N(SiMe_3)]^-$ with ellipsoids at 50% probability level and hydrogen atoms omitted for clarity. (Center) Overlay of both cluster geometries onto the X-ray crystallographic structure of FeMoco.[363] Adapted with permission from the American Chemical Society[414] and the National Academy of the Sciences of the USA.[416]

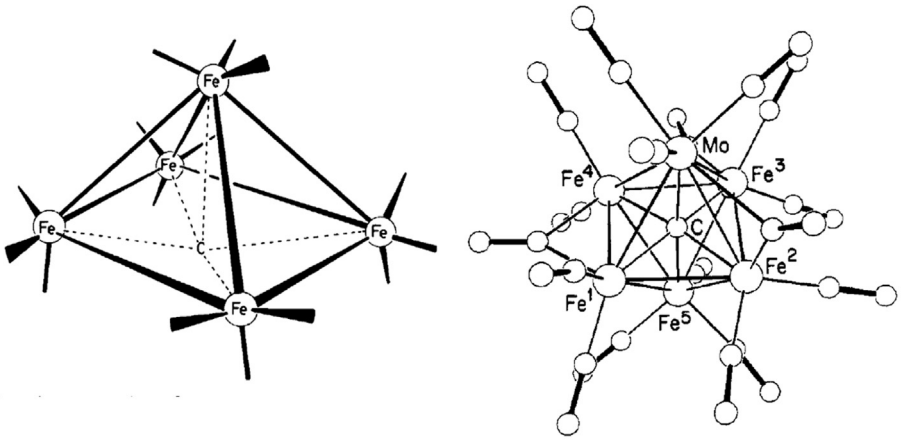

Fig. 51. (Left) 3D Crystal structure of $Fe_5(\mu_5\text{-}C)(CO)_{15}$.[424] The carbide carbon atom extends 0.08 A below the center of the basal plane of iron atoms. Terminal carbonyl ligand positions are indicated by solid lines projecting out from the iron atoms. Reproduced with permission from Wiley.[421] (Right) Crystal Structure of $[MoFe_5(\mu_6\text{-}C)(CO)_{17}]^{2-}$. Reproduced with permission from the American Chemical Society.[422]

analogy to FeMoco, though nitrogenase is not mentioned in these reports. The central carbide ligand originates from a CN^- ligand, and the identity of the central ligand was determined using ^{13}C labelling and NMR. [425]

While weak field iron carbide clusters at first row transition metals have yet to be achieved, some organometallic clusters containing carbon-based ligands are worthy of note. A small subset of Cp-ligated Fe heterocubane clusters (see Section 2.1) have been isolated by the laboratories of Ozawa, Ogino, and Okazaki. [60,72,430] These works have involved bridging methine (CH^{3-}) [60] ligands, or mixtures of methine and CO[60,430] or methine and isonitrile.[72] While these reports do not mention the topic of nitrogenase, they accomplish remarkable bio-relevant chemistry related to CO and acetylene (both alternative substrates for various nitrogenases[370]). Reduction of the $Fe_4(\mu_3\text{-}CO)_4Cp'_4$ cluster by a hydride source reduces two carbonyl ligands to methylidyne bridging ligands in $[Fe_4(\mu_3\text{-}CO)_2(\mu_3\text{-}CH)_2Cp'_4]^{2+}$. Further reduction by a hydride source results in C–C coupling to give an acetylene-type ligand. With excess reductant, the CO ligands can be reduced entirely to acetylene[60] (Fig. 53). A similar C–C coupling occurs with the isolobal phenylisonitrile ligands.[72]

5. The Ca-Mn-O cubane cluster of photosystem II and biomimetic systems

Embedded within the thylakoid membrane of higher green plants, algae, some cyanobacteria, and all oxygenic photosynthetic organisms, is a ~ 350 kDa homodimeric protein named Photosystem II (PSII, Fig. 54). Crucially integrated into oxygenic photosynthesis and which houses the active site where water-splitting

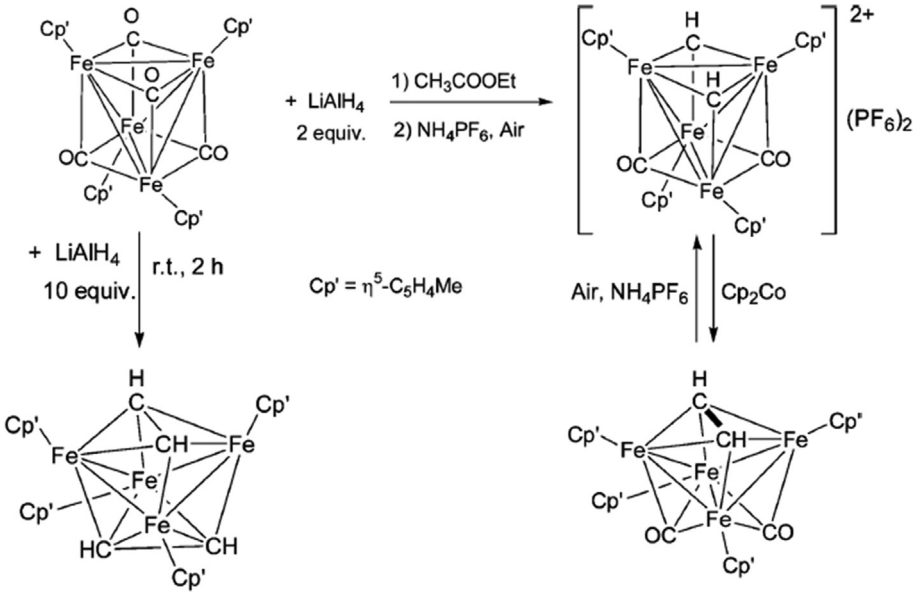

Fig. 53. Carbon-centered redox chemistry at an iron heterocubane cluster converting CO to methylidyne and acetylene. Adapted with permission from the American Chemical Society.[430]

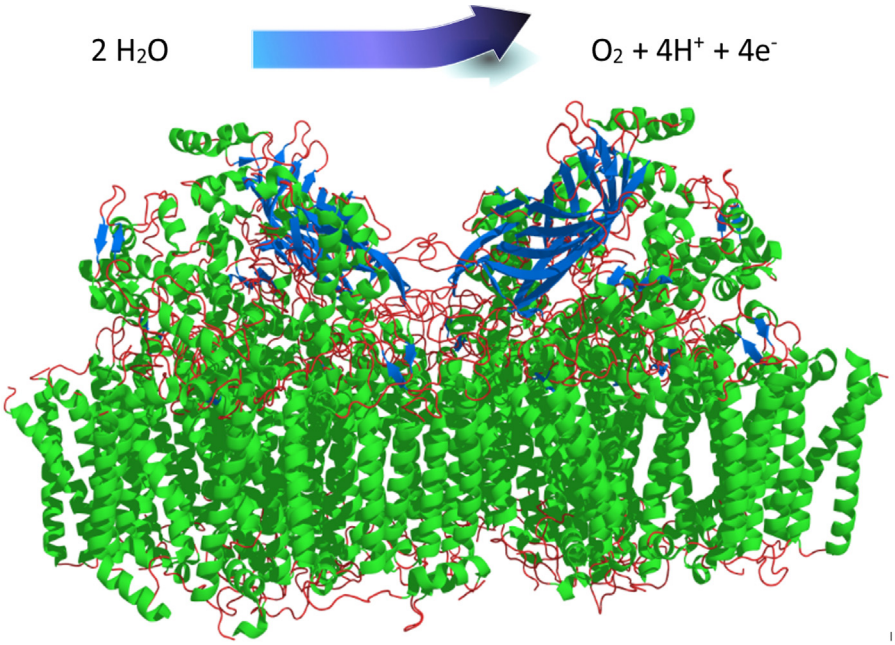

Fig. 54. Photosystem II protein effectively splits water to form dioxygen, four electrons, and four protons.[434]

catalysis occurs is the Oxygen Evolving Complex (OEC). Splitting highly stable water is no simple task, however PSII generates the strongest known biological oxidant via one-electron oxidation of the redox-active chlorophyll (P680) of PSII. This transient $P680^+$ species has a reduction potential estimated at ~ 1.25 V.[431,432] This species is poised to carry out the electrochemically extreme water oxidation reaction, creating dioxygen from water.[433]

The PSII protein absorbs red photons centered around 680 nm (the λ_{max} of the redox active P680), causing an excited charge transfer singlet state, with the electron delocalized into nearby pheophytin A.[435] Subsequent electron transfer events move the electron ultimately to a dissociable plastoquinone redox cofactor.[436] Having used light to drive this charge separation, the electron migrates within its hosts along the thylakoid membrane to cascade down a series of additional transmembrane-protein-bound redox cofactors, driving proton pumps to generate a proton-motive potential across the thylakoid membrane, which is used to synthesize ATP. After this cascade, the relaxed electron reaches Photosystem I, at which point it is excited again by red light to further harvest solar energy and generate $NADPH{\cdot}H^+$ (effectively a stored, soluble form of H_2).[437] In PSII, the resultant $P680^+$ generated by the initial photon absorption, acting as the oxidative driving force, drives a catalytic oxidation of two water molecules to form oxygen gas and four protons, effectively splitting water into O_2 and H_2.[438] The resultant protons are added to the chemiosmotic H^+ gradient within the thylakoid membrane which drives transmembrane ATP synthase, providing stored cellular energy.[439]

The evolution of oxygenic photosynthesis on earth resulted in the scavenging of CO_2 from the warm atmosphere, the simultaneous cooling of earth, and accumulation of O_2, which resulted in the extinction of vast numbers of anaerobes. The oxygenated atmosphere permitted the simultaneous evolution of aerobic heterotrophs, and higher organisms.[440] This evolutionary development transformed life from specialized organisms living, most likely, at undersea hydrothermal vents, into widespread, versatile organisms that spread through the sea and across the surface of the planet, terraforming the earth. As such, there has been no development in geohistory with a greater impact to the planet and its life forms than the evolution of OEC, implicating it as an important cubane structure of bioinorganic chemistry.

Early investigations of the interaction of short pulses of light with PSII demonstrated that predictable evolution of O_2 occurred after specific numbers of flashes.[441–446] Starting with a dark-adapted sample of PSII enzyme, it was noted by Kok et al.[447] that upon exposure of dark-adapted PSII to repeated short flashes of light, that a burst of O_2 could be detected evolving from the enzyme on the 3rd flash of light, and then on every 4th flash thereafter (Fig. 55).[448,449] This led to the proposal of a set of five OEC oxidation states (S_n, n = 0–4) now termed the Kok cycle, where n corresponds to the number of photo-induced oxidation events that have occurred since the last turnover of O_2. The result suggests that S_1 is the stable, dark-adapted state, and that the four-electron oxidation of two water molecules to O_2 occurs via stepwise transitions of the S-states from S_0 up to S_4, concomitant with the absorption of a photon with each oxidation event. O_2 is ultimately evolved in a dark reaction as S_4 relaxes back to S_0, eliminating a molecule of water-derived O_2, and reducing the cluster by $4e^-$ back to the S_0 state. The analytical determination of four manganese atoms in the cofactor[450] suggests an oxidative burden of one electron per metal atom. This theme of metalloenzymes featuring one redox-active metal site per each electron transferred is common to many multi-electron redox enzymes containing metallocofactors such as nitrogenase (8 metals for the 8-electron reduction of one N_2 and one H_2, see section 3.7)[284], diiron and nickel iron hydrogenases (2 metals for the 2-electron reduction of protons, see section 3.5),[330] cytochrome *C*-oxidase (two copper centers and two heme irons for the 4-electron reduction of O_2)[451], alkane monooxygenases such as methane monooxygenase (2 iron ions for 2-electron methane oxidation to methanol),[452] and even the heme-containing cytochrome P450, which uses one iron ion and one redox-active porphyrin to achieve 2-electron hydrocarbon oxidation.[453] While the latter two examples are dioxygenases that nominally transfer four electrons per turnover, in both cases the minimalistic peroxide shunt pathway uses a 2-electron-transfer mechanism.[453–455]

In addition to manganese, Ca^{2+}[456–458] and Cl^- [459–464] were found to be essential components for catalytic activity of PSII, and were frequently presumed to be atomic components of the molecular OEC. In the case of the Ca^{2+} Lewis acid component, only Sr^{2+} could be substituted and retain any activity (about 50%); no other Lewis acid results in any activity.[465–467]

5.1. Spectroscopic signatures of the OEC

The most distinctive spectroscopic feature of the OEC is the low-temperature EPR spectrum of the odd-electron S_2 state obtained by flashing the dark-adapted state once (Fig. 56). At liquid

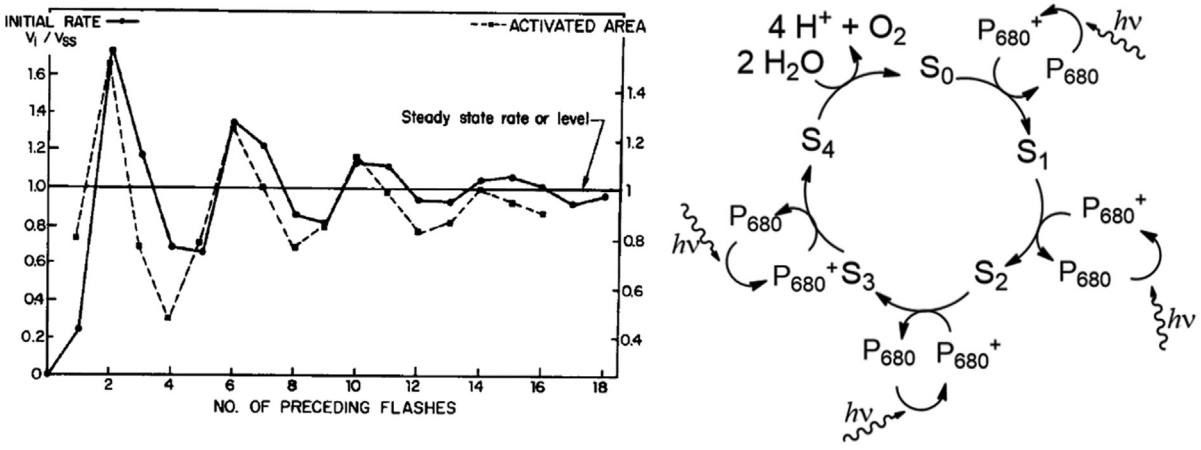

Fig. 55. Left: Quantification of O_2 evolution as a function of flash number from the original report of Kok et al, reproduced with permission from Wiley[447]: "Dots (left ordinate): initial rate V_i as a function of the number of preceding flashes, spaced 1 sec apart. . .Squares (right ordinate): relative areas bounded by the same rate transients as used for computing V_i, normalized to the area bounded by the 0 flash transient." Right: Kok cycle explaining the oxygen evolution profile, where the cycle begins in the dark-adapted S_1 state, and evolves O_2 on the 3rd flash, and every 4th flash thereafter.

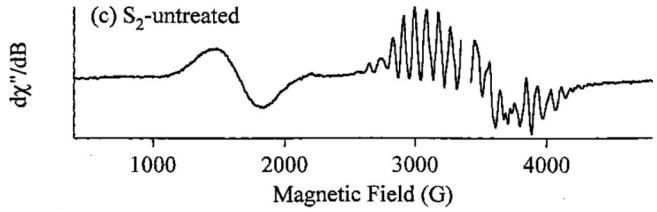

Fig. 56. Perpendicular mode X-band EPR spectrum of PSII in the S_2 state. Reproduced with permission from the American Chemical Society.[468]

helium temperatures, this state displays two EPR signatures: a broad axially distorted signal at g = 4.1 corresponding to a larger quadrupole spin state, and the sharp "multiline" signal at g = 2, corresponding to an S = ½ state. Careful experiments have ruled out the possibility that one of these signals is a contaminant, and the consensus has been reached that both signals represent active forms of the S_2 state, poised to proceed onto the S_3 state upon the next flash. The most commonly proposed explanation for the two signals is that the S_2 state exists in two possible geometries or tautomers in thermal equilibrium, and which are frozen out at the low temperature of the EPR experiment, and thus observed simultaneously. Any hypothetical or synthetic OEC models and structural proposals must therefore be rationalized against this piece of benchmark data.

A second spectroscopic aspect of the OEC that has been the subject of much contention is the analysis of the EXAFS (Extended X-ray Absorption Fine Structure) region of the X-ray absorption spectrum (XAS). An XAS possesses a distinct absorption edge with specific energy corresponding to element identity. This edge corresponds to the excitation of core electrons to higher energy orbitals. Beyond the edge (the EXAFS region), electrons are ionized and exit the sample as photoelectrons. EXAFS analysis operates by a fitting of the element-specific absorption edge of the XAS, to subtract the absorption profile. This subtraction leaves an oscillating pattern in the EXAFS region resulting from interference among outgoing backscattered photoelectrons. A Fourier transform of this oscillating pattern as a function of photoelectron energy gives a one-dimensional electronic probability distribution function illustrating *apparent* distances (described below) between the atom of interest and nearby atoms. These probability distribution functions can be compared to model structures. A manganese EXAFS analysis of the S_1 state of PSII is shown in Fig. 57.

In order for EXAFS analysis to work properly the absorption edge has to be accurately modeled before subtraction to avoid introducing systematic errors into the EXAFS analysis, and the *apparent* distances (such as those indicated by the peaks in Fig. 57) must have their α/2 phase shifts corrected using knowledge of the identities of neighboring atoms to give corrected interatomic distances. As such, confident knowledge of the structure and composition as well as the physical and electronic structure is needed to accurately model the absorption edge using parameterized cubic curves or, more ideally, theoretical methods such as time-dependent DFT (TD-DFT). After subtraction, a Fourier transform of the remaining oscillation pattern gives a probability distribution function: a histogram of apparent interaction distances, which may be compared to proposed model structures. This makes EXAFS analysis on unknown structures something of a Catch-22: to determine an accurate structure from EXAFS, one must input accurate structural and atomic information into the data analysis. The technique is nevertheless highly powerful, especially when high-quality diffraction data is not available to provide a high-confidence structural model. EXAFS examinations of the S_1 state of the OEC subtract the absorption edge assuming a 2-Mn^{III}/2-Mn^{IV} oxidation state assignment (referred to as the "high oxidation

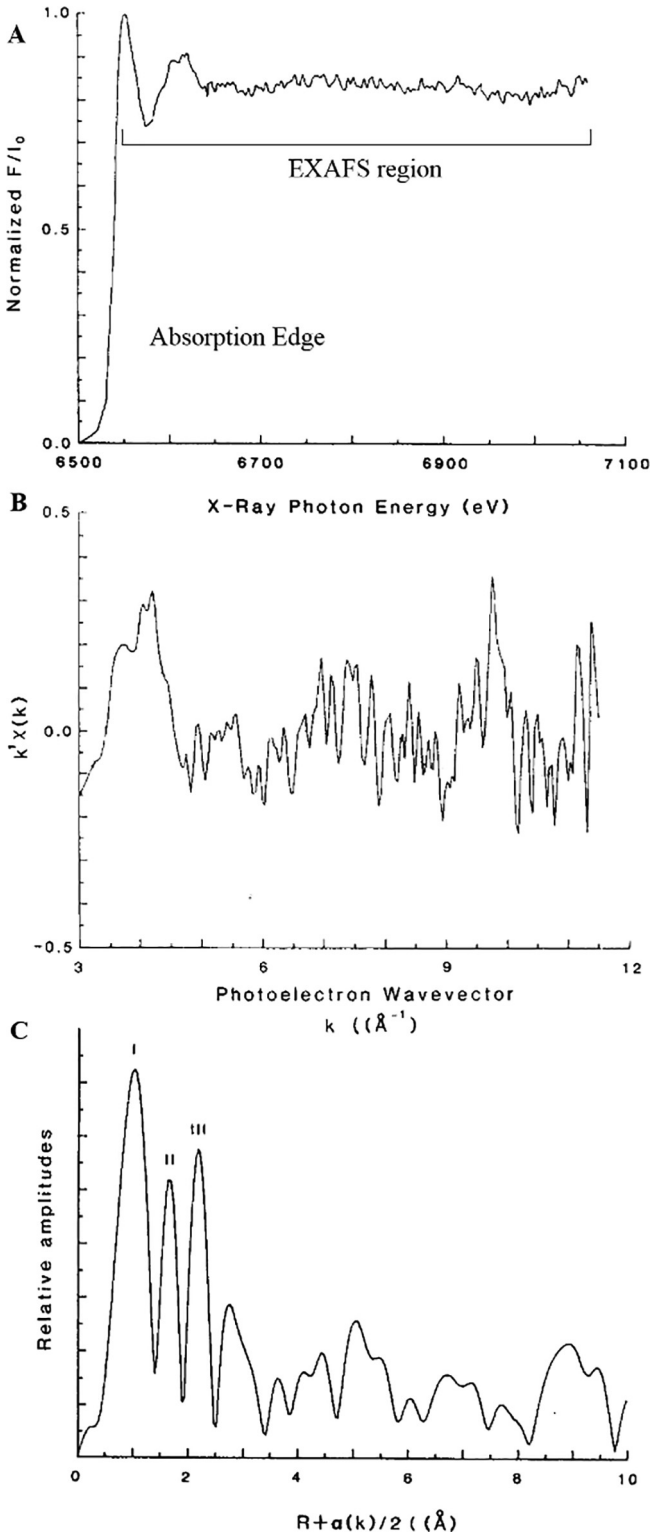

Fig. 57. Illustration of EXAFS analysis on the S_1 state of the OEC[469], reproduced with permission from Elsevier. A) XAS showing the absorption edge and the EXAFS region with visible oscillation pattern from interference between X-rays and backscattered electrons. B) XAS after theoretical subtraction of the absorption edge showing EXAFS oscillations as a function of backscattered electronic energy. C) Fourier transform of B showing probability distribution function of apparent distances. Note that these apparent distances are different from the actual interatomic distances by α/2, which corresponds to a phase shift between the absorbing and scattering atoms based upon their respective ionization potentials. For this reason, fits of specific proposed structural models to the data are required to extract the true interatomic distances.

state paradigm", which is the most commonly assigned set of oxidation levels for the OEC) with electronic transitions from the Mn 1 s electrons to unoccupied *p* orbitals responsible for the edge rise (see Fig. 57 above). The result generally gives a profile like that shown in Fig. 58, with three distinctive Fourier peaks corresponding to manganese-oxygen interatomic vectors at 1.8–2.15 Å (peak I), additional manganese atoms at 2.72 Å (peak II), and manganese and calcium interatomic vector(s) at 3.3 Å (peak III).[470] However, much more subtle information is inherent in this histogram of nearby neighbors; any proposed 3D model of the OEC can be collapsed to a 1D representation of overlaid radial electron densities as a function of distance from all manganese atom, and compared not only for a match in positions of large peaks, but for a match in the overall profile, including shoulders, valleys, and small near-baseline peak features. It is the required agreement with EXAFS analysis that has largely frustrated efforts to model the structure of the OEC using single-crystal X-ray diffraction (vide infra).

5.2. The evolution of OEC structural models.

Recent enhanced crystallographic data has illuminated ever more precise structures of the Oxygen Evolving Complex and Photosystem II by reducing the problems of radiation damage and low crystallographic resolution, with recent structures achieving resolution even below 2 Å.[434,472,473] Since the original consensus that the OEC was a tetramanganese calcium cluster,[450] discussion of the possible structure of the catalytic complex continued for several decades, with numerous proposals gaining (and some losing) traction, illustrated in Fig. 59. Any structural and mechanistic proposals were required to conform to the key biophysical observations about the OEC. 1st: Operation via the (at least) five distinct redox states S_n of the Kok cycle, 2nd, that the structure be comprised of four manganese atoms and one calcium atom, 3rd, that the structure be consistent with the EPR signatures in the S_2 state, and 4th, that the structure be consistent with available EXAFS data. This led to several proposals with disparate structures, but each of which was defensible in some way or another. As time continued, and as protein crystallographic technologies improved, a consensus of a cubane-type structure of the OEC gained traction, affirming the ubiquity of cubane motifs as cofactors in catalytic enzymes, though agreement between crystallographic structure and EXAFS has remained challenging.

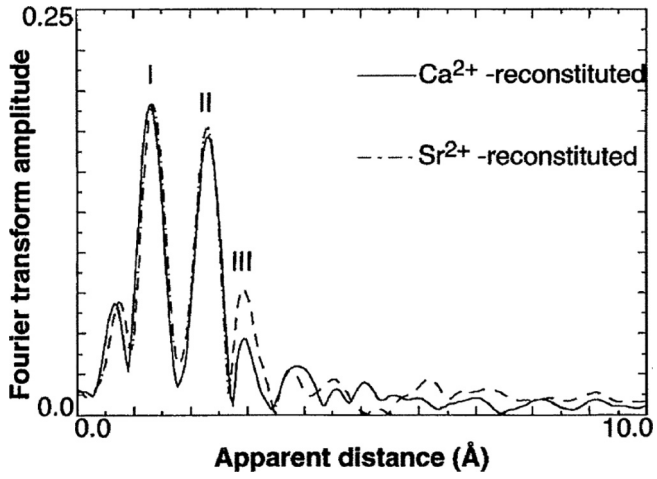

Fig. 58. EXAFS analysis of the OEC in the S_1 state.[471] The solid line corresponds to calcium-incorporated PSII, and the dotted line to strontium-incorporated PSII, which represent the only two catalytically active OEC compositions. Reproduced with permission from AAAS.

5.2.1. Early structural proposals from biophysical experiments and model chemistry

A general understanding of the history of biomimetic complexes must be understood to move forward into the newest discoveries. The importance of manganese and its stoichiometry in the biological OEC has been known for decades.[437,446,450,474–476] Applying these lessons to inorganic models was a priority of the scientific community.[477] As macromolecular structural technology has improved, the experimental picture of the OEC was clarified over the past few decades. Prior to this time, proposed OEC structures were based upon spectroscopic data and model chemistry. A number of the most significant early proposals for the OEC structure are covered here, and summarized in Fig. 59, and the evolution of synthetic model complexes are summarized in Fig. 60. Models postdating the obtainment of atomically resolved macromolecular crystal data will be discussed in section 4.2.5.

Among the earliest structures considered was indeed a cubane structure, proposed by Brudvig and Crabtree in 1986 using EPR spectral data from the S_2 state,[494] although this proposal involved a structural conversion to an adamantane Mn_4O_6 structure as the OEC advanced to the S_4 state. The adamantane-type tetramanganese cluster had already been prepared synthetically and reported three years earlier by Wieghardt and coworkers.[495] The group of Armstrong demonstrated the viability of a redox-dependent cluster structure in adamantine-type model complex chemistry[496] templated by the *N*,*N*,*N*′,*N*′-tetra-(2-methylpyridyl)-2-hydroxypropanediamide (tphpn) ligand. This work showed a redox-initiated conversion between a dimer of dimers cluster $[(Mn_2(\mu\text{-}O)_2(tphpn))_2]^{4+}$ with an oxidation state of 2-Mn^{III}:2-Mn^{IV} (S_1-like) and a one-electron oxidized adamantane-type Mn_4O_6 cluster $[Mn_4(\mu\text{-}O)_4(tphpn)_2]^{5+}$ with an oxidation state of 1-Mn^{III}:3-Mn^{IV} (S_2-like) (Fig. 61). This latter adamantane-type structure was similar to one member of the shapeshifting proposal of Brudvig and Crabtree[494] (Fig. 59). Further, Armstrong's dimer-of-dimer molecule exhibited an EPR spectrum remarkably similar to that of the analogous S_1 state of the OEC,[488] and its one-electron reduced analogue was analogous to the EPR spectrum of the S_0 state of photosystem II (Fig. 62),[496] which was rationalized as a possible indication of structural analogy. However, this history lesson well illustrates the risks of assigning atomic structure using EPR spectroscopy, which can exhibit similar spectral signatures for vastly different structures.

The proposal of a cubane Mn_4O_4 complex for the S_0 state by Brudvig and Crabtree in 1986 [494] represented an important historical proposal for the cofactor structure. The groups of Christou and Dismukes further contributed support for the probability of the cubane structure in their respective model complex chemistries.[137,497–499] A cubane cluster from the group of Dismukes, terminally ligated by six face-bridging diphenylphosphonates, $Mn_4O_4(O_2PPh_2)_6$, represents a 2-Mn^{III}:2-Mn^{IV} cluster: a presumed analogue of the S_1 state. This cluster exhibited release of O_2 upon laser irradiation,[498] resulting in formation of a cluster with mass spectral features consistent with the "butterfly" geometry cluster, $Mn_4O_2(O_2PPh_2)_3$(Scheme 4).[499] While this compound was not structurally characterized, its analog had been previously synthesized and characterized by single crystal X-ray diffraction by the group of Christou (Fig. 63),[500,501] demonstrating the fundamental stability of such species. In solution, the Dismukes cluster did not bind water to re-form the cubane cluster to close the cycle, but an analog of the reverse reaction—the generation of the butterfly geometry by hydrogen atom transfer to the cluster to extrude water—was achieved by the addition of the H-atom donor phenothiazine (pzH), which resulted in the isolation of the "pinned butterfly" cluster, $Mn_4O_2(O_2PPh_2)_4$, which retained all four diphenylphosphonate ligands (Scheme 4).[499] Additionally, the

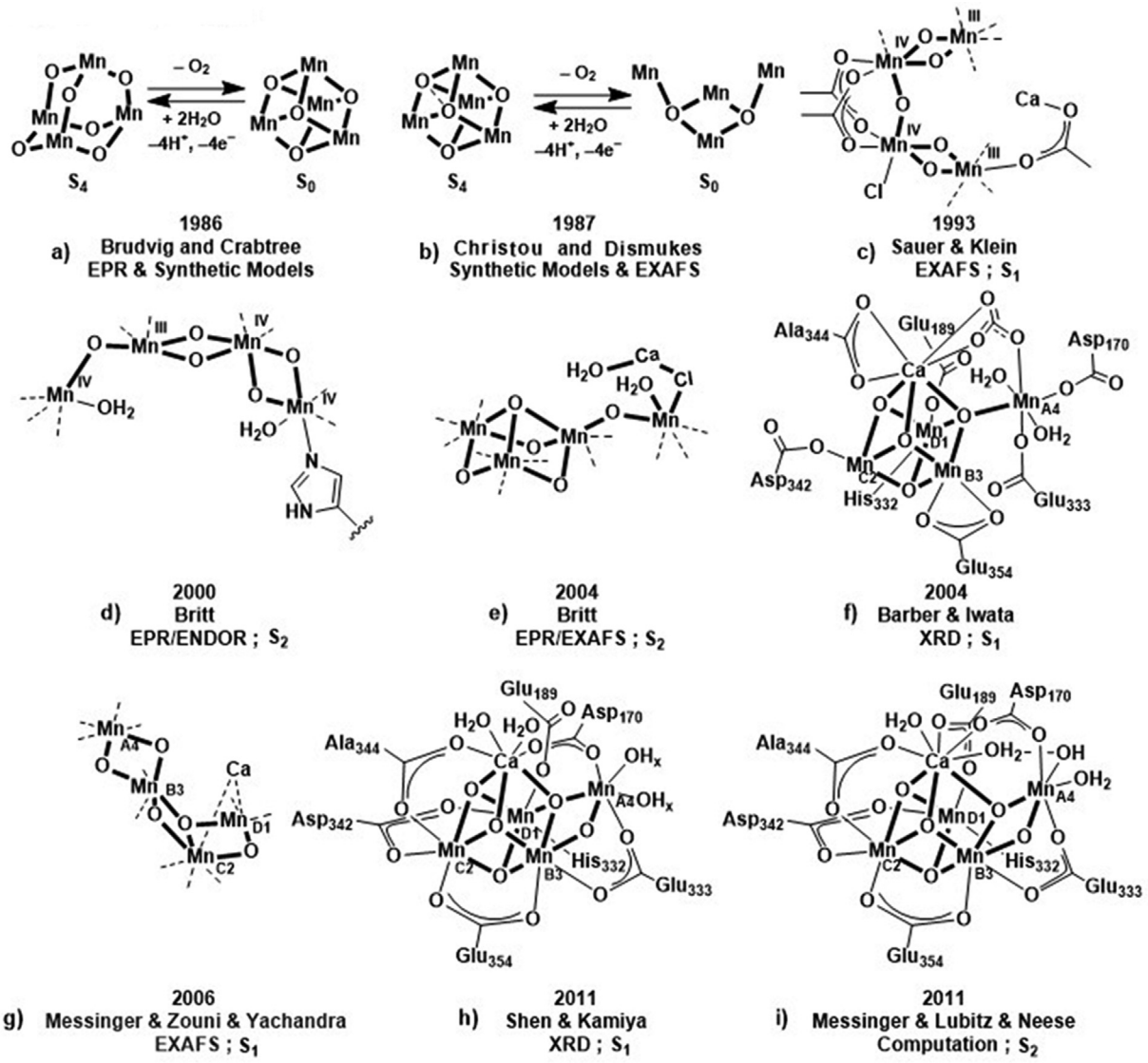

Fig. 59. Historically important structural proposals for the OEC. Research group, year, main spectroscopic methods, and S-state are stated below each figure. Dashed lines represent generic coordination sites and could represent either amino acids or water.[178,470,478–484]

cluster did serve as an electrochemical water oxidation precatalyst when diffused into a Naffion support.[502,503] Later, in 2015, a related cluster system was reported by the laboratory of Tilley, wherein the oxygen atom transfer from a Mn_4O_4 cubane cluster to triethylphosphine was achieved, with resulting isolation of a butterfly cluster (albeit with a *trans* geometry)[142] analogous to Dismukes' proposal (Fig. 64). Other similar models have been synthesized with various bidentate chelating ligands.[504–506] The proposal of O_2 formation via coupling of corner oxygens to form a pinned butterfly intermediate remains under consideration for the molecular mechanism of O_2 evolution in the OEC by some.[507] This, and other proposed mechanisms of O-O bond formation will be discussed in section 5.3.

Another example of a redox-dependent shape-shifting tetramanganese cluster from one of our groups[509] exhibited a redox-dependent geometry change from the "pinned butterfly" geometry, to an S_4 symmetric manganese cluster entitled the "twisted basket" (Fig. 65) This cluster work featured nitrene core ligand substitution in place of the biological oxide, containing a mixture of amide and hydrazine ligands. Hydrogen atom transfer to and from this cluster facilitated the breaking and forming (respectively) of an N-N bond, leading to cluster geometric rearrangements.

As Cl^- is an essential cofactor for PSII turnover, it was frequently presumed an atomic component of the OEC in early models. The laboratory of Christou was the first to prepare cubane clusters with a Cl^- ligand substituted for an oxygen atom in highly-distorted cubane complexes (Fig. 66).[143,510,511] However, later crystallographic analysis of PSII demonstrated the obligatory Cl^- ion is located elsewhere in the structure, distal from the OEC.[434]

The next class of OEC structural proposals to emerge were those of the end-fused Mn_2O_2 rhombs. Sauer and Klein proposed a pac-man shaped μ-oxo dimer of Mn_2O_2 rhombs that could template the formation of the O_2 bond within the cofactor's bite (Fig. 59).[470] This structure was rationalized based upon a good match to EXAFS data for the S_1 state of the OEC. A number of synthetic model complexes of oxygen-fused dimer-of-dimer molecules followed.[489,491] A similar topology was reported containing Mn ions joined by three bis-μ-oxo units, and it showed an X-band EPR signal similar to the multiline signal from the S_2 state of the biological OEC (Fig. 67).[512] These dimer-based proposals gained some traction by the discovery of structurally analogous

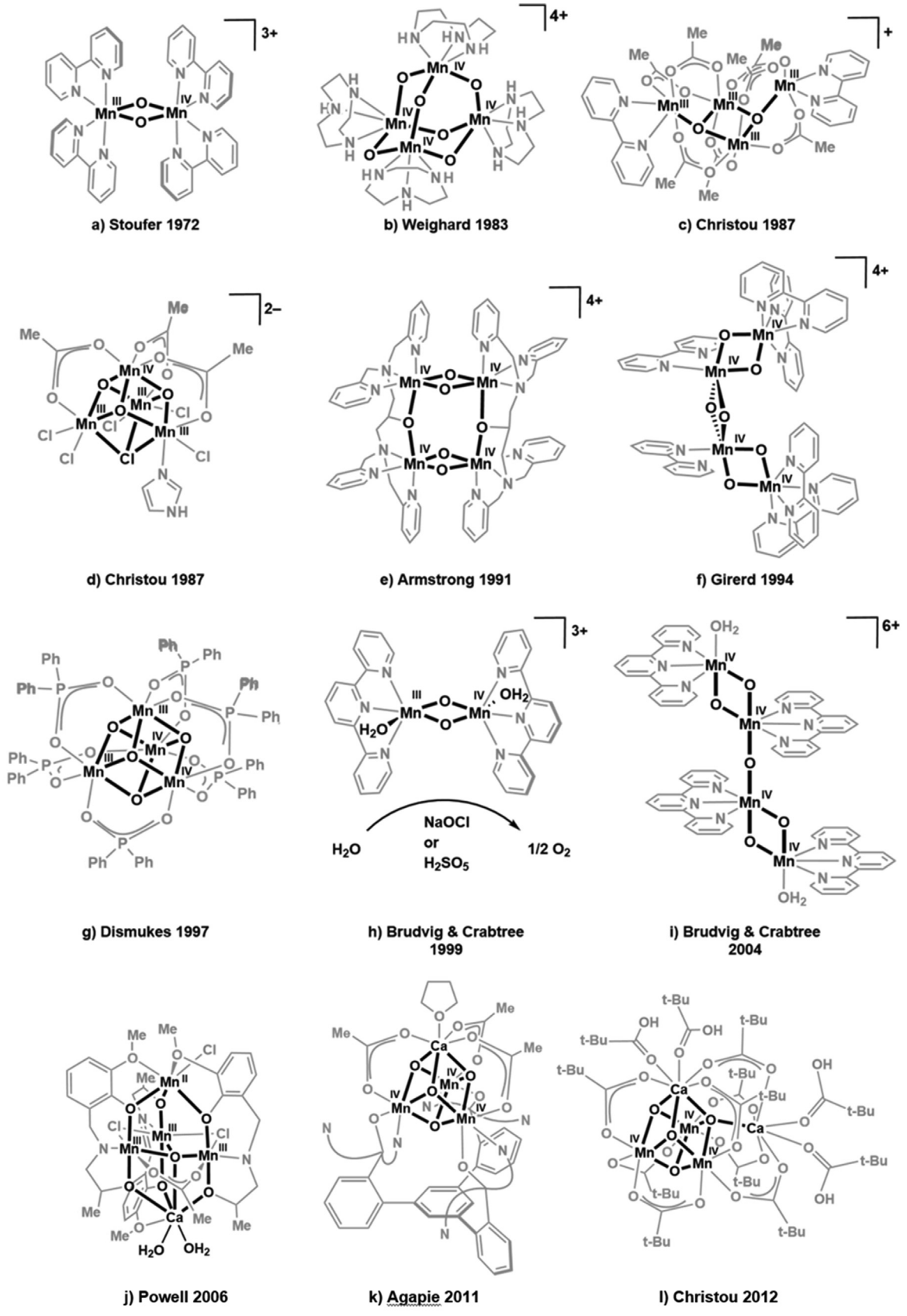

Fig. 60. Synthetic models relevant to the OEC.[136,137,485–493]

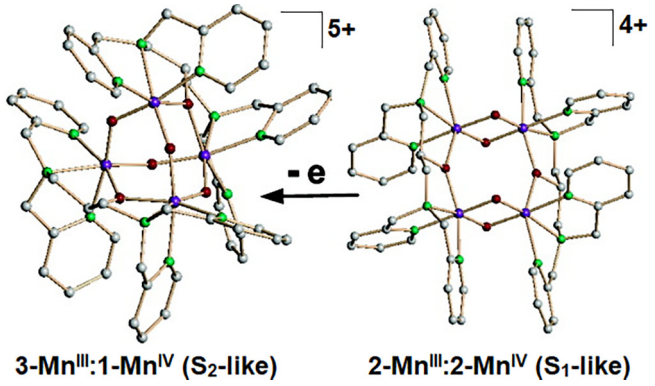

Fig. 61. Structures of shape-shifting Mn_4O_4 complexes from Armstrong.[496] (Left) the structure of the $[Mn_4(\mu\text{-}O)_4(tphpn)_2]^{5+}$ ion with adamantane-type geometry. (Right) the structure of the $[(Mn_2(\mu\text{-}O)_2(tphpn))_2]^{4+}$ ion with dimer-of-dimer geometry. Adapted with permission from the American Chemical Society.

$Mn_2(\mu\text{-}O)_2$ dimeric complexes from the groups of Crabtree and Brudvig that represented the first multinuclear Mn-O catalysts for O_2 evolution (Fig. 68).[490] The catalysis was driven by the chemical oxidants periodate or oxone (peroxysulfate), which are potent oxo-transfer agents, and catalysis was not achievable by the one-electron oxidant ceric ammonium nitrate (CAN). The use of two-electron oxo-transfer oxidants in water oxidation leads to concerns that the catalytic reaction is oxidant disproportionation rather than water oxidation. However, the authors addressed this concern by demonstrating that the O_2 product obtained from isotopically labelled water contains water-based oxygen rather than oxidant-based oxygen, and that the rate of exchange of the μ-oxo ligands with water is too slow to explain water-oxygen incorporation by any mechanism other than direct water oxidation. And while this catalyst achieved a meager turnover number of 4, it provided plausible evidence for the inclusion of Mn_2O_2 rhombs in OEC models. When incorporated into a metal organic framework

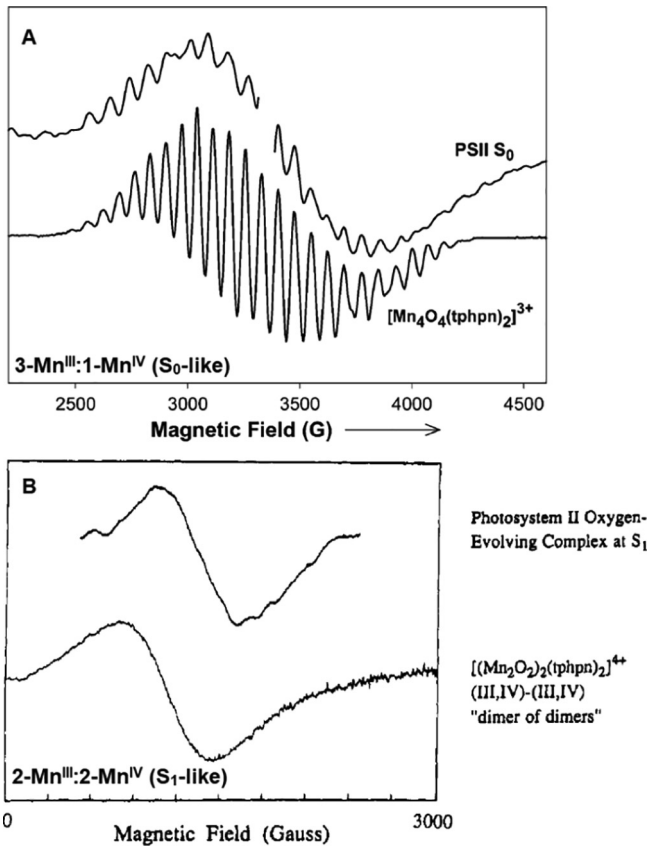

Fig. 62. EPR spectra comparing $[(Mn_2(\mu\text{-}O)_2(tphpn))_2]$ clusters of the group of Armstrong to those of the S_0 and S_1 states of the OEC. A) comparison of S_0 state EPR signature to the $[(Mn_2(\mu\text{-}O)_2(tphpn))_2]^{4+}$ cluster after in-situ one-electron reduction in perpendicular mode.[496] B) comparison of S_1 state EPR signature to the $[(Mn_2(\mu\text{-}O)_2(tphpn))_2]^{4+}$ cluster in parallel mode.[488] Adapted with permission from the American Chemical Society.

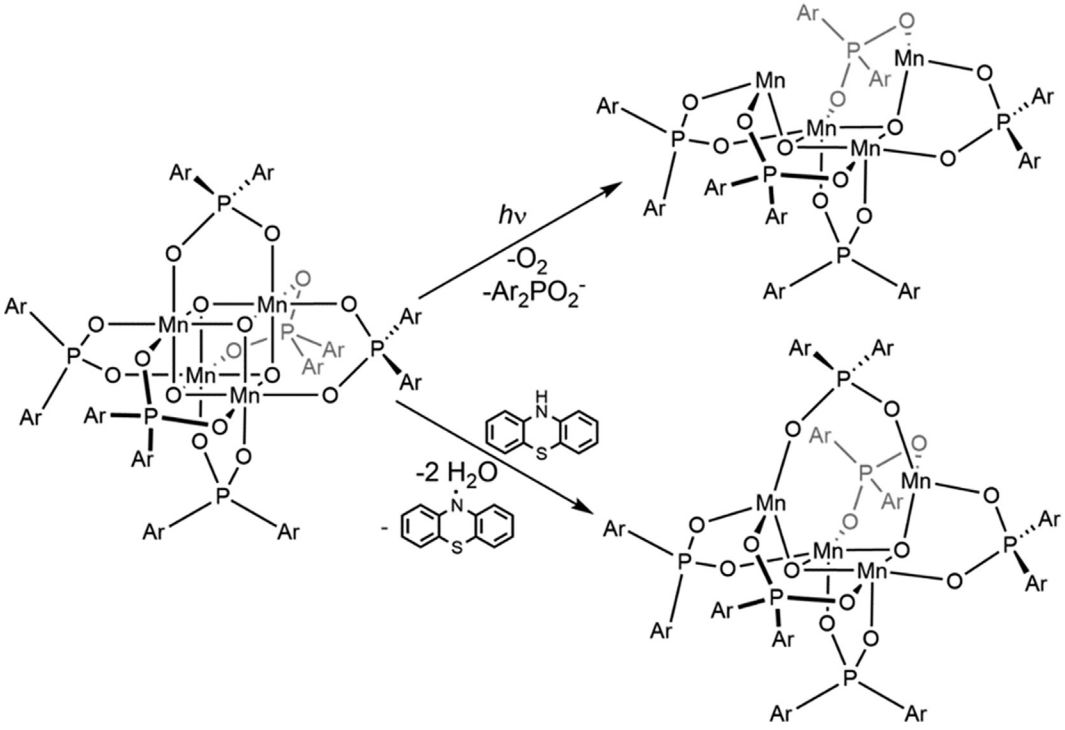

Scheme 4. Interconversions between the $Mn_4O_4(Ph_2PO_2)_6$ cubane clusters of Dismukes.[508]

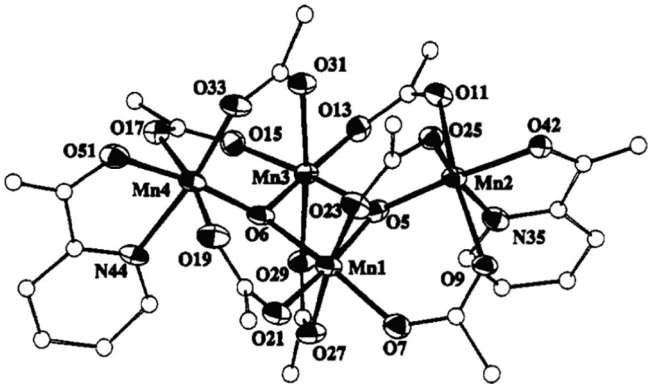

Fig. 63. The $(NBu^n_4)[Mn_4O_2(O_2CMe)_7(pic)_2$ butterfly cluster of Libby et al (pic = picolinate). Image reproduced with permission from the American Chemical Society. [500]

(MOF), the catalyst experienced a 20-fold increase in turnover number attributed to the mitigation of decompositional side reactions.[513]

Shortly after the discovery of the Mn_2O_2 water oxidation catalyst of Brudvig and Crabtree, the group of Britt suggested an

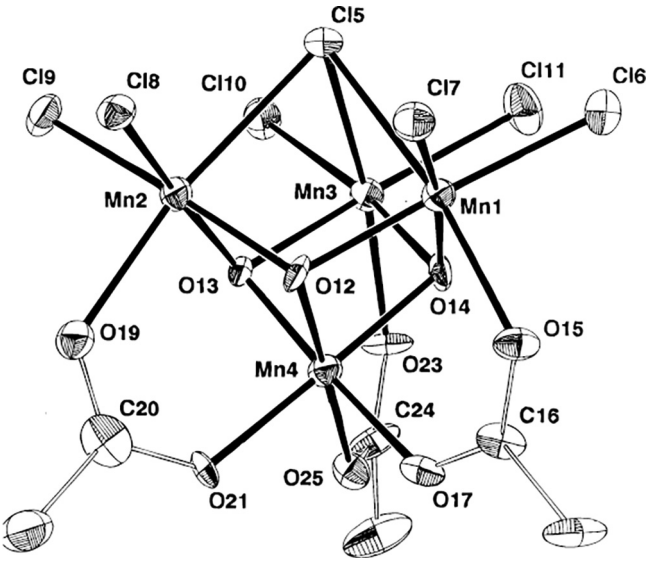

Fig. 66. The $[Mn_4O_3Cl_7(O_2CMe)_3]^{3-}$ chloride-substituted cubane cluster of Wang et al.[511] Image reproduced with permission from the American Chemical Society.

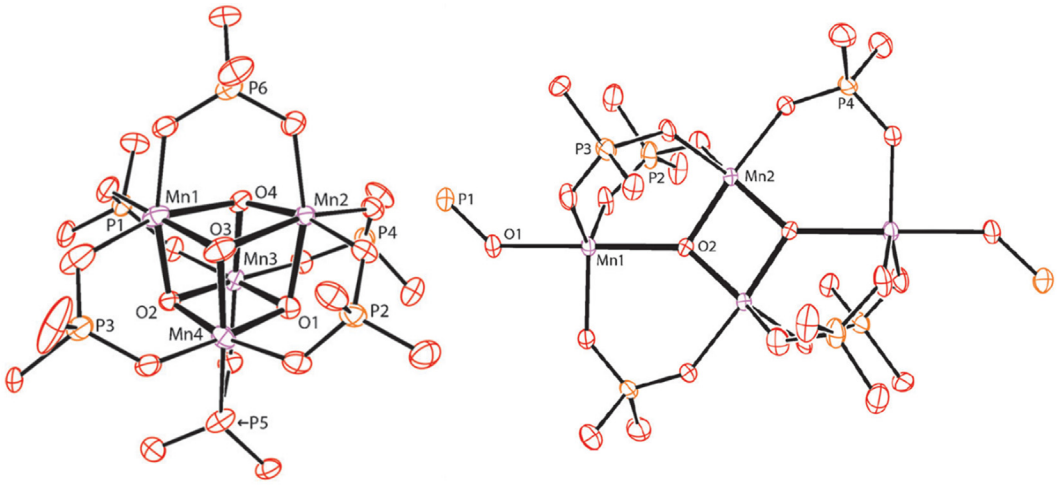

Fig. 64. Thermal ellipsoid plots of Mn_4 clusters from Van Allsburg et al.[142] Ellipsoids set at 50% probability level and C and H atoms omitted for clarity. (Left) $[Mn_4(\mu_3\text{-}O)_4(O_2P(O^tBu)_2)_6]$ cubane cluster. (Right) $[Mn_4(\mu_3\text{-}O)_2(O_2P(O^tBu)_2)_6(OPEt_3)_2]$ butterfly cluster resulting from oxygen atom transfer from the cubane cluster to Et_3P. Figure reproduced with permission from Wiley.

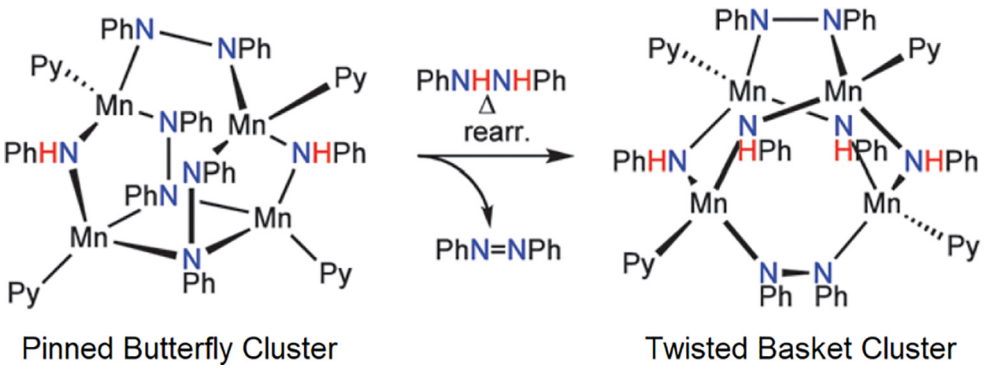

Fig. 65. Redox-dependent tetramanganese-nitrogen cluster rearrangement based on hydrogen-atom-mediated N-N bond cleavage. Figure reproduced with permission from the Royal Society for Chemistry.[509]

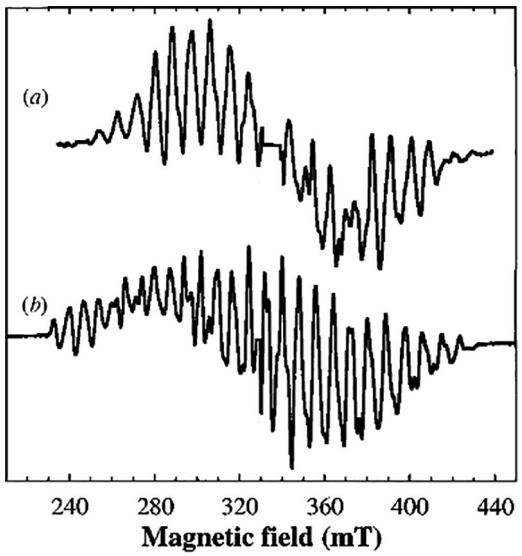

Fig. 67. (a) X-band EPR spectra of OEC (b) X-band EPR spectra of $[Mn^{III}Mn^{IV}_3O_6(bipy)_6]^{3+}$.[512] Reproduced from Ref.[512] with permission from the Royal Society of Chemistry.

improved model of an Mn_2O_2-rhomb-based model wherein the single μ-O bridge was placed at the edge of the linear cluster, and the two Mn_2O_2 rhombs where placed adjacent to one another (Fig. 59).[468] This new model provided an improved fit for both the CW-EPR and ESE ENDOR spectral data as well as the S_2 EXAFS data. A few years thereafter, this group improved this proposed model to one of a voided hemicubane based on ^{87}Sr ESEEM and CW-EPR on Sr- and Ca-substituted samples (Fig. 59).[514] This model was highly analogous to a computational model from Siegbahn several years prior[515] which was ahead of its time in that it featured corner calcium atoms and pendant manganese atoms (now known to be correct). Curiously, the revised structure from the group of Britt[514] bore remarkable similarities to the first atomic-resolution structure published by Ferreira et al[516] at almost the same time, and independently, and which was cited in its in-press form in a note in revision.[514] The structures were highly analogous but for the inclusion of the calcium atom in the main cubane core. This groundbreaking macromolecular crystal structure and its successors are the subject of discussion in the next section.

The ultimate determination and support for a calcium atom in the OEC was crucial in propagating the discussion forward. As time continued, a general consensus of a cubane-type structure of the OEC gained support, affirming the ubiquity of cubane motifs as cofactors in metalloenzymes. X-ray crystallographic structural analysis on model compounds illustrated cubane motifs in early proposals. However the crystallographic structural solution of the PSII enzyme implicated an additional pendant or "dangler" manganese. The structure featured terminal water molecules bound to both the cubane-corner-bound calcium atom and the dangler, and also revealed likely coordination modes of amino-acid residues to the complex.[484,518]

5.2.2. Barber-Iwata and related macromolecular crystal structures

The first published PSII structure at 3.5 Å in 2004 from Ferreira et al brought the discussion of OEC structure back to the heterocubane. As illustrated in Fig. 69, the crystallographic model described a heterocubane cluster of three manganese ions at three metal corners of the cube, and with the Ca^{2+} ion into the fourth corner, and a curious pendant or "dangler" manganese 3.3 Å away

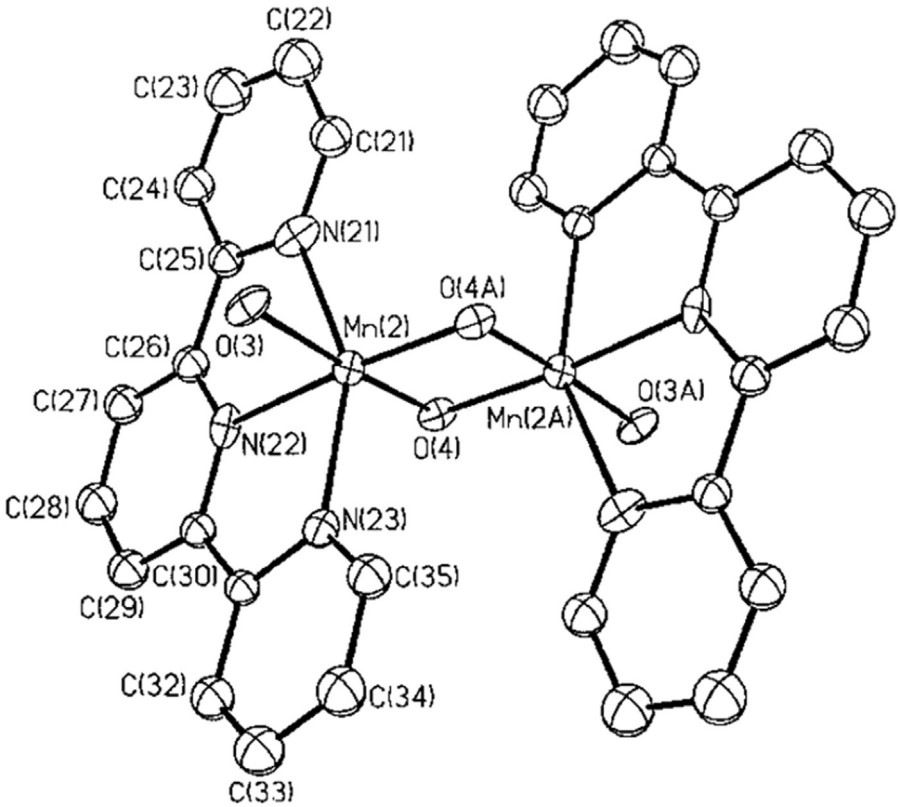

Fig. 68. The $[(OH_2)(terpy)MnO_2Mn(terpy))OH)_2]^{3+}$ dimeric oxygen evolving cluster of Crabtree and Brudvig. Hydrogen atoms omitted for clarity. Reproduced with permission from the American Association for the Advancement of Science.[490]

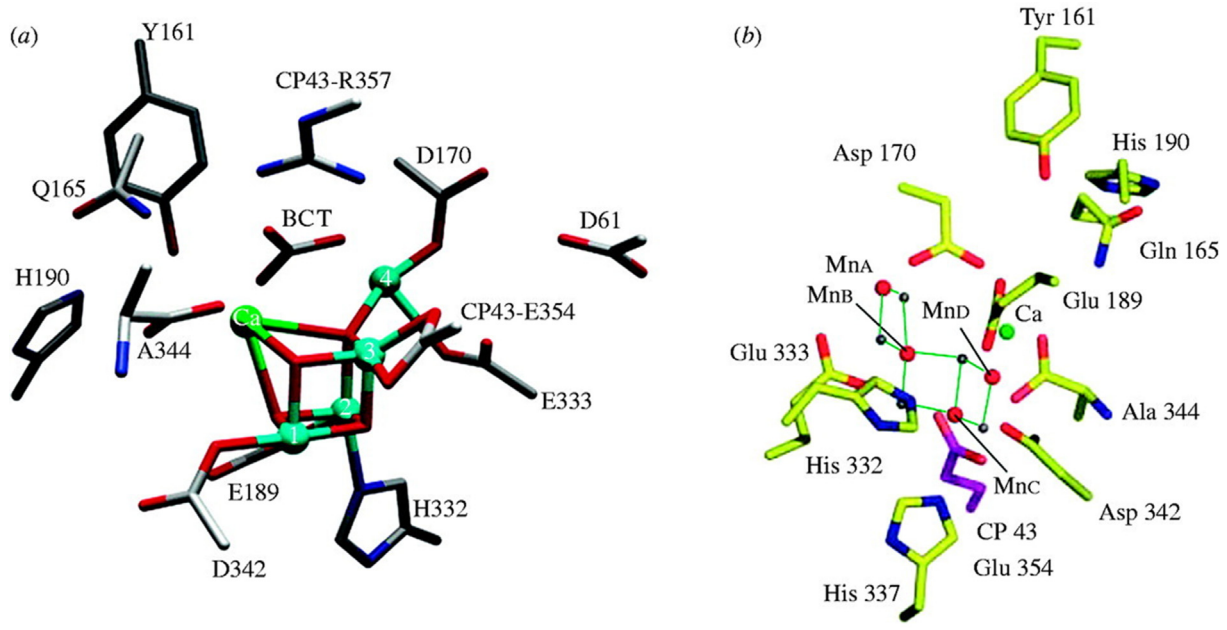

Fig. 69. (a) Structure of the OEC based on the X-ray diffraction measurements done by Barber and co-workers[516] and (b) the revised model of Yano et al from polarized Mn-EXAFS[522] and the 3.0 Å resolution X-ray structure of Loll et al.[521] Reproduced with permission from the American Chemical Society[523] and the American Association for the Advancement of Science.[484]

from the corner manganese atoms.[519] However, problems with the resolution of this crystal structure at 3.5 Å were a commonly cited concern, some suggested that the cubane-like crystallographic model was not yet a definitive structure. The too-long Mn-Mn contacts in the crystallographic model suggested that the heavily dosed crystals feature a larger cluster than those studied by the smaller-dosed XAS samples, implicating cryoreductive damage to the OEC during which the high-energy X-ray photons ionize atoms, and that the resulting high-energy electrons reduce the OEC to a lower oxidation state.[520]

As described at the end of the previous section, around the same time as the release of the Barber structure, the group of Britt released a new model of the S_2 state based on fitting to EXAFS and EPR data that represented a remarkable qualitative match to the new crystal structure: a hemicubane complex with a dangler manganese; Britt's group proposed this structure without knowledge of the new X-ray structure since the new structure work was mentioned as an afterthought in a note in revision[514] and was in press at the time. Unlike the X-ray crystallographic model, this proposal placed the calcium away from the hemicubane core, and also included a Cl^- ion in the model (Fig. 59), which is now known to be located distally from the OEC.[434] Another 3.0-Å-resolution X-ray diffraction analysis published the following year showed a similar overall arrangement of metal atoms, but significantly different interatomic distances,[521] supporting instead a distorted cubane structure. Around the same time in 2005, Yano et al released new high-resolution EXAFS analysis and proposed a similar model (minus the calcium) among the most likely structural candidates.[522] However, the following year, the same group proposed a revised model of the OEC geometry with similar relative atom placement to the crystallographic structure of Loll et al,[521] but with the overall geometry opened up into a dimer of dimers type model.[484] The authors argued that this geometric change with shorter overall interatomic distances was consistent with EXAFS data whereas the structural metrics of the crystallographic cubane models were too large.

The structure of Barber showed early crystallographic evidence for a cubane arrangement of the OEC, which was first proposed by Brudvig and Crabtree in 1986 using EPR spectral data from the S_2 state (Fig. 56).[479] Although this proposal involved a structural conversion between an adamantane Mn_4O_6 and cubane Mn_4O_4 complex, it represented an important historical proposal for the cofactor structure. Christou and Dismukes supported the probability of this cubane structure in their respective model complex chemistries,[524,525] and the group of Armstrong demonstrated the viability of a redox-dependent cluster structure in adamantine-type model complex chemistry,[480] but it was the X-ray crystallographic structure reported in 2004 that led to the first steps on a path to consensus despite concerns about cryoreduction.[526] The cubane structure of the OEC was reaffirmed again in 2007 by Kargul et al who solved the first crystal structure of the catalytically active Sr^{2+} substituted enzyme, and observed a similar placement of the Sr^{2+} cation 3.5 Å away from the Mn cluster.[523] However, none of these X-ray structures featured well-resolved oxygen atom locations, and none matched the EXAFS data, suggesting cryoreduction is a perpetual problem in X-ray crystallographic analysis of the OEC. This challenge left the cubane assignment of OEC geometry somewhat in doubt for some time.

5.2.3. Umena structure and use of slide-oscillation to reduce X-ray damage

Crystallographic data had previously supported cubane geometries proposed from biophysical and model chemistries for the Oxygen Evolving Complex, but reliance on low-resolution crystal data left plenty of room for doubt.[518,521,527] Then Umena et al[434] reported a structure of the OEC starting at the S_1, dark-adapted, state using XRD data at 1.9 Å resolution using Synchrotron radiation, and they mitigated the problem of X-ray damage by using a large crystal and a small beam, which permitted the local position of interaction of the X-ray beam with the crystal to be varied such that the beam was always striking "fresh" solid sample. This so-called "slide-oscillation method" greatly reduced the level of X-ray damage to the crystals, significantly mitigating the problem of cryoreduction-induced X-ray damage.[434] The higher-resolution structure featured resolved oxygen atoms, and more confidently located the calcium atom. This higher-

resolution structure also at last identified the location of the Cl^- ion in a proton conduction channel, implicating it as a charge-balancing counterion in proton shuttling as opposed to a component of the OEC. The structure reaffirmed the cubane cluster core, the corner calcium, and the dangler manganese. In addition, it unveiled oxygen locations, and water or hydroxide ligands bound to the calcium and the pendant manganese atom (Fig. 70).

Despite the groundbreaking quality of the Umena structure, concerns remained about radiation damage. While the new model was much more satisfactory in comparison to EXAFS data and theoretically calculated expectations,[528] bond lengths remained overall too long in comparison with XAS data, suggesting to many that cryoreduction was still a problem despite the reduced X-ray damage.[529] Theoretical examination of the crystallographic model suggested that the OEC was cryoreduced by as much as three full electrons, making the oxidation state formally 2-Mn^{II}:2-Mn^{III}, or the "S_{-3}" state.[530] Experimental examination of the OEC by XAS after controlled exposure experiments suggested it could be reduced even farther — entirely to the all-Mn^{II} state — while still maintaining diffraction-quality crystals.[520] Despite the recapitulation of a cubane geometry in the Umena et al structure, doubt about the cubane geometry persisted due to the continued concerns of X-ray damage by cryoreduction of the OEC. Ames et al[478] performed geometry optimization of the OEC in the S_2 state using the BP86 density functional, and predicted that the crystallographic structure is more stable if opened up into the popular dimer-of-dimers structure.[468,470,484,489,491,494]

Hybrid density functional theory (DFT) geometry optimizations also showed some disagreements with the new structure from Umena et al. For instance, the XRD bond length of the Mn_1-Mn_3 bond was reported as 3.3 Å, while geometry optimizations using a B3LYP functional and lacvp basis set of an S_0 model using coordinates from Umena et al showed a shorter distance of 3.19 Å.[531] This study indicated that a hydroxide at Mn_4 with a distance of 2.5 Å from the calcium atom was inconsistent with the S_1 oxidation states.[531]

While X-ray damage remained a worrisome problem (to which most attributed the XRD-EXAFS mismatch) several other groups proposed an alternative explanation: that the presumed oxidation state of an all-Mn^{IV} cluster for the S_1 state — a longtime consensus of the community — was in need of reevaluation, and that the actual operative forms of the OEC are in reality *two electrons more reduced* than previously believed.[507,532–535] These groups have thus argued that the longer bond metrics resulted not from a cryoreduced S_{-1} state for example, but actually the proper oxidation assignment for the S_1 state. This argument was also supported by reconsiderations of the XAS and RIXS and NIR data,[532–534] EPR data,[533,536] OEC cofactor maturation experiments,[537,538] water exchange rates,[539] and DFT studies,[507,532,535] yet still remains controversial. This so-called "low-oxidation-state paradigm" describing the OEC oxidation states as two-electrons more reduced than traditionally believed will be discussed in more detail in Section 4.2.3.

5.2.4. Femtocrystallography using the X-ray free electron Laser [473,517]

The X-ray Free Electron Laser (XFEL) has been introduced for better high-intensity data collection, introducing a new technique termed serial femtosecond crystallography (SFX) sometimes referred to as "diffraction before destruction".[478,521,540] Femtosecond, ultra-bright X-ray pulses reduce radiation damage since the pulses are short enough to allow diffraction data to be collected before the sample is damaged. These methods have been used to fine-tune the structural model of the OEC,[473] and obtain X-ray data on higher S-states for the first time ever,[517,541,542] and even visualize possible mechanisms of O-O formation.[541,542] As such, femtocrystallography has revolutionized macromolecular structural determination of the OEC more than any other technique.

The most resounding observation to be made about new macromolecular structures in the age of the XFEL, is that the cubane geometry is further strengthened as a consensus. Each of the new high-resolution XFEL structures uncovers essentially the same cubane-with-dangler geometry unveiled in the Umena et al report using slide-oscillation (Fig. 71),[434] albeit with significantly reduced interatomic distances, suggesting the approach is successful at further mitigating X-ray damage to the sample during collection.

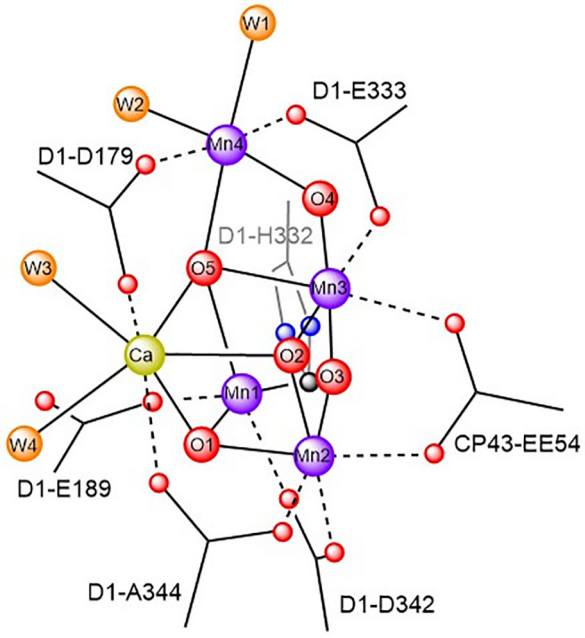

Fig. 70. Crystallographic model of the OEC from Umena et al obtained using Synchrotron radiation with slide-oscillation, and illustrating the proposed Mn_3CaO_5 heterocubane structure with pendant manganese atom.[434]

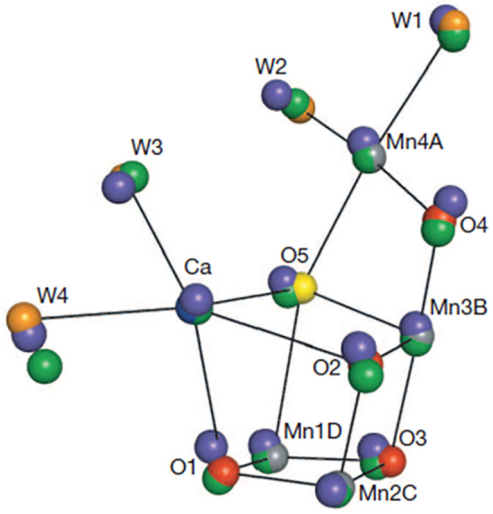

Fig. 71. Comparison of the two OEC structures using XFEL,[473] and one using synchrotron radiation.[434] Atoms from the XFEL structures from Suga et. Al.[473] are colored by atomic element. Atoms from a second, smaller XFEL dataset of Suga et al are colored green, and data from synchrotron radiation with slide-oscillation are labelled in Purple.[434] Image reproduced with permission from Springer-Nature.

Following the initial high-resolution structures from Umena et al,[434] it was found that the OEC had been reduced by cryoreduction to the S_0 state[531,543] or lower,[520,530] even using the reduced-intensity X-ray doses from stage-oscilation. Since it had been noted that the threshold of reduction for OEC was below 0.12 MGy — well below the dose encountered in the Umena structure, this clearly indicated that the slide-oscillation structure of Umena et al had also experienced significant cryoreduction from X-ray exposure. It was initially presumed that the use of the XFEL might solve this problem entirely.

This new XFEL structure featured revised atom locations that improved the fit with EXAFS data, yet retained the overall structural motif from the original Umena XFEL structure, further solidifying the relevance of the cubane motif under reduced X-ray damage. B3LYP DFT geometry optimizations on this structure [473] resolved some conflicting Mn–O–bond distances between computational and XRD methods.[543] Some differences between XRD and predicted structure from theory were noted. Refinement of the structure Hybrid B3LYP DFT[531] and QM/MM[540] methods resulted in the loss of the a Mn–O–Mn contact that is present in the XRD S_1 structure results.[434] One Mn···Mn distance from XRD, reported as 2.5 Å, was actually predicted to lengthen to 3.0 Å by both DFT and QM/MM.

However, despite the use of the XFEL to mitigate concerns, the possibility of X-ray damage still cast doubt on these findings, and it was later confirmed from Suga et al. that the XRD data experienced at least some damage from the high energy X-rays, despite the use of the XFEL technology.[541] Following this, UB3LYP DFT geometry optimizations were calculated for a new XFEL structures of the S_1 and S_3 states[544] that exhibited a rather puzzling missing hydroxide on Mn1 at the S_3 state.[545] It was determined through the study that the lowest energy description for this XFEL structure [544] without this hydroxide was found to be 18.1 kcal/mol higher in energy than the model[473] with a hydroxide.[545] Thus, the crystallographic structure for S_3 without OH can be likely ruled out energetically.[545] These studies illustrate the rapidly changing results and paradigms of the OEC as instrumental methods improve.

Evidence from studies of other proteins have supported concerns that even the XFEL structures experience some X-ray damage. An early concern came from XFEL studies on ferredoxin crystals that showed that X-ray damage still occurs in single crystals during a short pulse, potentially altering electron density distribution prior to complete crystal destruction.[546] There is some evidence that suggests there can be rapid diffusion of oxygenic free radicals through the sample.[547] This shows a possibility of contamination since oxygen atoms are observed to be added to the protein residues.[548] Other reports indicated cryoreduction of the OEC itself, and that the structural metrics in (presumed) S_1 state structures were a better fit to the S_0 state than the dark adapted S_1 state.[549] Several very-low-exposure synchrotron datasets are consistent with these explanations, as these low-dose datasets exhibit structure models at exposure levels comparable to those used for EXAFS.[550].

While it may ultimately be impossible to collect a high-resolution X-ray structure without X-ray damage, the picture of the OEC has become clearer and clearer over the past decade with X-ray doses and damage becoming better and better mitigated. What remains to be agreed upon is how the structure of the OEC changes between transition states, and the mechanism of O-O formation, though excellent progress has been made in this area in the past few years. For studying the $S_1 \rightarrow S_2$ transition, most contributions have been made using Fourier transform infrared spectroscopy (FTIR),[552,553] extended X-ray absorption fine structure (EXAFS),[525,554,555] and EPR.[556] Inducing changes in PSII using a two-flash illumination before XFEL crystallographic analysis, Suga et al noted electron density changes around the Q_B/non-heme iron and the Mn_4CaO_5 cluster. Due to the disappearance of a water molecule 3.5 Å away from the cluster, they concluded that protonation of hydroxide and dissociation of the resulting water ligand also occurred during the two-flash illumination.[541] These findings have been in support with previously proposed mechanisms of O-O formation involving O5 (see Fig. 71), which will be further discussed in Section 4.2. [543,557]

Isomorphous difference Fourier analysis is another technique that has provided significant insight to the changes in transition states of the Oxygen Evolving Complex using crystallography. This technique permits the observation of small differences in electronic density in structures with the same cell parameters and orientation.[551] Using these methods, it was shown that the $S_1 \rightarrow S_2$ transition exhibits a displacement of the dangling 4th manganese from the protein membrane and its movement to the coordination mode of an ideal octahedron.[540] Several recent serial femto-crystallography experiments have permitted the visualization of higher-S-state structures, and the assignment of electron density Fourier difference peaks to oxygen atoms participating in O-O bond formation, though individual accounts differ in the assigned location of the attacking oxygen atom [541,542,558] These results and full implications of the various reports on the mechanism of O-O bond formation will be discussed in Section 4.2, Mechanism of the OEC. Nevertheless, analysis of XFEL structures has limitations, especially when arguments about the small changes in electron density resulting from Isomorphous Fourier difference analysis are the crucial findings. Since there is not a sufficient signal in individual XFEL images at high resolution, the averaging of multiple images from multiple crystal samples is required to better resolve small differences in electron density in Fourier difference analysis, especially those used to identify shifting atoms in transitions between S-states.[551]

5.2.5. Model complexes inspired by high-resolution macromolecular crystal structures

The structure of Ferreira et al,[516] displaying a corner calcium ion, a dangler manganese atom, and no cluster-incorporated chloride (Fig. 69), gave the synthetic community a more concrete target for biomimetic synthetic compounds. And while initial concerns about the relevance of this structure due to X-ray damage were justified, the overall atomic arrangement has withstood the test of time (as outlined in the previous section), and as such the synthetic target has not changed over the course of the past decade and a half. It has been an intention of the scientific community to introduce the 4th dangler manganese ion once its importance to photosynthetic water oxidation was known.[559–566] Studies of binding of ammonia in competition with water[560,561] suggest that water coordinates to the 4th manganese ion during water oxidation catalysis (ammonia binding will be further discussed in section 4.2.2). Selected examples of the progress in synthetic chemistry inspired by crystallographic developments are presented in this section.

A necessary component of any OEC model is a calcium ion, which has a crucial role in the OEC, especially in the formation of the S_3 state.[567] Its incorporation adds asymmetry to the structure that is integral for the oxygen evolving complex.[554,568–570] This is supported by studies that show decreased oxygen evolution when a Sr^{2+} ion replaces the Ca^{2+} ion.[571,572] Some examples of $Mn^{II}Ca^{II}$ complexes[573] are too reduced to be relevant to OEC turnover, but are potentially related to early stages of photoassembly of the OEC from dissolved Mn^{2+} ions. The lab of Christou was the first to incorporate a calcium atom into a cubane

fragment of a higher oxidation state MnO cluster.[194] This system involved a larger Ca_2Mn_{12} cluster that nevertheless contained an internal $CaMn_3O_4$ cubane fragment with additional neighboring dangler-like manganese ions with interionic distances similar to that of the OEC (Fig. 72). Magnetic susceptibility suggested very strong antiferromagnetic coupling within the cluster, giving a ground spin state of S = 5/2. As such, the cluster was not a precise model, but more accurately "contained" an accurate model fragment within a larger cluster. The result is consistent with the high degree of antiferromagnetic coupling observed in the EPR spectrum of the OEC.

In light of increasing crystallographic evidence for cubane structure of the OEC, this and several other groups have since published additional papers on Ca-containing Mn cubane models with improved accuracy. The first isolated $CaMn_3O_4$ single-cubane cluster was from the group of Agapie, and featured a trigonally symmetric 1,3,5-triarylbenzene functionalized with six pyridine and three alkoxide ligands.[136] This trigonal template permitted the formation of a voided-cubane architecture, followed by the controlled insertion of either a manganese or a calcium ion into the 4th metal site (Fig. 73). These models showed that alteration of the identity of the corner metal atom altered the reduction potential of the cluster, suggesting a potential role for the calcium ion of tuning redox potentials for efficient electron transfer and catalysis. Further structural modifications permitted the addition of a "dangler" silver ion in a similar location to that of the pendant manganese atom of the OEC.[574]

At almost the same time, the group of Christou published another cubane cluster [164] containing a calcium ion on one corner, and a second dangling calcium (but not manganese) ion (Fig. 74). This cluster exhibited a ground-state S = 9/2 spin manifold examined by both magnetometry and EPR spectroscopy. The

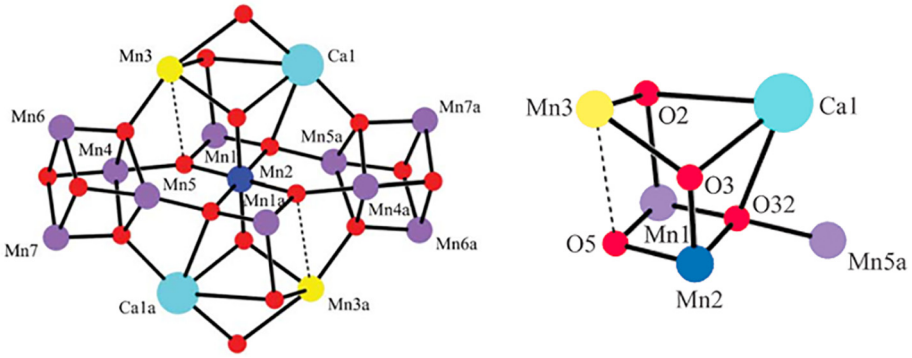

Fig. 72. (Left) core atoms of the $[Mn_{13}Ca_2O_{10}(OH)_2(OMe)_2(O_2CPh)_{18}(H_2O)_4]$ cluster of Mishra et al.[194] (Right) view of the atoms from the upper cubane fragment showing analogous atomic arrangement to the OEC. Reproduced with permission from the Royal Society of Chemistry.

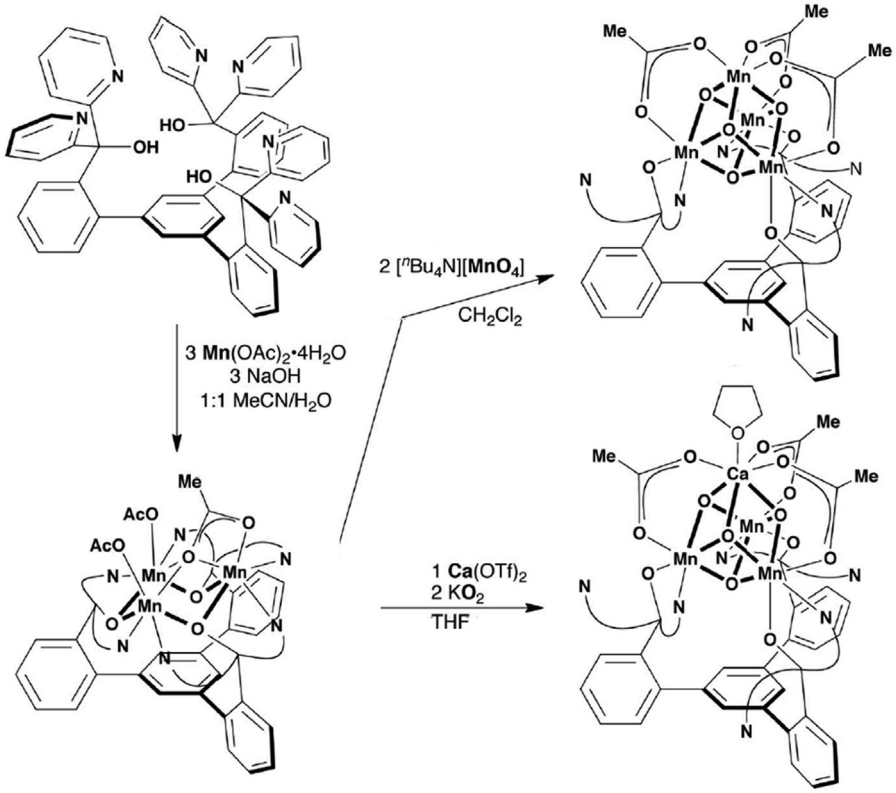

Fig. 73. Preparation of the MMn_3O_4 clusters of Agapie.[575] M = Mn, Ca. Adapted with permission from the American Association for the Advancement of Science.

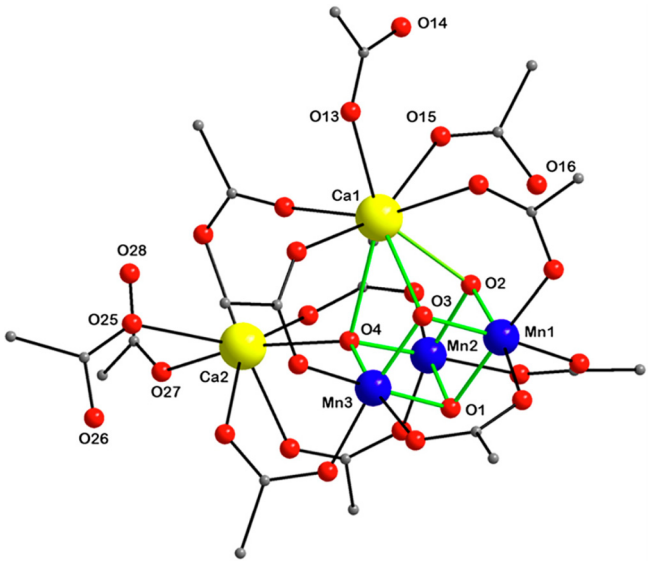

Fig. 74. Structure of Mn_3Ca_2 cubane cluster from Mukherjee et al.[493] Reproduced with permission from the National Academy of the Sciences of the USA.

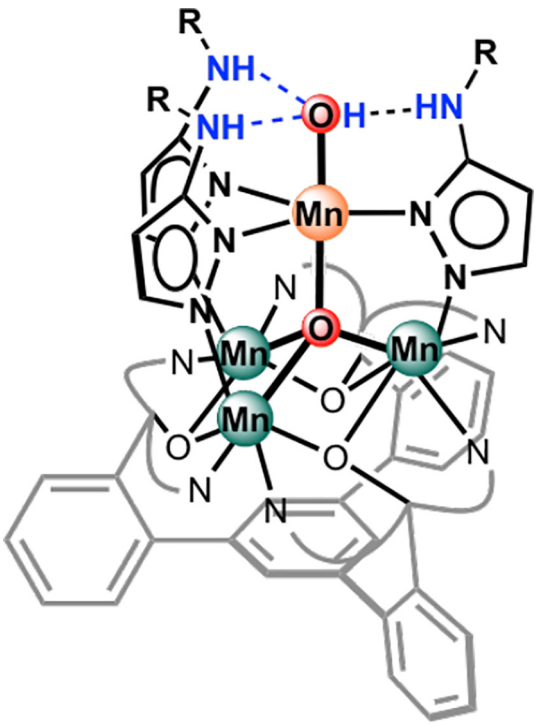

Fig. 75. Tetranuclear dangler system of Han et al. Reproduced with permission from the American Chemical Society.[577]

EPR spectrum exhibited both a low-field signal around g = 8, and another around g = 2 resulting from the thermally populated spin manifold of a S = 9/2 system of Mn^{IV} ions with strong ferromagnetic coupling. Another ether example of a (non-manganese) dangler ion at an OEC models is one containing a pendant strontium ion from Cheng et al,[576] and one including a calcium ion from Mukherjee et al.[493]

Biologically relevant cluster systems with a single pendant manganese atom are rare. The group of Agapie reported the use of a tripodal triarylbenzene-based ligand to template a trinuclear (non-cuboidal) cluster through pyridyl and alkoxide ligands, with a single bridging inorganic oxide between the metal centers. Pendant pyrazolyl ligands at the ligand periphery permitted the addition of a fourth dangler metal (Fig. 75), which in the case of the manganese system, resulted in a catalyst that could oxidize water to peroxide.[577]

The group of Zdilla reported a Li-Mn-N^{t}Bu cubane cluster with a pendant Mn≡N group. Though the dangler manganese of this cluster differed in geometry from the OEC and this cluster featured Li Lewis acid incorporation (instead of Ca). A biomimetic four electron reductive elimination of azo-*tert*-butane ensued upon the removal of the lithium Lewis acid cation (Fig. 76). This reaction represents a nitrene analog of the four-electron reductive elimination of O_2 from OEC oxide ligands.[174] The resulting cluster-based product is a simple manganese-imide cubane cluster of formal Mn^{IV} ions. The pseudotetrahedral geometry of the Mn ions brings them much closer to one another in the interior of the cluster than what is observed in the more common six-coordinate manganese clusters and in the OEC. As a result, neither ferromagnetic nor antiferromagnetic coupling, but instead full Mn-Mn bonding is invoked to describe the interaction between the manganese *d*-electrons. A full complement of six covalent Mn-Mn bonds is formed, evidenced by the temperature independent diamagnetism, suggesting full pairing of all d-electrons in this idealized 60-electron[39] cluster (see section 2.1).

When this synthesis is performed in the presence of trace water, a biomimetic cubane cluster with a dangler Mn=O moiety is obtained.[175] Water protolyzes the pendant $Mn(NR)_3N$ fragment (Fig. 77) to give an $[O_3Mn^{VII}N]^{2-}$ tetrahedral metalloligand that incorporates into the bridging positions of the cluster. Being that it is the same charge, and almost identical size and shape to the *tert*-butylamido ligand, this fragment incorporates into the cluster at random, giving a mixture that is approximately 90% the all-*tert*-butyl cluster, $Mn_4(\mu_3\text{-}N^tBu)_4(N^tBu)_4$, <10% singly-incorporated cluster, $Mn_4(O_3Mn^{VII}N)(\mu_3\text{-}N^tBu)_3(N^tBu)_4$, and trace amount of multi-incorporated clusters with more than one metalloligand. This results in the presence of about 10% of the $Mn_4(O_3Mn^{VII}N)(\mu_3\text{-}N^tBu)_3(N^tBu)_4$ cluster, containing a biologically inspired pendant Mn=O group, related to the proposed active intermediate of the so-called "nucleophilic attack" mechanism of the OEC [557,578,579] (the nucleophilic attack mechanistic proposal will be discussed further in section 4.2.2). While this compound has not been shown to oxidize water, the pendant manganese moiety is reactive with alkenes, and leads to dioxygenated products such as diketones and diols.[175]

In general, there is a paucity of biomimetic synthetic manganese cluster systems that can oxidize water[580,581] and even among them, a dearth of OEC model complexes that are both structural mimics, and reactive mimics. A possible exception is illustrated in a report of the most structurally accurate biomimetic model reported to date: the cluster of Zhang et al,[582] which features a nearly perfect topological and compositional map of the OEC, including carboxylate-based ligation, a corner calcium atom, and a dangler manganese bridged by a carboxylate (Fig. 78). A solution of the product showed a pair of EPR signatures (Fig. 79) strikingly similar to those of the S_2 state of the OEC (see Fig. 54 in section 4.1). The authors further claim four biomimetic S-states based on cyclic voltammetry, and catalytic water oxidation capability. While this model clearly features the most striking similarity to the OEC of any reported system, a number of major concerns exist, including the poor quality of the crystal structure (R_1 > 16%), incomplete characterization (including a complete lack of purity assessment), a standard CV whose oxidation and reduction waves do not integrate to one electron each as claimed, and a catalytic CV showing an onset potential for catalytic water oxidation below the thermodynamic potential of 1.23 V vs. NHE (a physical impossibility).

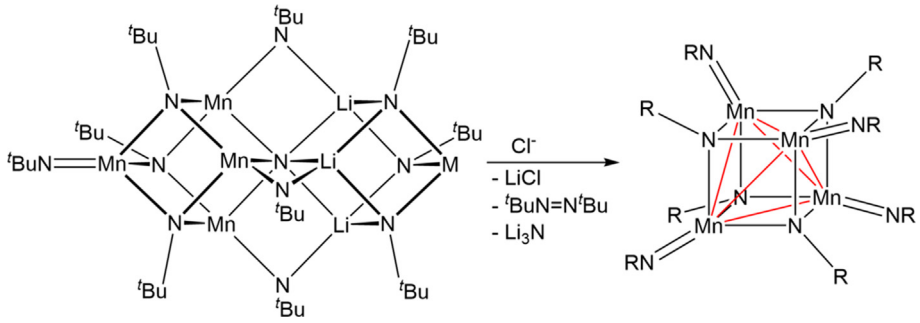

Fig. 76. Reductive elimination of azo-*tert*-butane from a manganese imide cubane, triggered by removal of lithium. M = Li or pendant Mn≡N group. A cubane cluster with six covalent M-M bonds is formed.[174]

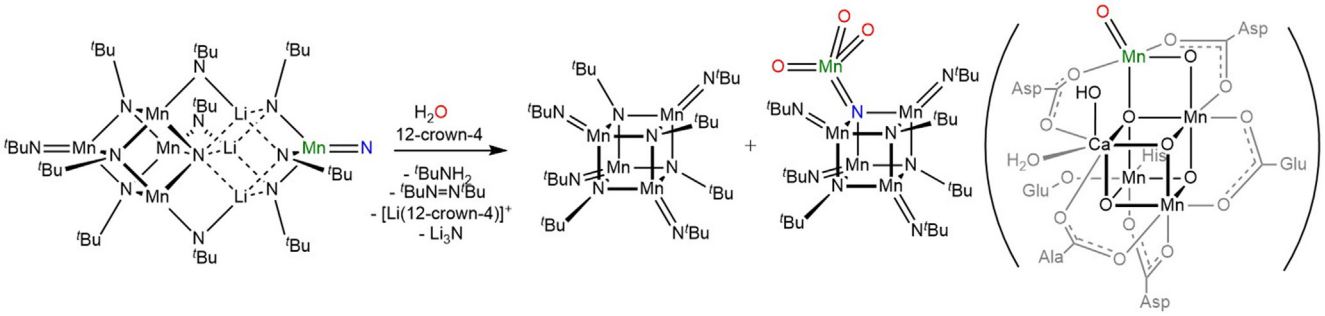

Fig. 77. Formation of a pendant-Mn=O containing cubane cluster from Vaddypally et al[175] by partial hydrolysis of a precursor dicubane cluster, and comparison to a proposed "nucleophilic attack" intermediate of photosystem II (in parenthesis).

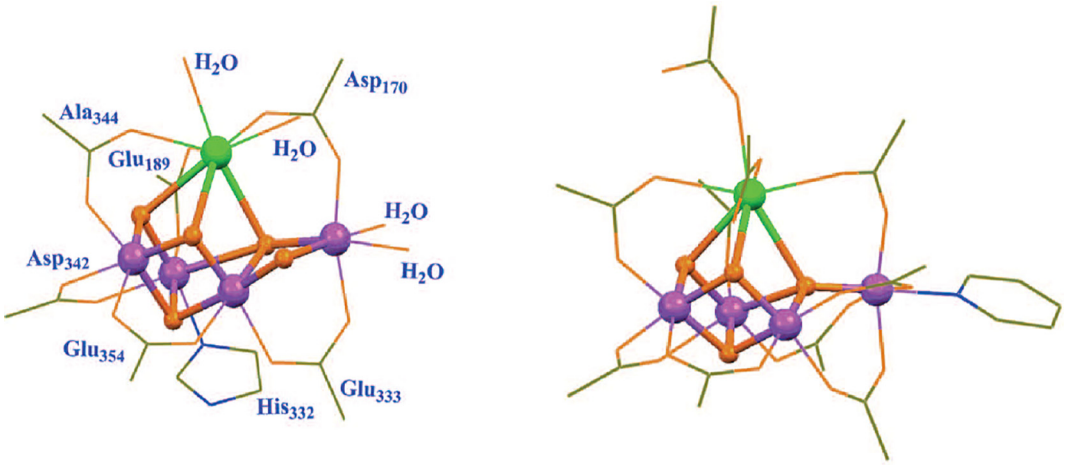

Fig. 78. Comparison of the OEC (left) to the $Mn_4CaO_4(Bu^tCO_2)_8(^tBuCO_2H)_2(py)$ cubane model cluster of Zhang et al.[582] Figure reproduced with permission from the American Association for the Advancement of Science.

5.3. Proposed mechanisms of the OEC

The cubane geometry is pervasive across redox catalysis in biological enzymes. Yet, the relevance of the cubane cluster in catalysis extends to synthetic and solid-state systems as well.[207,583–586] It has been well documented that the OEC cycles through at least five redox states via photon-driven oxidation, denoted S_0, S_1, S_2, S_3, S_4 (See Fig. 55).[447] This repeating cycle serves as the foundation of empirical and theoretical methods that aim to study the OEC, with the S_4 state the area of focus for O-O bond formation mechanistic considerations. Recent studies supporting various mechanisms of O-O bond formation (Fig. 80) in the context of the consensus OEC cubane structure and water splitting at biomimetic catalysts will be introduced and discussed in this section. Earlier mechanisms proposed at pre-crystallographic non-cuboidal OEC proposed structures are not covered here, but have been discussed in previous papers.[494,587,588] An excellent review on proposed mechanism of a wide array of water oxidation catalysts using varied transition metals is worth noting.[589]

5.3.1. Nucleophilic attack mechanism

One of the earliest mechanisms proposed for O-O bond formation in the cubane cofactor was the so-called nucleophilic attack mechanism (See Fig. 80), originally proposed by Brudvig and McE-

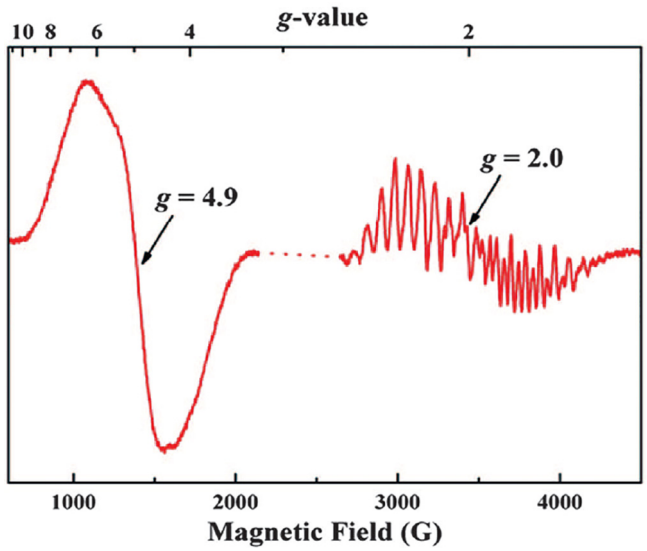

Fig. 79. EPR spectrum of the $Mn_4CaO_4(Bu^tCO_2)_8(^tBuCO_2H)_2(py)$ cubane model cluster of Zhang et al.[582] showing remarkable similarity to the EPR spectrum of the S_2 state of the OEC (Fig. 55). Figure reproduced with permission from the American Association for the Advancement of Science.

voy.[523] This mechanism proposed a highly intuitive role for both the pendant manganese and the calcium ion. The proposed role of the pendant manganese is to stabilize an electrophilic oxide bound to a Mn^V center in the S_4 state, while the calcium ion's role is to carry a nucleophilic hydroxide, as is commonly found in calcium-based hydrolases such as Staphylococcal nuclease.[593] Similar mechanisms have also been proposed for the activity of non-manganese water-oxidizing systems such as copper,[594] iridium,[594] iron,[595,596] ruthenium,[597,598] cobalt[599] and others.[589] The plausibility of a nucleophilic attack mechanism at manganese is supported by a few synthetic studies, including one from Åkermark where a solution-phase Mn^V=O moiety was stabilized by a corrole ancillary ligand. This system forms O_2 by reacting with solution-phase hydroxide[600] (Fig. 81). A catalytic water oxidation system from Mohamed et al[601] was also proposed to occur through a nucleophilic attack mechanism. In contrast, work from one of our groups isolated a cubane cluster with a Mn^{VII}=O moiety, which did not generate detectable O_2 when reacted with water or hydroxide ion, even though a Mn^{VII}=O unit is expected to be much more electrophilic than the putative Mn^V=O responsible for S_4 state turnover in this proposed mechanism.

Although the nucleophilic attack mechanism has garnered much support, particularly from the synthetic inorganic chemistry community, this mechanism has been claimed to be a near impossibility by some in the computational community due to the high energy barriers.[557,603] This mechanism was calculated to have an incredibly high activation energy (29.8 kcal/mol being the lowest) compared to the oxyl-oxo mechanism coupling mechanism predicted by Siegbahn to have a much lower barrier (6.2 kcal/mol, vide infra). The rationale for this high barrier for the water attack mechanism is that a transition between two potential energy surfaces with different spin is required. Very poor energetic stabilization occurs upon the formation of the product O-O bond on this spin surface.[603] While the synthetic inorganic chemistry

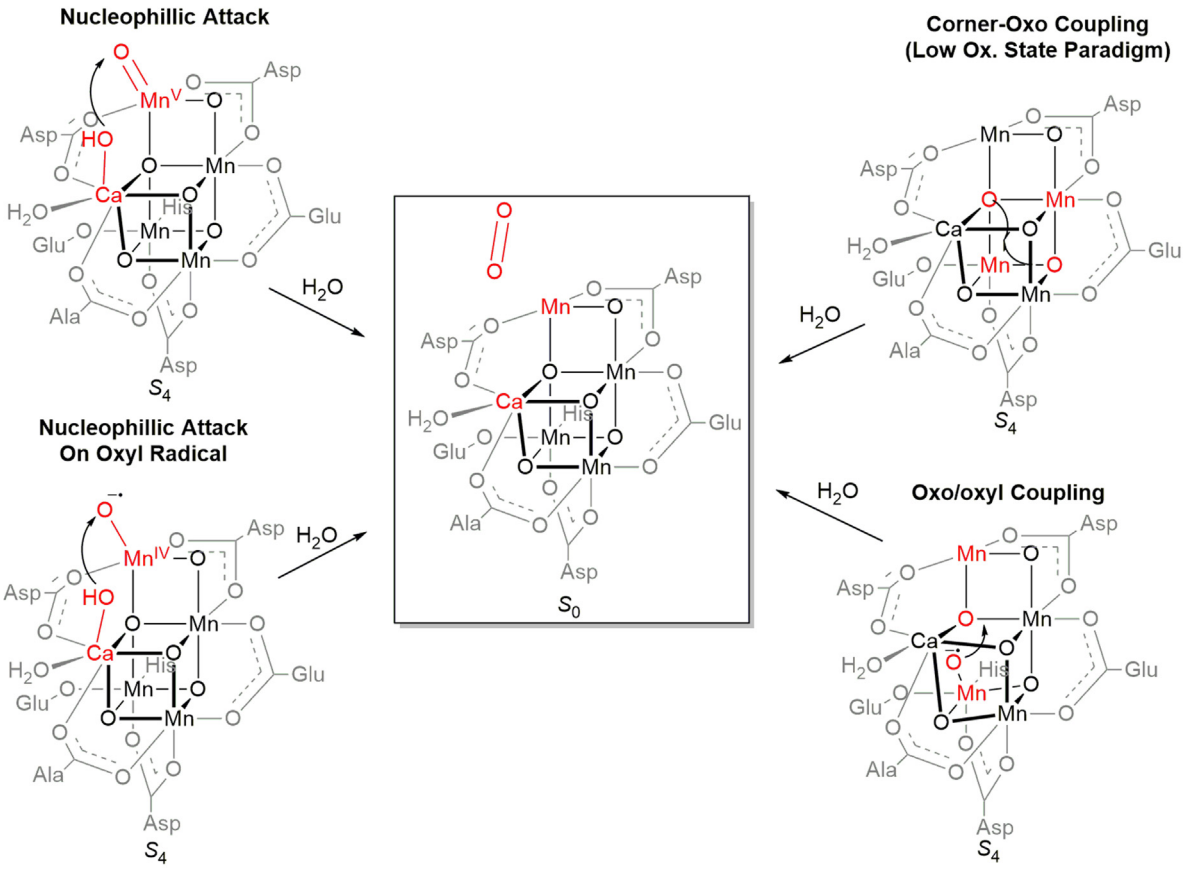

Fig. 80. Illustration of several proposed mechanisms of O-O bond formation supported using theoretical methods. These include the nucleophilic attack,[590] modified nucleophilic attack/oxyl radical,[591] oxo-oxyl coupling,[592] and corner oxo coupling/low-oxidation-state paradigm.[507]

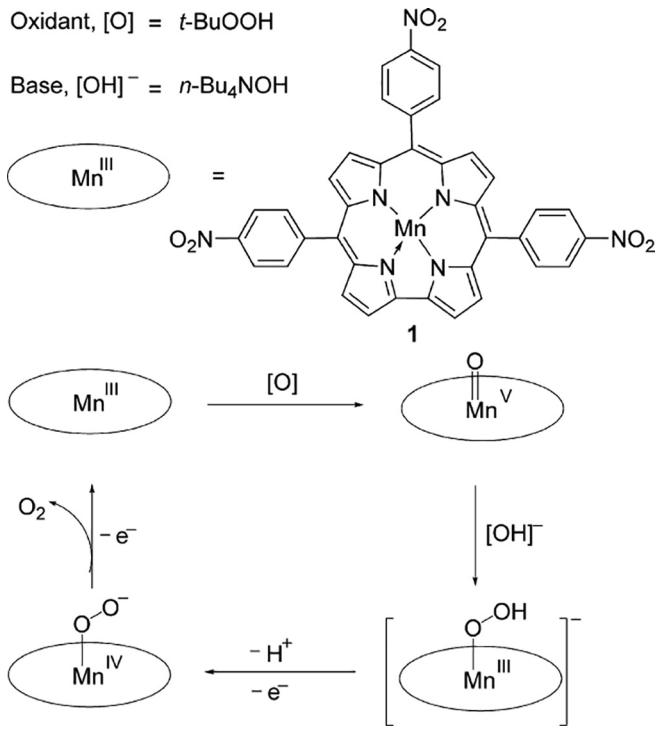

Fig. 81. Proposed mechanism for water oxidation via nucleophilic attack by OH^- on a Mn^V = O oxide.[602]

community has tended to favor the nucleophilic attack mechanism, the theoretical and biophysical communities have tended to support a radical coupling mechanism involving a requirement for radical character on the oxygen atom(s) for bond formation. However, the description of spin delocalization onto oxygen in Mn^V=O systems was disfavored by spectroscopic characterization of a Mn^V=O model complex by the group of Borovik, which demonstrated a paucity of radical character on the terminal oxo as determined from the extent of magnetic hyperfine interaction between an isotopically labelled ^{17}O nucleus and the unpaired electrons (Fig. 82).[604] It has also been proposed that a nucleophilic attack mechanism could be possible through a low oxidation paradigm [605–606] (See Section 4.2.3).

5.3.2. Radical mechanisms and ammonia binding studies

An alternative explanation that has gradually gained favor by many groups is that radical oxygen character is required for O-O bond formation in the OEC. Even the original proposers of the nucleophilic attack mechanism revised this to a version where the electrophilic Mn^V = O is better described as a Mn^{IV}-O·, a manganese(IV)-oxyl radical, but still receives a nucleophilic attack from a water oxygen atom.[591] Other mechanisms involve radical coupling with the central O5 oxygen atom of the OEC with one of the bridging oxide ligands[603] or with an incoming substrate water oxygen atom.[541,542] A longtime proponent of the oxyl-oxo mechanism has been Siegbahn. The proposed mechanism claims an oxyl radical in the center of the OEC (O5) forms an O-O bond with a bridging oxo group.[479,519,531,557,603,607,608] This radical mechanism, first proposed in 2006,[609] received early support, such as in the work of Batista et al who proposed the presence of an oxyl radical in the OEC mechanism.[524] Experimental data using W-band electron–electron double resonance (^{17}-OELDOR) detected NMR spectroscopy suggests the involvement of the bridging O5 in dioxygen formation,[610] which is more consistent with the diradical mechanism proposal of Siegbahn.[603] However, most of the recent computational endeavors studying the biological OEC rely on the newest and most reliable crystallographic data.[480,543,611] Newer empirical data coupled with computation has continued to draw support for the radical mechanism. For example, a broken symmetry DFT (BS-DFT) study of ammonia coordination indicated that ammonia binding occurred at the W1 ligand as opposed to O5 in the OEC.[612] Guo et al claimed these findings increase support for the oxo-oxyl coupling mechanism, for the calculated free energy barrier of 30 kcal mol^{-1} for ammonia entrance into the OEC was evaluated as forbidden. Another BS-DFT study from Lomiller et al[559] affirmed previous work[613] that Sr^{2+} substitution of the Ca^{2+} ion and NH_3 coordination do not change the geometric or electronic structure of the S_2 state significantly, supporting O5 as the exchangeable μ-oxo bridge and first area of substrate introduction.[560] Studies of methanol binding showed that structural flexibility is important for the OEC mechanism, which is best reflected in Siegbahn's model.[614]

Once the oxygen evolving complex reaches the S_2 transition state, water coordination and introduction pathways can shed light on the OER. Water binding mechanisms have been studied using ammonia substitution because of analogous electronic properties that make it a model marker.[561,562,615] Pérez-Navarro et al. [560] utilized pulsed EPR spectroscopy methods and mass spectrometry to study ammonia binding to the S_2 state, concluding that NH_3 replaces a terminal water ligand (W1), *not* substrate water, at the Mn_A *trans* to the bridging O5 ligand (Fig. 83). The study was accompanied by quantum chemical studies, yet these were restricted to only the W1 position, and the chosen model clusters were not large enough to include crucial hydrogen-bonding interactions with the bound ammonia ligand. EPR techniques combined with broken-symmetry DFT performed by Schraut and Kaupp showed ammonia displacing a water coordinated to the outer dangling fourth manganese (Fig. 83).[562] The computational finding

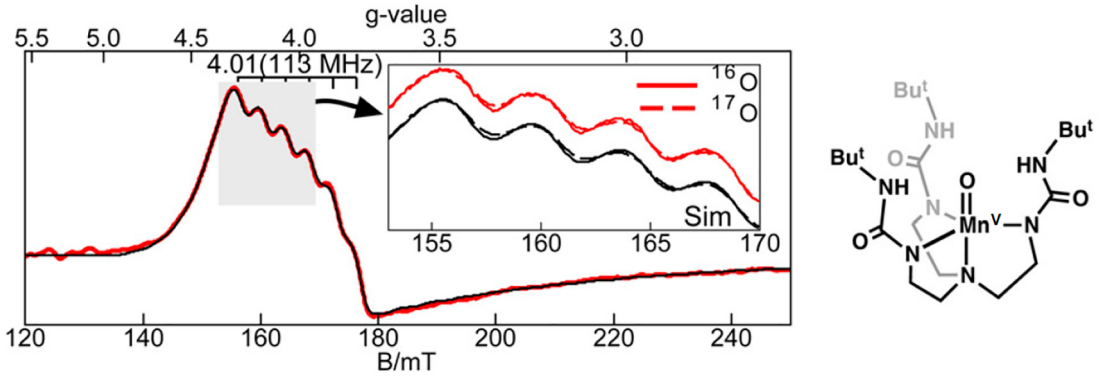

Fig. 82. EPR spectrum of Mn^VH_3buea(O) showing an essentially identical EPR signature for the ^{16}O and ^{17}O labelled metal oxide, suggesting minimal delocalization of radical character onto the terminal oxide. Adapted with permission from the National Academy of Science.[604]

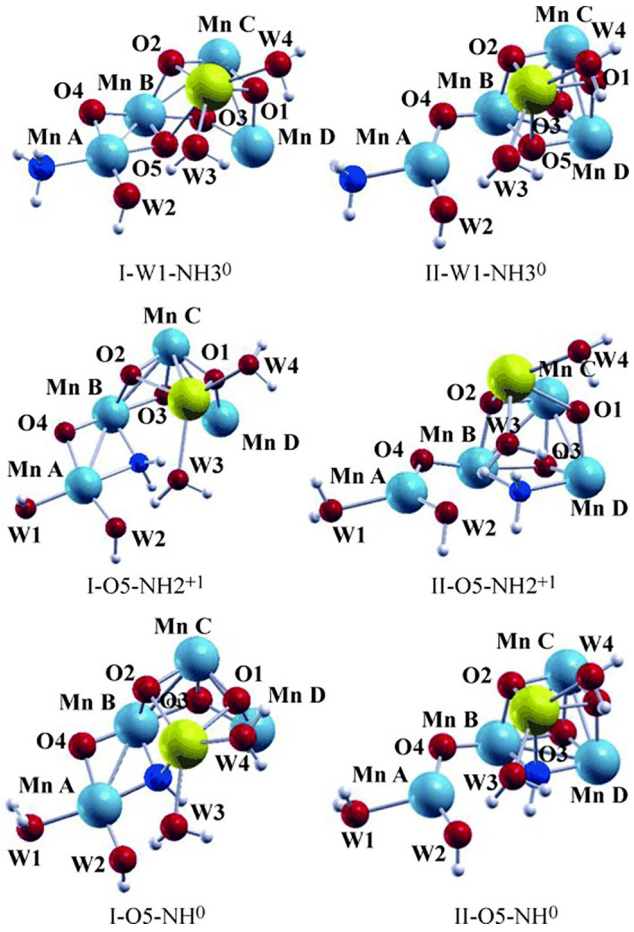

Fig. 83. Various proposals of ammonia binding to the OEC investigated computationally by Schraut and Kaupp.[562] Reproduced with permission from Wiley.

of substitution of bridging oxygen O5 by NH_2 found that the Mn_A–Mn_B distance increased by 0.12 Å (from 2.76 to 2.88 Å) upon ammonia binding, in agreement with an EXAFS study[616] (0.15 Å elongation). However, it has been claimed that that particular EXAFS study likely suffered unavoidable radiation damage [562] and the only binding mode consistent with EXAFS data (NH_2 bridging at O5), was calculated to be extremely unfavorable in energy in comparison to W1 terminal binding by about 20–30 kcal/mol.[562]

Ammonia binding was also found to occur in a secondary site (Fig. 84),[615] which the authors claim gives rise to an S = 5/2 spin state that occurs in the S_2 transition state. This coordination was used to explain the high spin S = 5/2 state in the EPR of ammonia-bound OEC[615] (in contrast to an alternative explanation given in the low-oxidation-state paradigm hypothesis, section 4.2.3). The ammonia is competitive with the chloride ion, which is approximately 7 Å from the 4th dangler manganese and has been shown to be intimately involved with its OEC function.[615] Combined with QM/MM modeling, it is proposed that ammonia replaces D1-D61 as a hydrogen bond acceptor that is associated with the chloride binding site.[567,617] Ammonia's binding to this secondary site of the OEC is thermodynamically driven by the > 120 mV (>2.7 kcal mol^{-1}) stabilization of S_2, whereas the binding of NH_3 to the primary site occurred at temperatures above 250 K. Additionally, in K317A PSII where there is no chloride within the OEC they found no binding of NH_3 in the secondary site, supporting their hypothesis that NH_3 competes with D61 as a hydrogen acceptor for W1 forcing its displacement (Fig. 84). This further illustrates the use of ammonia as a model binding tool [561,562,615,616,618,619] to identify likely sites of substrate water binding; the results of these studies offer evidence for the oxo-oxyl radical type mechanisms by implicating the same water binding sites as proposed in those mechanisms.[615]

Newer alternative radical mechanisms have been suggested as well,[608] where the "inner oxo" O5 arranges between Mn3 and Mn1.[620,621] This results in radical coupling of W2 and O5 [611], which contrasts to the originally proposed "outer oxo" of Mn3 and Mn4.[578] The "outer oxo" proposal has been supported by EDNMR experiments using a rapid mix-freeze approach where it was found the oxo-bridge (O5) exchanges rapidly with water in the S_1 state (within 10–15 s).[610] This evidence supports the suggestion that O5 is indeed substrate-water-derived. The radical mechanism is also helpful in explaining why the exchange rate of slowly exchanging water (W_s) is fairly unchanged during the $S_2 \rightarrow S_3$ transition despite apparent changes in oxidation state and structure.[621] The best suggestion currently is that the exchange mechanism in the S_3 state involves a structural and/or redox equilibrium that may also include a $Mn^{III}Mn^{IV}Mn^{IV}Mn^{IV}$ tyrosyl radical state that allows water exchange to occur like in the S_2 state.[622–624]

UV–vis difference spectroscopy[625,626] and FTIR spectroscopy [627] propose an early deprotonation event (0–300 μs) during the

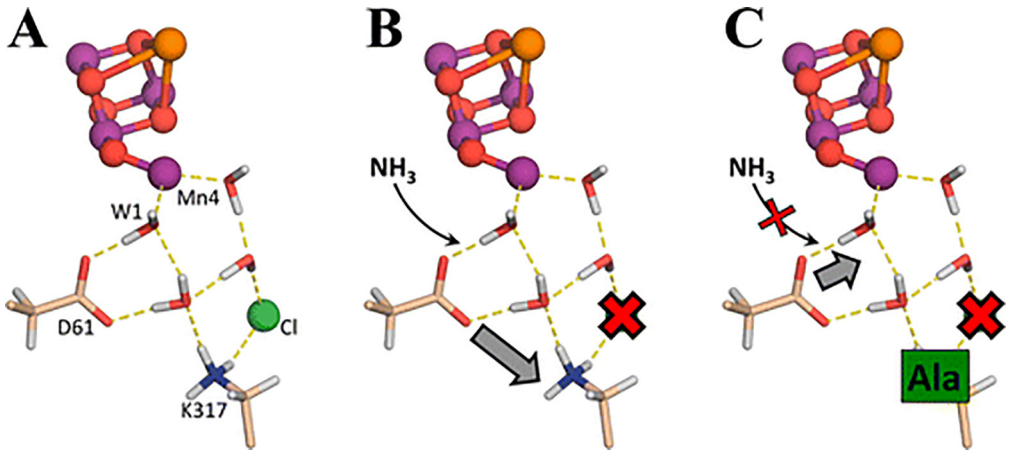

Fig. 84. Proposed model of chloride-competitive ammonia binding outside the OEC. (A) Native structure of the S_2 state $S = {}^5/_2$ spin isomer. (B) Ammonia competes with D61 as a hydrogen bond acceptor to W1. (C) In K317A PSII, chloride does not bind. D61 remains a strong hydrogen bond acceptor to W1, and ammonia does not bind. Reproduced with permission from the American Chemical Society.[615]

S_3-S_4-S_0 transitions. A study from Davis et al, while not excluding this hypothesis, suggests that it would require a significant electronic rearrangement of the 3d Mn frontier orbitals to explain the observed absorption spectra. The spectroscopic results combined with their work can be better rationalized if the formation of the (Tyr_Z•) S_3 state triggers a sequence of events resulting in significant redox or structural changes to the OEC, such as the formation of the O—O bond. Davis et al thus proposed a new mechanistic model in which O—O bond formation occurs prior to the transfer of the final fourth electron from the Mn_4Ca cluster, suggesting that the S_4 state is actually transient, and explaining why no $Mn^{V}Mn_3^{IV}$ or Mn^{IV}-O· radical state is observed in their time resolved X-ray emission spectroscopic kinetic experiments.[628] An XFEL study of the S_3 state by Suga et al[541] produced an S_3-state structure virtually indistinguishable from the DFT model within the experimental resolution of X-ray diffraction.[629] These observations support the hypothesis that O-O bond formation may be occurring in the S_3 state, earlier than previously suggested, though there could be an intermediate precursor structure related to other mechanistic proposals, such a formal $Mn^{V}Mn_3^{IV}$ intermediate, or a Mn_4^{IV} species coupled to a radical Tyr_Z•.

5.3.3. Low oxidation state paradigm

Throughout the entire history of analysis of the structure of the OEC, it has proven difficult to provide a picture of the OEC consistent with all biophysical data. XRD structures tend to suggest a greater level of reduction than EXAFS data, even using damage-reducing ultrafast femto crystallography.[473,517,546,549,550,630] However, a few groups have argued that all inconsistencies can be resolved by the revision of the presumptive S-state oxidation state model to a new set of assigned oxidation states two-electrons more reduced, termed the "low-oxidation-state paradigm," formally ranging from 1-Mn^{II}:3-Mn^{III} for S_0 up to 1-Mn^{III}:3-Mn^{IV} for S_4. By comparison, the more traditional set of assigned formal oxidation states (3-Mn^{III}:1-Mn^{IV} for S_0 up to 3-Mn^{IV}:1-Mn^{V} for S_4) is now sometimes referred to as the high-oxidation-state paradigm by contrast (Fig. 85). A theoretical report from Terrett et al suggested O-O bond formation from corner O atoms was feasible from the proposed 1-Mn^{III}:3-Mn^{IV} S_4 state.[507] A technique that is commonly used to probe the S-states of the OEC is electron paramagnetic resonance (EPR). In particular, the S_2 state has received extensive study using EPR techniques.[571,631–634] However, spin state assignments from EPR do not usually offer direct evidence of any oxidation states, but rather, the total number of unpaired electrons, and their distributions across atoms. These spectra may be consistent with more than one possible electronic structure, though specific values of hyperfine (a), and types of anisotropy in g and in a can lend support to some electronic assignments over others. The S_2 spectrum (Fig. 86) suggests two species with separate spin states, S = 1/2 and S = 5/2, but the S = 1/2 "open cubane" spin state predominates in normal environmental conditions. The S = 5/2 spin state exhibits a "closed cubane", where the 5th oxygen is not bonded to the dangling 4th manganese.[633] The split EPR signal was originally attributed to an amino acid radical, either histidine[635] or tyrosine[636], magnetically interacting with the Mn cluster. A combination of spectral and ^{55}Mn ENDOR simulations performed by Peloquin et al[637] were able to reproduce the split signal observed in both EPR and ENDOR spectra (Fig. 86), providing evidence that the split signal is resultant from tyrosine radical (Y_Z·) coupled to the Mn cluster.[638]

Consistent with theoretical predictions,[639] this high spin "closed cubane" structure is proposed to undergo transition into the S_3 state through low energy barriers and fast kinetics.[633] Even though the $S=^1/_2$ isomer is favored, it has been shown higher order plants can use this equilibrium to carefully tune efficiency from thermodynamics and charge recombination.[640] It has been proposed that the $S=^5/_2$ isomer is stabilized by the surrounding hydrogen bonding network, allowing the OEC to transition into the S_3 state.[482] These observations thus made understanding the hyperfine interactions of the $S=^5/_2$ signal an integral piece to understand the oxygen evolving mechanism.

However, due to the complex nature of the S_2 state, usual EPR methods cannot distinguish hyperfine interaction tensors of the manganese ions of the S = $^5/_2$ signal, requiring electron nuclear double resonance (ENDOR) spectroscopy.[633] Recent ^{55}Mn ENDOR spectroscopy of the S_2 state below 4.2 K bolsters support for the low-oxidation-state paradigm[634] with three Mn hyperfine couplings containing anisotropy. This indicates that three Mn(III) ions are likely present within PSII.[639] When comparing

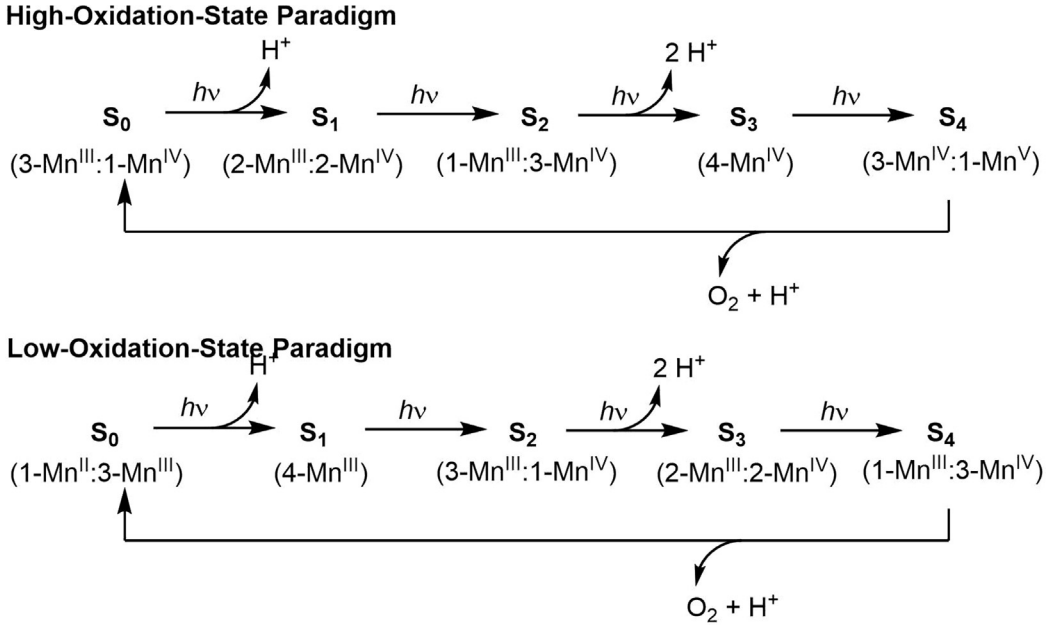

Fig. 85. High and low oxidation pathway proposals for the OEC.

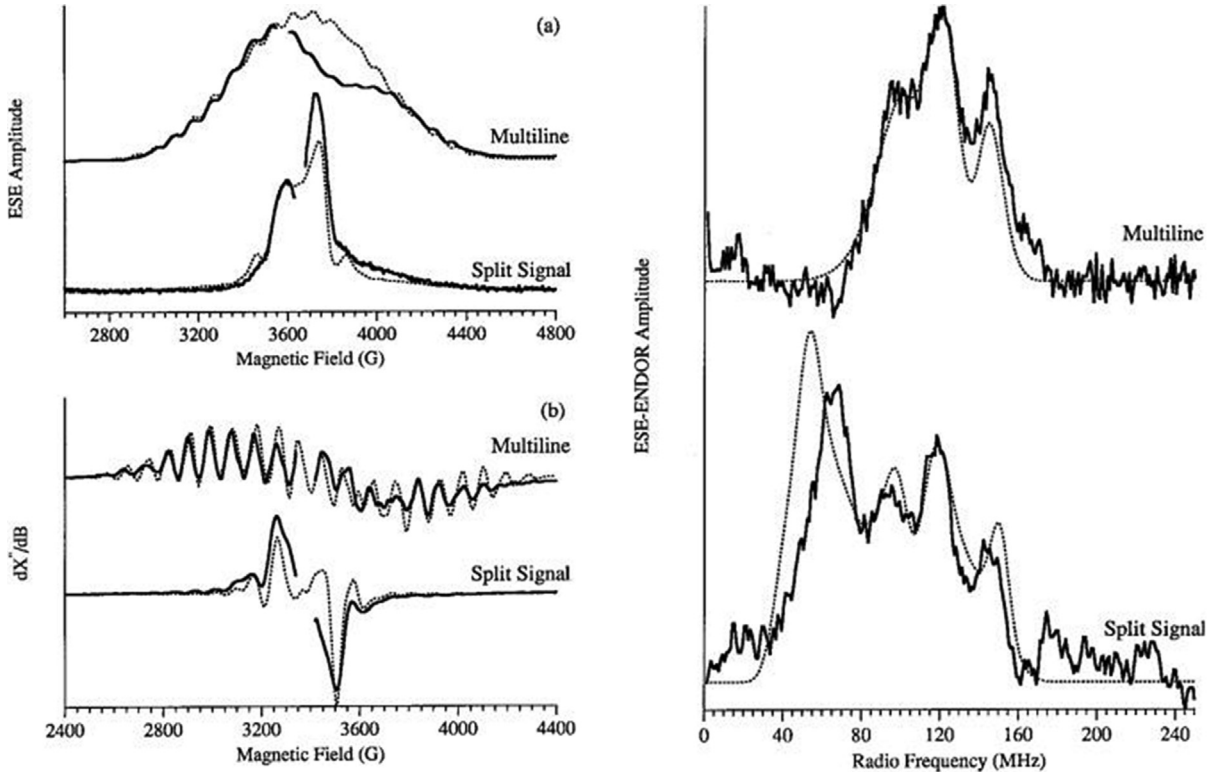

Fig. 86. Left: (a) Two-pulse ESE and (b) CW-EPR, field swept "illuminated minus annealed" difference spectra of the S_2-state multiline signal PSII membranes and the split EPR signal of acetate-treated membranes. The black lines represent experimental data and the gray lines numerical simulations. Right: Davies ESE-ENDOR "illuminated minus annealed" difference spectra of the S_2-state multiline signal and the split EPR signal of acetate treated samples. Black lines represent experimental data and gray lines numerical simulations. Reproduced with permission from the American Chemical Society.[637]

the 1.9 Å and 1.95 Å structures of Umena et al[434] and Suga et al [473] respectively, the low oxidation state paradigm was supported since computational root means squared deviation (RMSD) of M-M and M−O distances was significantly smaller than the high oxidation state paradigm (0.086 Å and 0.164 Å respectively).[641]

The low-oxidation-state paradigm is further supported by experimental work from Dismukes on the photo-assembly of the OEC from aqueous Mn^{II}.[538] OEC maturation requires the oxidation of aqueous Mn^{II} ions using photooxidation of P680 using the normal electron transfer pathway. When using light to excite electron transfer from the unmetallated PSII in the presence of Mn^{II}, the regeneration of P680 occurs via oxidation of Mn^{II} to Mn^{III} with concomitant cluster assembly. In this work, only 7 flashes were required to evolve O_2. Since four flashes are required to evolve O_2 from the S_0 state, only three flashes are required to assemble the S_0 state from Mn^{II}, suggesting that S_0 has the oxidation state assignment 1-Mn^{II}:3-Mn^{III}, consistent with the low-oxidation-state paradigm.[538]

5.3.4. High oxidation state Paradigm-New findings

More support has recently come into agreement with the high valent scheme of S state cycling.[606] Krewald et al replicated the recent ^{55}Mn Davies ENDOR experiment of Jin et al,[642] and in contrast to proponents of the low-oxidation state paradigm, [533] did not observe any Mn(III) ion evidenced by large anisotropy at 2.5 K. They suggest their data represents tetramer-like magnetic coupling with all Mn ions exhibiting similar hyperfine couplings.[606] This supports the claim that there are no structurally consistent low oxidation state schemes for the S_0 and S_1 states, as high valent models agree with geometric constraints from EXAFS and are argued to be more stable.[643]

As discussed earlier, XFEL methods have produced structures with less radiation damage, which do not reduce the manganese complex as severely, mitigating resulting increases in the Mn-Mn distances.[473,541] Ambiguity of experimental data along with structural disorder of even these images has left some room for concern.[644] Recent DFT studies of the 1.95 Å structure determined that the structure that was in best in agreement with experiment was obtained by removing a proton from the water W2 ligand and protonating the O5.[645] Leaving the His337 residue neutral in their S_1 model, the group adopts the high oxidation state paradigm to better agree with the newest XFEL findings.[645] The protonation of O5 in the S_1 state has been supported by the work of several,[530,532] although Petrie et al,[532] while agreeing with the presence of the protonated OH ligand, claimed that the identity of the OH was the W2 ligand, and favored the low oxidation state paradigm.

The high oxidation state paradigm has historically seen more support from experimental data in comparison to the low-valent scheme.[468,632,641,643,646] For instance, simulation of the vibrational difference spectra between the S_1 and S_2 state using a QM/MM approach showed that the changes in the IR spectrum were more consistent with the high-oxidation-state paradigm (Fig. 87).[647] They concluded that the high-oxidation models 1 and 2 (see Fig. 87), corresponded most consistently with carboxylate shifts in IR spectra.[678,649,650] ^{55}Mn pulse ENDOR at the Q-band of the S_0 state with subsequent revisiting of the hyperfine interaction parameters for the S_2 state disfavors the presence of Mn(II), a requisite in the low-valent scheme, and instead explicitly favor the high-valent scheme of Mn_4(III, III, III, IV) and Mn_4(III, IV, IV, IV) for S_0 and S_2 respectively.[641] Similarly, an EPR study utilizing the inversion-recovery method on OEC model compounds

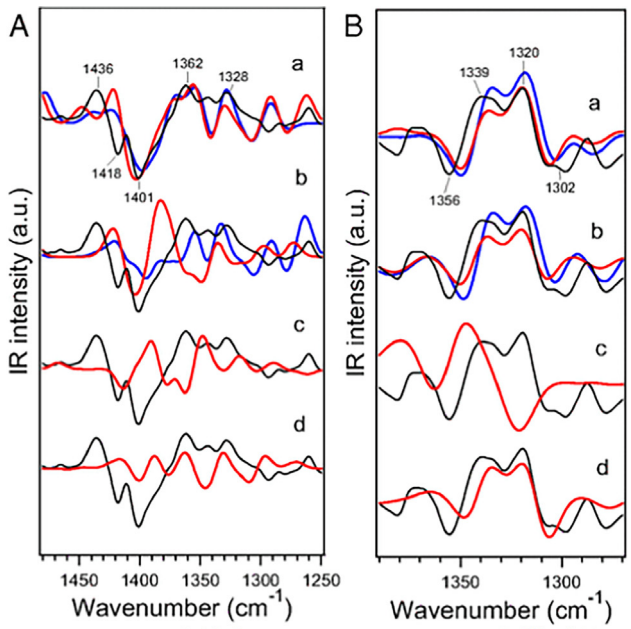

Model	Oxidation states in S_1*	W2	O5	Oxidized Mn in S_2
1	High (III, IV, IV, III)	H_2O	O^{2-}	Mn_1 or Mn_4
2	High (III, IV, IV, III)	OH^-	O^{2-}	Mn_1 or Mn_4
3	Low (III, III, III, III)	OH^-	H_2O	Mn_2
4	Low (III, IV, III, II)	H_2O	OH^-	Mn_4
5 (Ca depleted)	High (III, IV, IV, III)	H_2O	O^{2-}	Mn_4

*Oxidation states of (Mn_1, Mn_2, Mn_3, Mn_4).

Fig. 87. Experimental [680,681] and calculated [647] IR spectra in the symmetric COO^- stretching vibrations of carboxylate groups (red or blue lines) compared with experimental FTIR difference spectra (black lines). (A) S_2/S_1 difference spectra. (B) $^{12}C/^{13}C$-A344 S_2/S_1 double-difference spectra. (a) Model 1 (blue line, Mn_1-oxidized S_2; red line, Mn_4-oxidized S_2), (b) model 2 (blue line, Mn_1-oxidized S_2; red line, Mn_4-oxidized S_2), (c) model 3, and (d) model 4. Model 5 not plotted. Reproduced with permission from the National Academy of Sciences.[647]

$[Mn(II)Mn(III)(\mu\text{-}OH)(\mu\text{-}piv)_2(Me_3tacn)_2](ClO_4)_2$ and $Mn(III)Mn(IV)(\mu\text{-}O)_2bipy_4]ClO_4$ suggested that the S_0 could be described as a Mn(II)Mn(III) dimer, coupled antiferromagnetically to *either* a Mn(III, III) (low oxidation state) or Mn(IV,IV) (high oxidation state) dimer.[648] However, since this result was obtained from biomimetic analogues it should be taken understanding the limitations of these synthetic models in simulating the OEC environment. These findings from experiment summarize some of the more recent support for the high-oxidation paradigm yet also illustrate the ever-ongoing search for a definitive explanation to the OEC's cycle and mechanism in a yet unresolved debate.

6. Concluding statements

The importance of cubane clusters in biological chemistry has been well appreciated for nearly 50 years. For even longer synthetic exploration and characterization of cubane cluster reactivity and electronic structure has been ongoing. There exists a wealth of literature deliberately connecting biological systems to synthetic model systems, but this review has sought to make broader connections between biology and synthetic research across all the cubane literature. This review describes the current state of understanding across multiple biological metalloprotein systems and synthetic cubane clusters of a wide array of types. It is hoped that this review will enlighten readers about the broad array of cubane literature available outside the biomimetic modelling community, as well as provide new connections between mechanistic and electronic structure questions surrounding these important biological systems.

Declaration of Competing Interest

The authors declare that they have no known competing financial interests or personal relationships that could have appeared to influence the work reported in this paper.

Acknowledgment

Support of MJZ and SV by the National Science Foundation under award 1800105, and support for MJZ via a sabbatical award from Temple University are gratefully acknowledged.

References

[1] P. Venkateswara Rao, R.H. Holm, Chem. Rev. 104 (2004) 527–559.
[2] G.F. Swiegers, J.K. Clegg, R. Stranger, Chem. Sci. 2 (2011) 2254–2262.
[3] H. Seino, M. Hidai, Chem. Sci. 2 (2011) 847–857.
[4] L.-H. Hou, C.-M. Wu, H.-H. Huang, H.-A. Chu, Biochemistry 50 (2011) 9248–9254.
[5] R.H. Holm, W. Lo, Chem. Rev. 116 (2016) 13685–13713.
[6] S.C. Lee, R.H. Holm, Chem. Rev. 104 (2004) 1135–1158.
[7] J. Zhou, Z. Hu, E. Münck, R. Holm, J. Am. Chem. Soc. 118 (1996) 1966–1980.
[8] B. Gerey, E. Gouré, J. Fortage, J. Pécaut, M.-N. Collomb, Coord. Chem. Rev. 319 (2016) 1–24.
[9] G.C. Dismukes, R. Brimblecombe, G.A. Felton, R.S. Pryadun, J.E. Sheats, L. Spiccia, G.F. Swiegers, Acc. Chem. Res. 42 (2009) 1935–1943.
[10] D.J. Evans, Coord. Chem. Rev. 249 (2005) 1582–1595.
[11] R.A. Henderson, Chem. Rev. 105 (2005) 2365–2437.
[12] X. Liu, J.A. McAllister, M.P. De Miranda, B.J. Whitaker, C.A. Kilner, M. Thornton-Pett, M.A. Halcrow, Angew. Chem. Int. Ed. Engl. 41 (2002) 756–758.
[13] R. Holm, S. Ciurli, J. Weigel, Subsite-Specific Structures and Reactions in Native and Synthetic [4Fe-4S] Cubane-Type Clusters, Prog. Inorg. Chem. (2007) 1–74.
[14] Q.-F. Zhang, W.-H. Leung, X. Xin, Coord. Chem. Rev. 224 (2002) 35–49.
[15] J.-P. Lang, S.-J. Ji, Q.-F. Xu, Q. Shen, K. Tatsumi, Coord. Chem. Rev. 241 (2003) 47–60.
[16] R. Hernandez-Molina, M.N. Sokolov, A.G. Sykes, Acc. Chem. Res. 34 (2001) 223–230.
[17] M. Hidai, S. Kuwata, Y. Mizobe, Acc. Chem. Res. 33 (2000) 46–52.
[18] R. Hernandez-Molina, A. Geoffrey Sykes, Coord. Chem. Rev. 187 (1999) 291–302.
[19] K. Dehnicke, M. Krieger, W. Massa, Coord. Chem. Rev. 182 (1999) 19–65.
[20] H. Ogino, S. Inomata, H. Tobita, Chem. Rev. 98 (1998) 2093–2122.
[21] T. Shiga, H. Oshio, Sci. Techno. Adv. Mater. 6 (2005) 565–570.
[22] F.G. Mann, D. Purdie, A.F. Wells, J. Chem. Soc. (1936) 1503–1513.
[23] A.F. Wells, Z. Krist-Cryst, Mater. 94 (1936) 447–460.
[24] F.G. Mann, A.F. Wells, D. Purdie, J. Chem. Soc. (1937) 1828–1836.
[25] E.O. Fischer, K. Ulm, H.P. Fritz, Chem. Ber. 93 (1960) 2167–2173.
[26] F. Bottomley, D.E. Paez, P.S. White, J. Am. Chem. Soc. 103 (1981) 5581–5582.
[27] R. Schunn, C.J. Fritchie Jr, C. Prewitt, Inorg. Chem. 5 (1966) 892–899.
[28] C.H. Wei, G.R. Wilkes, P.M. Treichel, L.F. Dahl, Inorg. Chem. 5 (1966) 900–905.
[29] F. Bottomley, D.E. Paez, P.S. White, J. Am. Chem. Soc. 104 (1982) 5651–5657.
[30] F. Bottomley, D.E. Paez, L.C. Sutin, P.S. White, F.H. Koehler, R.C. Thompson, N. P. Westwood, Organometallics 9 (1990) 2443–2454.
[31] F. Bottomley, J. Chen, S.M. MacIntosh, R.C. Thompson, Organometallics 10 (1991) 906–912.
[32] K. Nishikawa, K. Kido, J.i. Yoshida, T. Nishioka, I. Kinoshita, B.K. Breedlove, Y. Hayashi, A. Uehara, K. Isobe, Appl. Organomet. Chem. 17 (2003) 446–448.
[33] Y. Hayashi, K. Toriumi, K. Isobe, J. Am. Chem. Soc. 110 (1988) 3666–3668.
[34] S.H. Bertz, G. Dabbagh, J. Am. Chem. Soc. 110 (1988) 3668–3670.
[35] Y. Do, X.Z. You, C. Zhang, Y. Ozawa, K. Isobe, J. Am. Chem. Soc. 113 (1991) 5892–5893.
[36] G.L. Simon, L.F. Dahl, J. Am. Chem. Soc. 95 (1973) 2164–2174.
[37] A. Pasynskii, I. Eremenko, Y.V. Rakitin, V. Novotortsev, O. Ellert, V. Kalinnikov, V. Shklover, Y.T. Struchkov, S. Lindeman, T.K. Kurbanov, J. Organomet. Chem. 248 (1983) 309–320.
[38] H. Blonk, J. Van der Linden, J. Steggerda, R. Geleyn, J. Smits, G. Beurskens, P.T. Beurskens, J. Jordanov, Inorg. Chem. 31 (1992) 957–962.
[39] T. Toan, B.K. Teo, J.A. Ferguson, T.J. Meyer, L.F. Dahl, J. Am. Chem. Soc. 99 (1977) 408–416.
[40] H. Seino, H. Mori, A. Shinozaki, Y. Mizobe, J. Organomet. Chem. 695 (2010) 1878–1882.
[41] D.A. Dobbs, R.G. Bergman, J. Am. Chem. Soc. 114 (1992) 6908–6909.
[42] H. Mori, H. Seino, M. Hidai, Y. Mizobe, Angew. Chem. Int. Ed. 46 (2007) 5431–5434.
[43] J. Amarasekera, T.B. Rauchfuss, S.R. Wilson, J. Chem. Soc. Chem. Commun. (1989) 14–16.

[44] E.J. Houser, J. Amarasekera, T.B. Rauchfuss, S.R. Wilson, J. Am. Chem. Soc. 113 (1991) 7440–7442.
[45] Q. Feng, T.B. Rauchfuss, S.R. Wilson, J. Am. Chem. Soc. 117 (1995) 4702–4703.
[46] P. Baird, J.A. Bandy, M.L. Green, A. Hamnett, E. Marseglia, D.S. Obertelli, K. Prout, J. Qin, J. Chem. Soc. Dalton Trans. (1991) 2377–2393.
[47] L.Y. Goh, W. Chen, J. Chem. Soc. Dalton Trans. (1994) 2697–2704.
[48] A. Venturelli, T.B. Rauchfuss, J. Am. Chem. Soc. 116 (1994) 4824–4831.
[49] S. Schulz, M. Andruh, T. Pape, T. Heinze, H.W. Roesky, L. Haeming, A. Kuhn, R. Herbst-Irmer, Organometallics 13 (1994) 4004–4007.
[50] E.J. Houser, S. Dev, A.E. Ogilvy, T.B. Rauchfuss, S.R. Wilson, Organometallics 12 (1993) 4678–4681.
[51] H. Seino, Y. Mizobe, M. Hidai, New J. Chem. 24 (2000) 907–911.
[52] E.J. Houser, T.B. Rauchfuss, S.R. Wilson, Inorg. Chem. 32 (1993) 4069–4076.
[53] I. Eremenko, S. Nefedov, A. Pasynskii, B. Orazsakhatov, O. Ellert, Y.T. Struchkov, A. Yanovsky, D. Zagorevsky, J. Organomet. Chem. 368 (1989) 185–192.
[54] S. Guo, R. Hauptmann, S. Losi, P. Zanello, J.J. Schneider, J. Clust. Sci. 18 (2007) 237–251.
[55] H. Suzuki, T. Kakigano, M. Igarashi, A. Usui, K. Noda, M. Oshima, M. Tanaka, Y. Moro-oka, Chem. Lett. 22 (1993) 1707–1710.
[56] A. Hörnig, U. Englert, U. Koelle, J. Organomet. Chem. 453 (1993) 255–261.
[57] R. Liu, X. Li, H. Zhang, L. Weng, X. Zhou, Dalton Trans. 39 (2010) 11053–11059.
[58] M.A. Neuman, L.F. Dahl, J. Am. Chem. Soc. 94 (1972) 3383–3388.
[59] M.D. Westmeyer, M.A. Massa, T.B. Rauchfuss, S.R. Wilson, J. Am. Chem. Soc. 120 (1998) 114–123.
[60] M. Okazaki, T. Ohtani, M. Takano, H. Ogino, Organometallics 23 (2004) 4055–4061.
[61] C. Wei, L.Y. Goh, T.C. Mak, Organometallics 5 (1986) 1997–2002.
[62] T. Kimura, N. Koiso, K. Ishiwata, S. Kuwata, T. Ikariya, J. Am. Chem. Soc. 133 (2011) 8880–8883.
[63] G.L. Simon, L.F. Dahl, J. Am. Chem. Soc. 95 (1973) 2175–2183.
[64] O.J. Scherer, S. Weigel, G. Wolmershäuser, Chem-Eur. J. 4 (1998) 1910–1916.
[65] S. Reisinger, M. Bodensteiner, E.M. Pineda, J.J. McDouall, M. Scheer, R.A. Layfield, Chem. Sci. 5 (2014) 2443–2448.
[66] W.-X. Zhang, Z. Wang, M. Nishiura, Z. Xi, Z. Hou, J. Am. Chem. Soc. 133 (2011) 5712–5715.
[67] M. Akita, R. Hua, Y. Moro-oka, J. Organomet. Chem. 539 (1997) 205–207.
[68] M. Akita, R. Hua, S. Nakanishi, M. Tanaka, Y. Moro-oka, Organometallics 16 (1997) 5572–5584.
[69] M. González-Moreiras, M. Mena, A. Pérez-Redondo, C. Yélamos, Chem-Eur. J. 23 (2017) 3558–3561.
[70] R. Andrés, P. Gómez-Sal, E. de Jesús, A. Martín, M. Mena, C. Yélamos, Angew. Chem. Int. Ed. Eng. 36 (1997) 115–117.
[71] L.C. Roof, W.T. Pennington, J.W. Kolis, Angew. Chem. Int. Ed. Eng. 31 (1992) 913–915.
[72] M. Okazaki, K. Suto, N. Kudo, M. Takano, F. Ozawa, Organometallics 31 (2012) 4110–4113.
[73] J.R. Bowser, A. Bonny, J.R. Pipal, R.N. Grimes, J. Am. Chem. Soc. 101 (1979) 6229–6236.
[74] D.M.P. Mingos, D.J. Wales, Introduction to cluster chemistry, Prentice Hall, 1990.
[75] J.R. Pipal, R.N. Grimes, Inorg. Chem. 18 (1979) 257–263.
[76] T.A. Scott, C.P. Berlinguette, R.H. Holm, H.-C. Zhou, Proc. Natl. Acad. Sci. U.S.A. 102 (2005) 9741–9744.
[77] W.A. Herrmann, A. Egli, E. Herdtweck, R. Alberto, F. Baumgärtner, Angew. Chem. Int. Ed. Eng. 35 (1996) 432–434.
[78] K. TravisáHolman, O. Jeffrey, J. Chem. Soc. Dalton Trans. (1995) 2233–2243.
[79] S.B. Copp, S. Subramanian, M.J. Zaworotko, J. Am. Chem. Soc. 114 (1992) 8719–8720.
[80] S.B. Copp, S. Subramanian, M.J. Zaworotko, Angew. Chem. Int. Ed. Eng. 32 (1993) 706–709.
[81] M.D. Clerk, M.J. Zaworotko, J. Chem. Soc. Chem. Commun. (1991) 1607–1608.
[82] J. Breimair, C. Robl, W. Beck, J. Organomet. Chem. 411 (1991) 395–404.
[83] T.J. McNeese, M.B. Cohen, B.M. Foxman, Organometallics 3 (1984) 552–556.
[84] R.L. Geerts, J.C. Huffman, K. Folting, T.H. Lemmen, K.G. Caulton, J. Am. Chem. Soc. 105 (1983) 3503–3506.
[85] N.A. Pushkarevsky, S.N. Konchenko, M. Zabel, M. Bodensteiner, M. Scheer, Dalton Trans. 40 (2011) 2067–2074.
[86] S. Onaka, Y. Katukawa, J. Coord. Chem. 39 (1996) 135–146.
[87] D.S. Choi, S.H. Hong, S.S. Lee, Y.K. Chung, J. Organomet. Chem. 579 (1999) 385–390.
[88] M. Reyes-Lezama, R.A. Toscano, N. Zuñiga-Villareal, J. Organomet. Chem. 517 (1996) 19–23.
[89] T.A. Scott, H.C. Zhou, Angew. Chem. Int. Ed. 43 (2004) 5628–5631.
[90] M. Laing, P.M. Kiernan, W.P. Griffith, J. Chem. Soc. Chem. Commun. (1977) 221–222.
[91] S.L. Estes, M.R. Antonio, L. Soderholm, J. Phys. Chem. C 120 (2016) 5810–5818.
[92] Y.M. Gayfulin, A.I. Smolentsev, Y.V. Mironov, J. Coord. Chem. 68 (2015) 409–421.
[93] O.A. Efremova, Y.V. Mironov, N.V. Kuratieva, V.E. Fedorov, Acta Cryst. E 60 (2004) m1817–m1818.
[94] O.A. Efremova, Y.V. Mironov, D.Y. Naumov, S.G. Kozlova, V.E. Fedorov, Polyhedron 25 (2006) 1233–1238.
[95] N. Zhu, R. Appelt, H. Vahrenkamp, J. Organomet. Chem. 565 (1998) 187–192.
[96] R.S. Gall, N.G. Connelly, L.F. Dahl, J. Am. Chem. Soc. 96 (1974) 4017–4019.
[97] C.T.W. Chu, R.S. Gall, L.F. Dahl, J. Am. Chem. Soc. 104 (1982) 737–746.
[98] R.S. Gall, C.T. Chu, L.F. Dahl, J. Am. Chem. Soc. 96 (1974) 4019–4023.
[99] M.J. Scott, R.H. Holm, Angew. Chem. Int. Ed. Eng. 32 (1993) 564–566.
[100] C.-C. Tsou, Z.-S. Lin, T.-T. Lu, W.-F. Liaw, J. Am. Chem. Soc. 130 (2008) 17154–17160.
[101] N. Zhu, J. Pebler, H. Vahrenkamp, Angew. Chem. Int. Ed. Eng. 35 (1996) 894–895.
[102] B. Segal, H. Hoveyda, R. Holm, Inorg. Chem. 37 (1998) 3440–3443.
[103] M. Harmjanz, W. Saak, D. Haase, S. Pohl, Chem. Commun. (1997) 951–952.
[104] K.S. Hagen, M. Uddin, Inorg. Chem. 47 (2008) (1815) 11807–11811.
[105] V. Fedin, I. Kalinina, D. Samsonenko, Y.V. Mironov, M. Sokolov, S. Tkachev, A. Virovets, N. Podberezskaya, M. Elsegood, W. Clegg, Inorg. Chem. 38 (1999) 1956–1965.
[106] J.Y. Kwon, Y. Kim, S.-J. Kim, S.H. Lee, H. Kwak, C. Kim, Inorg. Chim. Acta 361 (2008) 1885–1890.
[107] C. Magliocchi, X. Xie, T. Hughbanks, Inorg. Chem. 43 (2004) 1902–1911.
[108] E. Fischer, Pure Appl. Chem. 30 (1972) 353–372.
[109] V.P. Fedin, I.V. Kalinina, A. Gerasimenko, A.V. Virovets, Inorg. Chim. Acta 331 (2002) 48–51.
[110] I.V. Kalinina, A.V. Virovets, F.M. Dolgushin, M.Y. Antipin, R. Llusar, V.P. Fedin, Inorg. Chim. Acta 357 (2004) 3390–3396.
[111] K. Takenaka, Y. Obora, Y. Tsuji, Inorg. Chim. Acta 357 (2004) 3895–3901.
[112] R.P. Pesavento, C.P. Berlinguette, R. Holm, Inorg. Chem. 46 (2007) 510–516.
[113] T.A. Scott, R. Holm, Inorg. Chem. 47 (2008) 3426–3432.
[114] X.-L. You, Y.-L. Liu, Acta Cryst. E 65 (2009).
[115] Z.-G. Ren, H.-X. Li, L.-L. Li, Y. Zhang, J.-P. Lang, J.-Y. Yang, Y.-L. Song, J. Organomet. Chem. 692 (2007) 2205–2215.
[116] Q.-F. Xu, J.-X. Chen, W.-H. Zhang, Z.-G. Ren, H.-X. Li, Y. Zhang, J.-P. Lang, Inorg. Chem. 45 (2006) 4055–4064.
[117] Q. Liu, Z.-G. Ren, L. Deng, W.-H. Zhang, X. Zhao, Z.-R. Sun, J.-P. Lang, Dalton Trans. 44 (2015) 130–137.
[118] X. Chen, H.-X. Li, Z.-Y. Zhang, W. Zhao, J.-P. Lang, B.F. Abrahams, Chem. Commun. 48 (2012) 4480–4482.
[119] M. Gnida, R. Ferner, L. Gremer, O. Meyer, W. Meyer-Klaucke, Biochemistry 42 (2003) 222–230.
[120] R. Hille, J. Hall, P. Basu, Chemical reviews 114 (2014) 3963–4038.
[121] H. Dobbek, L. Gremer, O. Meyer, R. Huber, Proc. Natl. Acad. Sci. U.S.A. 96 (1999) 8884–8889.
[122] P. Hänzelmann, H. Dobbek, L. Gremer, R. Huber, O. Meyer, J. Mol. Biol. 301 (2000) 1221–1235.
[123] L.L. Nelson, F.Y.-K. Lo, A.D. Rae, L.F. Dahl, J. Organomet. Chem. 225 (1982) 309–329.
[124] M. Ryzhikov, S. Kozlova, S. Gabuda, J. Struct. Chem. 49 (2008) 587–594.
[125] A. Savin, R. Nesper, S. Wengert, T.F. Fässler, Angew. Chem. Int. Ed. Eng. 36 (1997) 1808–1832.
[126] R.F. Bader, Chem. Rev. 91 (1991) 893–928.
[127] A. Müller, W. Eltzner, W. Clegg, G.M. Sheldrick, Angew. Chem. Int. Ed. Eng. 21 (1982) 536–537.
[128] L.F. Dahl, A.S. Foust, J. Am. Chem. Soc. 92 (1970) 7337–7341.
[129] S.J. Yoo, H.C. Angove, B.K. Burgess, M.P. Hendrich, E. Münck, J. Am. Chem. Soc. 121 (1999) 2534–2545.
[130] M. Chakrabarti, L. Deng, R. Holm, E. Münck, E.L. Bominaar, Inorg. Chem. 48 (2009) 2735–2747.
[131] M. Chakrabarti, E. Münck, E.L. Bominaar, Inorg. Chem. 50 (2011) 4322–4326.
[132] R. King, Inorg. Chem. 5 (1966) 2227–2230.
[133] J.C. Green, M.L. Green, G. Parkin, Chem. Commun. 48 (2012) 11481–11503.
[134] G.E. Kostakis, A.M. Ako, A.K. Powell, Chem. Soc. Rev. 39 (2010) 2238–2271.
[135] R. Bagai, G. Christou, Chem. Soc. Rev. 38 (2009) 1011–1026.
[136] J.S. Kanady, E.Y. Tsui, M.W. Day, T. Agapie, Science 333 (2011) 733–736.
[137] W.F. Ruettinger, C. Campana, G.C. Dismukes, J. Am. Chem. Soc. 119 (1997) 6670–6671.
[138] F. Wang, Y. Ding, L. Guo, J. Du, X. Zhang, Z. Anorg, Allg. Chem. 641 (2015) 1762–1766.
[139] M. Mikuriya, Y. Hashimoto, A. Kawamori, Chem. Lett. 24 (1995) 1095–1096.
[140] J.S. Kanady, R. Tran, J.A. Stull, L. Lu, T.A. Stich, M.W. Day, J. Yano, R.D. Britt, T. Agapie, Chem. Sci. 4 (2013) 3986–3996.
[141] S.T. Meally, S.M. Taylor, E.K. Brechin, S. Piligkos, L.F. Jones, Dalton Trans. 42 (2013) 10315–10325.
[142] K.M. Van Allsburg, E. Anzenberg, W.S. Drisdell, J. Yano, T.D. Tilley, Chem-Eur. J. 21 (2015) 4646–4654.
[143] M.W. Wemple, D.M. Adams, K. Folting, D.N. Hendrickson, G. Christou, J. Am. Chem. Soc. 117 (1995) 7275–7276.
[144] T. Kuroda-Sowa, T. Nogami, H. Konaka, M. Maekawa, M. Munakata, H. Miyasaka, M. Yamashita, Polyhedron 22 (2003) 1795–1801.
[145] C. Lampropoulos, G. Redler, S. Data, K.A. Abboud, S. Hill, G. Christou, Inorg. Chem. 49 (2010) 1325–1336.
[146] M. Soler, W. Wernsdorfer, Z. Sun, J.C. Huffman, D.N. Hendrickson, G. Christou, Chem. Commun. (2003) 2672–2673.
[147] S.M. Aubin, Z. Sun, L. Pardi, J. Krzystek, K. Folting, L.-C. Brunel, A.L. Rheingold, G. Christou, D.N. Hendrickson, Inorg. Chem. 38 (1999) 5329–5340.
[148] A. Masello, M. Murugesu, K.A. Abboud, G. Christou, Polyhedron 26 (2007) 2276–2280.
[149] H. Zhao, C.P. Berlinguette, J. Bacsa, A.V. Prosvirin, J.K. Bera, S.E. Tichy, E.J. Schelter, K.R. Dunbar, Inorg. Chem. 43 (2004) 1359–1369.
[150] A.-L. Barra, A. Caneschi, A. Cornia, D. Gatteschi, L. Gorini, L.-P. Heiniger, R. Sessoli, L. Sorace, J. Am. Chem. Soc. 129 (2007) 10754–10762.

[151] R. Sessoli, H.L. Tsai, A.R. Schake, S. Wang, J.B. Vincent, K. Folting, D. Gatteschi, G. Christou, D.N. Hendrickson, J. Am. Chem. Soc. 115 (1993) 1804–1816.
[152] P. Parois, S.A. Moggach, J. Sanchez-Benitez, K.V. Kamenev, A.R. Lennie, J.E. Warren, E.K. Brechin, S. Parsons, M. Murrie, Chem. Commun. 46 (2010) 1881–1883.
[153] N.E. Chakov, S.-C. Lee, A.G. Harter, P.L. Kuhns, A.P. Reyes, S.O. Hill, N. Dalal, W. Wernsdorfer, K.A. Abboud, G. Christou, J. Am. Chem. Soc. 128 (2006) 6975–6989.
[154] N.E. Chakov, M. Soler, W. Wernsdorfer, K.A. Abboud, G. Christou, Inorg. Chem. 44 (2005) 5304–5321.
[155] N. Vries, J. Chem. Soc. Chem. Commun. (1994) 1745–1746.
[156] H.J. Eppley, H.-L. Tsai, N. de Vries, K. Folting, G. Christou, D.N. Hendrickson, J. Am. Chem. Soc. 117 (1995) 301–317.
[157] M. Soler, S.K. Chandra, D. Ruiz, E.R. Davidson, D.N. Hendrickson, G. Christou, Chem. Commun. (2000) 2417–2418.
[158] A.R. Schake, H.-L. Tsai, N. de Vries, R.J. Webb, K. Folting, D.N. Hendrickson, G. Christou, J. Chem. Soc. Chem. Commun. (1992) 181–183.
[159] C.-I. Yang, H.-L. Tsai, G.-H. Lee, C.-S. Wur, S.-F. Yang, Chem. Lett. 34 (2005) 288–289.
[160] J.T. Brockman, K.A. Abboud, D.N. Hendrickson, G. Christou, Polyhedron 22 (2003) 1765–1769.
[161] G.-Q. Bian, T. Kuroda-Sowa, H. Konaka, M. Hatano, M. Maekawa, M. Munakata, H. Miyasaka, M. Yamashita, Inorg. Chem. 43 (2004) 4790–4792.
[162] S.M. Aubin, Z. Sun, H.J. Eppley, E.M. Rumberger, I.A. Guzei, K. Folting, P.K. Gantzel, A.L. Rheingold, G. Christou, D.N. Hendrickson, Inorg. Chem. 40 (2001) 2127–2146.
[163] C. Boskovic, M. Pink, J.C. Huffman, D.N. Hendrickson, G. Christou, J. Am. Chem. Soc. 123 (2001) 9914–9915.
[164] A.J. Tasiopoulos, A. Vinslava, W. Wernsdorfer, K.A. Abboud, G. Christou, Angew. Chem. Int. Ed. 43 (2004) 2117–2121.
[165] C. Ritchie, A. Ferguson, H. Nojiri, H.N. Miras, Y.F. Song, D.L. Long, E. Burkholder, M. Murrie, P. Kögerler, E.K. Brechin, Angew. Chem. Int. Ed. 47 (2008) 5609–5612.
[166] C.-C. Wu, S. Datta, W. Wernsdorfer, G.-H. Lee, S. Hill, E.-C. Yang, Dalton Trans. 39 (2010) 10160–10168.
[167] S. Wang, K. Folting, W.E. Streib, E.A. Schmitt, J.K. McCusker, D.N. Hendrickson, G. Christou, Angew. Chem. Int. Ed. Eng. 30 (1991) 305–306.
[168] J.-Z. Wu, E. Sellitto, G.P. Yap, J. Sheats, G.C. Dismukes, Inorg. Chem. 43 (2004) 5795–5797.
[169] K.L. Taft, A. Caneschi, L.E. Pence, C.D. Delfs, G.C. Papaefthymiou, S.J. Lippard, J. Am. Chem. Soc. 115 (1993) 11753–11766.
[170] T.A. Hudson, K.J. Berry, B. Moubaraki, K.S. Murray, R. Robson, Inorg. Chem. 45 (2006) 3549–3556.
[171] H.J. Mai, R.M. zu Köcker, S. Wocadlo, W. Massa, K. Dehnicke, Angew. Chem. Int. Ed. Eng. 34 (1995) 1235–1236.
[172] U. Riese, B. Neumüller, N. Faza, W. Massa, K. Dehnicke, Z. Anorg, Allg. Chem. 623 (1997) 351–356.
[173] S. Vaddypally, S.K. Kondaveeti, M.J. Zdilla, Inorg. Chem. 51 (2012) 3950–3952.
[174] S. Vaddypally, S.K. Kondaveeti, J.H. Roudebush, R.J. Cava, M.J. Zdilla, Chem. Commun. 50 (2014) 1061–1063.
[175] S. Vaddypally, S.K. Kondaveeti, S. Karki, M.M. Van Vliet, R.J. Levis, M.J. Zdilla, J. Am. Chem. Soc. 139 (2017) 4675–4681.
[176] R. Chakrabarty, P. Sarmah, B. Saha, S. Chakravorty, B.K. Das, Inorg. Chem. 48 (2009) 6371–6379.
[177] R. Chakrabarty, S.J. Bora, B.K. Das, Inorg. Chem. 46 (2007) 9450–9462.
[178] K. Dimitrou, A.D. Brown, T.E. Concolino, A.L. Rheingold, G. Christou, Chem. Commun. (2001) 1284–1285.
[179] K. Dimitrou, J.-S. Sun, K. Folting, G. Christou, Inorg. Chem. 34 (1995) 4160–4166.
[180] G. Aromí, A.S. Batsanov, P. Christian, M. Helliwell, A. Parkin, S. Parsons, A.A. Smith, G.A. Timco, R.E. Winpenny, Chem-Eur. J. 9 (2003) 5142–5161.
[181] K. Dimitrou, K. Folting, W.E. Streib, G. Christou, J. Chem. Soc. Chem. Commun. (1994) 1385–1386.
[182] K. Dimitrou, K. Folting, W.E. Streib, G. Christou, J. Am. Chem. Soc. 115 (1993) 6432–6433.
[183] M. Murrie, S. Parsons, R.E. Winpenny, I.M. Atkinson, C. Benelli, Chem. Commun. (1999) 285–286.
[184] L. Akhter, W. Clegg, D. Collison, C.D. Garner, Inorg. Chem. 24 (1985) 1725–1728.
[185] M. Eshel, A. Bino, Inorg. Chim. Acta 329 (2002) 45–50.
[186] E.M. Zueva, W. Sameera, D.M. Pinero, I. Chakraborty, E. Devlin, P. Baran, K. Lebruskova, Y. Sanakis, J.E. McGrady, R.G. Raptis, Inorg. Chem. 50 (2011) 1021–1029.
[187] P. Baran, R. Boca, I. Chakraborty, J. Giapintzakis, R. Herchel, Q. Huang, J.E. McGrady, R.G. Raptis, Y. Sanakis, A. Simopoulos, Inorg. Chem. 47 (2008) 645–655.
[188] H. Oshio, N. Hoshino, T. Ito, J. Am. Chem. Soc. 122 (2000) 12602–12603.
[189] G. Seeber, G.J. Cooper, G.N. Newton, M.H. Rosnes, D.-L. Long, B.M. Kariuki, P. Kögerler, L. Cronin, Chem. Sci. 1 (2010) 62–67.
[190] J. Lewiński, K. Suwała, M. Kubisiak, Z. Ochal, I. Justyniak, J. Lipkowski, Angew. Chem. Int. Ed. 47 (2008) 7888–7891.
[191] D. Franz, H.-W. Lerner, M. Bolte, Acta Cryst. E, 67 (2011) m1395-m1395. https://doi.org/10.1107/S160053681103697X. https://journals.iucr.org/e/issues/2011/10/00/kj2188/index.html.
[192] E.L.-M. Wong, R.W.-Y. Sun, N.P.-Y. Chung, C.-L.S. Lin, N. Zhu, C.-M. Che, J. Am. Chem. Soc. 128 (2006) 4938–4939.
[193] A. Yanagisawa, S. Habaue, H. Yamamoto, J. Am. Chem. Soc. 113 (1991) 5893–5895.
[194] A. Mishra, W. Wernsdorfer, K.A. Abboud, G. Christou, Chem. Commun. (2005) 54–56.
[195] A.R. Schake, H.-L. Tsai, R.J. Webb, K. Folting, G. Christou, D.N. Hendrickson, Inorg. Chem. 33 (1994) 6020–6028.
[196] X. Fang, M. Luban, Chem. Commun. 47 (2011) 3066–3068.
[197] S. Polarz, F. Neues, M.W. Van den Berg, W. Grünert, L. Khodeir, J. Am. Chem. Soc. 127 (2005) 12028–12034.
[198] S. Jana, R.J. Berger, R. Fröhlich, T. Pape, N.W. Mitzel, Inorg. Chem. 46 (2007) 4293–4297.
[199] C. Redshaw, S. Jana, C. Shang, M.R. Elsegood, X. Lu, Z.X. Guo, Chem. Commun. 46 (2010) 9055–9057.
[200] A. Charette, A. Beauchemin, S. Francoeur, F. Bélanger-Gariépy, G.D. Enright, Chem. Commun. (2002) 466–467.
[201] J. Lewiński, W. Marciniak, J. Lipkowski, I. Justyniak, J. Am. Chem. Soc. 125 (2003) 12698–12699.
[202] Q. Li, K. Nie, B. Xu, Y. Yao, Y. Zhang, Q. Shen, Polyhedron 31 (2012) 58–63.
[203] D. Cui, M. Nishiura, Z. Hou, Angew. Chem. Int. Ed. 44 (2005) 959–962.
[204] J. Deutscher, T. Corona, K. Warm, X. Engelmann, S. Sobottka, B. Braun-Cula, B. Sarkar, K. Ray, Eur. J. Inorg. Chem. 2018 (2018) 4925–4929.
[205] A.I. Nguyen, M.S. Ziegler, P. Oña-Burgos, M. Sturzbecher-Hohne, W. Kim, D.E. Bellone, T.D. Tilley, J. Am. Chem. Soc. 137 (2015) 12865–12872.
[206] M.W. Kanan, D.G. Nocera, Science 321 (2008) 1072–1075.
[207] P.F. Smith, C. Kaplan, J.E. Sheats, D.M. Robinson, N.S. McCool, N. Mezle, G.C. Dismukes, Inorg. Chem. 53 (2014) 2113–2121.
[208] F. Evangelisti, R. Güttinger, R. Moré, S. Luber, G.R. Patzke, J. Am. Chem. Soc. 135 (2013) 18734–18737.
[209] S. Berardi, G. La Ganga, M. Natali, I. Bazzan, F. Puntoriero, A. Sartorel, F. Scandola, S. Campagna, M. Bonchio, J. Am. Chem. Soc. 134 (2012) 11104–11107.
[210] A.M. Ullman, Y. Liu, M. Huynh, D.K. Bediako, H. Wang, B.L. Anderson, D.C. Powers, J.J. Breen, H.c.D. Abruña, D.G. Nocera, J. Am. Chem. Soc. 136 (2014) 17681–17688.
[211] H. Link, D. Fenske, Z. Anorg, Allg. Chem. 625 (1999) 1878–1884.
[212] A.K. Verma, S.C. Lee, J. Am. Chem. Soc. 121 (1999) 10838–10839.
[213] M.J. Zdilla, A.K. Verma, S.C. Lee, Inorg. Chem. 50 (2011) 1551–1562.
[214] A.K. Verma, T.N. Nazif, C. Achim, S.C. Lee, J. Am. Chem. Soc. 122 (2000) 11013–11014.
[215] S.D. Brown, J.C. Peters, J. Am. Chem. Soc. 127 (2005) 1913–1923.
[216] M. Imaji, Y. Tanabe, Y. Mutoh, Y. Ishii, Inorg. Chem. 48 (2009) 773–780.
[217] Y. Tanabe, S. Kuwata, Y. Ishii, J. Am. Chem. Soc. 124 (2002) 6528–6529.
[218] U. Riese, K. Harms, J. Pebler, K. Dehnicke, Z. Anorg, Allg. Chem. 625 (1999) 746–754.
[219] T. Miekisch, K. Harms, S. Wocadlo, W. Massa, B. Neumüller, C. Frommen, K. Dehnicke, Z. Naturforsch, B 52 (1997) 1484–1490.
[220] U. Riese, K. Harms, B. Neumüller, K. Dehnicke, Z. Anorg, Allg. Chem. 624 (1998) 1279–1284.
[221] K. Harms, J. Merle, C. Maichle-Mössmer, W. Massa, M. Krieger, Inorg. Chem. 37 (1998) 1099–1104.
[222] M. Krieger, R.O. Gould, J. Pebler, K. Dehnicke, Z. Anorg, Allg. Chem. 624 (1998) 781–786.
[223] H.J. Mai, H.C. Kang, S. Wocadlo, W. Massa, K. Dehnicke, Z. Anorg, Allg. Chem. 621 (1995) 1963–1968.
[224] S. Abram, U. Abram, R.M. zu Köcker, K. Dehnicke, Z. Anorg. Allg. Chem. 622 (1996) 867–872.
[225] D. Coucouvanis, K.D. Demadis, C.G. Kim, R.W. Dunham, J.W. Kampf, J. Am. Chem. Soc. 115 (1993) 3344–3345.
[226] J.D. McCall, S. Vaddypally, S.K. Kondaveeti, M.J. Zdilla, Inorg. Chem. Commun. 37 (2013) 225–227.
[227] G.J. Cooper, G.N. Newton, P. Kögerler, D.L. Long, L. Engelhardt, M. Luban, L. Cronin, Angew. Chem. Int. Ed. 46 (2007) 1340–1344.
[228] A.A. Danopoulos, G. Wilkinson, T.K. Sweet, M.B. Hursthouse, J. Chem. Soc. Dalton Trans. (1995) 205–216.
[229] M.H. Zeng, M.X. Yao, H. Liang, W.X. Zhang, X.M. Chen, Angew. Chem. Int. Ed. 46 (2007) 1832–1835.
[230] C. He, S.J. Lippard, J. Am. Chem. Soc. 122 (2000) 184–185.
[231] G.N. Newton, G.J. Cooper, P. Kögerler, D.-L. Long, L. Cronin, J. Am. Chem. Soc. 130 (2008) 790–791.
[232] X. Liu, J.A. McAllister, M.P. de Miranda, E.J. McInnes, C.A. Kilner, M.A. Halcrow, Chem-Eur. J. 10 (2004) 1827–1837.
[233] P.L. Dedert, T. Sorrell, T.J. Marks, J.A. Ibers, Inorg. Chem. 21 (1982) 3506–3517.
[234] A. Igashira-Kamiyama, J. Fujioka, S. Mitsunaga, M. Nakano, T. Kawamoto, T. Konno, Chem-Eur. J. 14 (2008) 9512–9515.
[235] T.D. Keene, M.B. Hursthouse, D.J. Price, New J. Chem. 28 (2004) 558–561.
[236] J.P. Wikstrom, A.Y. Nazarenko, W.M. Reiff, E.V. Rybak-Akimova, Inorg. Chim. Acta 360 (2007) 3733–3740.
[237] M. Ahmed, H. Fjellvåg, A. Kjekshus, P. Dietzel, Z. Anorg, Allg. Chem. 633 (2007) 1371–1381.
[238] J.F. Berry, F.A. Cotton, C.Y. Liu, T. Lu, C.A. Murillo, B.S. Tsukerblat, D. Villagrán, X. Wang, J. Am. Chem. Soc. 127 (2005) 4895–4902.
[239] J. Bertrand, T.C. Hightower, Inorg. Chem. 12 (1973) 206–210.
[240] S. Diewald, Y. Lan, R. Clérac, A.K. Powell, C. Feldmann, Z. Anorg, Allg. Chem. 634 (2008) 1880–1886.
[241] E. Richard, Chem. Commun. (1996) 1439–1440.
[242] R. Wang, M. Hong, W. Su, R. Cao, Acta Cryst. E 57 (2001) m325–m327.

[243] A. Mukherjee, M. Nethaji, A.R. Chakravarty, Angew. Chem. Int. Ed. 43 (2004) 87–90.
[244] P.O. Oguadinma, F. Schaper, Organometallics 28 (2009) 4089–4097.
[245] S. Yoon, S.J. Lippard, J. Am. Chem. Soc. 127 (2005) 8386–8397.
[246] L.A. Vermeulen, J.L. Snover, L.S. Sapochak, M.E. Thompson, J. Am. Chem. Soc. 115 (1993) 11767–11774.
[247] F. Piga, F. Moro, I. Krivokapic, A.J. Blake, R. Edge, E.J. McInnes, D.J. Evans, J. McMaster, J. van Slageren, Chem. Commun. 48 (2012) 2430–2432.
[248] P.L. Feng, C.C. Beedle, C. Koo, W. Wernsdorfer, M. Nakano, S. Hill, D.N. Hendrickson, Inorg. Chem. 47 (2008) 3188–3204.
[249] P.L. Feng, C.C. Beedle, W. Wernsdorfer, C. Koo, M. Nakano, S. Hill, D.N. Hendrickson, Inorg. Chem. 46 (2007) 8126–8128.
[250] M.D. Godbole, O. Roubeau, A.M. Mills, H. Kooijman, A.L. Spek, E. Bouwman, Inorg. Chem. 45 (2006) 6713–6722.
[251] L.B. Jerzykiewicz, J. Utko, M. Duczmal, P. Starynowicz, P. Sobota, Eur. J. Inorg. Chem. 2010 (2010) 4492–4498.
[252] L.E. Pence, A. Caneschi, S.J. Lippard, Inorg. Chem. 35 (1996) 3069–3072.
[253] S. Brooker, V. McKee, T. Metcalfe, Inorg. Chim. Acta 246 (1996) 171–179.
[254] V. McKee, W.B. Shepard, J. Chem. Soc. Chem. Commun. (1985) 158–159.
[255] J.-W. Ran, S.-Y. Zhang, B. Xu, Y. Xia, D. Guo, J.-Y. Zhang, Y. Li, Inorg. Chem. Commun. 11 (2008) 73–76.
[256] S.-H. Zhang, N. Li, C.-M. Ge, C. Feng, L.-F. Ma, Dalton Trans. 40 (2011) 3000–3007.
[257] W.L. Gladfelter, M.W. Lynch, W.P. Schaefer, D.N. Hendrickson, H.B. Gray, Inorg. Chem. 20 (1981) 2390–2397.
[258] A.B. Charette, C. Molinaro, C. Brochu, J. Am. Chem. Soc. 123 (2001) 12160–12167.
[259] J.M. Burlitch, S.E. Hayes, G.E. Whitwell, Organometallics 1 (1982) 1074–1083.
[260] F. Chemla, F. Dulong, F. Ferreira, A. Pérez-Luna, Beilstein J. Org. Chem. 9 (2013) 236–245.
[261] A. Orlov, A. Roy, M. Lehmann, M. Driess, S. Polarz, J. Am. Chem. Soc. 129 (2007) 371–375.
[262] H. Shearer, C. Spencer, Acta Cryst. B 36 (1980) 2046–2050.
[263] J. Lewiński, M. Dutkiewicz, M. Lesiuk, W. Śliwiński, K. Zelga, I. Justyniak, J. Lipkowski, Angew. Chem. 122 (2010) 8442–8445.
[264] M.L. Ziegler, J. Weiss, Angew. Chem. 82 (1970) 931–932.
[265] T.J. Boyle, S.D. Bunge, N.L. Andrews, L.E. Matzen, K. Sieg, M.A. Rodriguez, T.J. Headley, Chem. Mater. 16 (2004) 3279–3288.
[266] M. Murrie, S.J. Teat, H. Stœckli-Evans, H.U. Güdel, Angew. Chem. Int. Ed. 42 (2003) 4653–4656.
[267] R.G. Pearson, J. Am. Chem. Soc. 85 (1963) 3533–3539.
[268] S.C. Lee, W. Lo, R. Holm, Chem. Rev. 114 (2014) 3579–3600.
[269] P. Barbaro, A. Bencini, I. Bertini, F. Briganti, S. Midollini, J. Am. Chem. Soc. 112 (1990) 7238–7246.
[270] S.B. Yu, G. Papaefthymiou, R. Holm, Inorg. Chem. 30 (1991) 3476–3485.
[271] C.W. Carter, S. Freer, N.H. Xuong, R. Alden, J. Kraut, in: Cold Spring Harbor Laboratory Press, Cold Spring Harbor Laboratory Press, 1972, pp. 381-385..
[272] M. Emptage, T. Kent, B. Huynh, J. Rawlings, W. Orme-Johnson, E. Münck, J. Biol. Chem. 255 (1980) 1793–1796.
[273] A. Robbins, C. Stout, Proteins 5 (1989) 289–312.
[274] T. Herskovitz, B. Averill, R. Holm, J.A. Ibers, W. Phillips, J. Weiher, Proc. Natl. Acad. Sci. USA 69 (1972) 2437–2441.
[275] S.C. Kennedy, R. Rauner, O. Gawron, Biochem. Biophys. Res. 47 (1972) 740–745.
[276] F.J. Ruzicka, H. Beinert, J. Biol. Chem. 253 (1978) 2514–2517.
[277] H. Beinert, M.H. Emptage, J.-L. Dreyer, R.A. Scott, J.E. Hahn, K.O. Hodgson, A.J. Thomson, Proc. Natl. Acad. Sci. USA 80 (1983) 393–396.
[278] H. Beinert, M.C. Kennedy, C.D. Stout, Chem. Rev. 96 (1996) 2335–2374.
[279] D.H. Flint, R.M. Allen, Chem. Rev. 96 (1996) 2315–2334.
[280] L. Banci, I. Bertini, C. Luchinat, P. Turano, I. in Bertini, H. Gray, E. Stiefel, J. Valentine, Biological Inorganic Chemistry: Structure and Reactivity, University Science Books, 2007, pp. 261..
[281] G. Bertini, H. Gray, H.B. Gray, E. Stiefel, J.S. Valentine, E.I. Stiefel, Biological Inorganic Chemistry: structure and reactivity, University Science Books, 2007.
[282] L.C. Seefeldt, B.M. Hoffman, J.W. Peters, S. Raugei, D.N. Beratan, E. Antony, D. R. Dean, Acc. Chem. Res. 51 (2018) 2179–2186.
[283] Y. Hu, M.W. Ribbe, Angew. Chem. Int. Ed. 55 (2016) 8216–8226.
[284] B.M. Hoffman, D. Lukoyanov, Z.-Y. Yang, D.R. Dean, L.C. Seefeldt, Chem. Rev. 114 (2014) 4041–4062.
[285] B.M. Hoffman, D. Lukoyanov, D.R. Dean, L.C. Seefeldt, Acc. Chem. Res. 46 (2013) 587–595.
[286] J.C. Fontecilla-Camps, A. Volbeda, C. Cavazza, Y. Nicolet, Chem. Rev. 107 (2007) 4273–4303.
[287] R.H. Holm, Acc. Chem. Res. 10 (1977) 427–434.
[288] E. Münck, T.A. Kent, Hyperfine Interact. 27 (1986) 161–172.
[289] R. Holm, B. Averill, T. Herskovitz, R. Frankel, H. Gray, O. Siiman, F. Grunthaner, J. Am. Chem. Soc. 96 (1974) 2644–2646.
[290] E. Laskowski, R. Frankel, W. Gillum, G. Papaefthymiou, J. Renaud, J.A. Ibers, R. Holm, J. Am. Chem. Soc. 100 (1978) 5322–5337.
[291] T. O'Sullivan, M.M. Millar, J. Am. Chem. Soc. 107 (1985) 4096–4097.
[292] V. Papaefthymiou, M.M. Millar, E. Muenck, Inorg. Chem. 25 (1986) 3010–3014.
[293] L. Deng, R. Holm, J. Am. Chem. Soc. 130 (2008) 9878–9886.
[294] Y. Ohki, Y. Sunada, K. Tatsumi, Chem. Lett. 34 (2005) 172–173.
[295] C.R. Sharp, J.S. Duncan, S.C. Lee, Inorg. Chem. 49 (2010) 6697–6705.
[296] L. Ryden, L. Ofverstedt, H. Beinert, M. Emptage, M.C. Kennedy, J. Biol. Chem. 259 (1984) 3141–3144.
[297] H. Beinert, A.J. Thomson, Arch. Bioch. Biophys. 222 (1983) 333–361.
[298] T.A. Kent, J.-L. Dreyer, M.C. Kennedy, B.H. Huynh, M.H. Emptage, H. Beinert, E. Münck, Proc. Natl. Acad. Sci. USA 79 (1982) 1096–1100.
[299] H. Beinert, M.C. Kennedy, FASEB 7 (1993) 1442–1449.
[300] C.H. Williams, T.J. Stillman, V.V. Barynin, S.E. Sedelnikova, Y. Tang, J. Green, J. R. Guest, P.J. Artymiuk, Nature Struct. Biol. 9 (2002) 447–452.
[301] S. Lloyd, H. Lauble, G. Prasad, C. Stout, Protein Sci. 8 (1999) 2655–2662.
[302] T.A. Kent, M. Emptage, H. Merkle, M. Kennedy, H. Beinert, E. Münck, J. Biol. Chem. 260 (1985) 6871–6881.
[303] C.D. Stout, J. Biol. Chem. 268 (1993) 25920–25927.
[304] C.R. Kissinger, E.T. Adman, L.C. Sieker, L.H. Jensen, J. Am. Chem. Soc. 110 (1988) 8721–8723.
[305] E. Merritt, G. Stout, S. Turley, L. Sieker, L. Jensen, W. Orme-Johnson, Acta Cryst. D 49 (1993) 272–281.
[306] J. Zhou, R. Holm, J. Am. Chem. Soc. 117 (1995) 11353–11354.
[307] E. Münck, K. Ksurerus, M.P. Hendrich, [17] Combining Mössbauer spectroscopy with integer spin electron paramagnetic resonance, in: Methods in enzymology, Elsevier, 1993, pp. 463-479..
[308] J.L. Vey, C.L. Drennan, Chem. Rev. 111 (2011) 2487–2506.
[309] J.B. Broderick, B.R. Duffus, K.S. Duschene, E.M. Shepard, Chem. Rev. 114 (2014) 4229–4317.
[310] J.B. Broderick, T.F. Henshaw, J. Cheek, K. Wojtuszewski, S.R. Smith, M.R. Trojan, R.M. McGhan, A. Kopf, M. Kibbey, W.E. Broderick, Biochem. Biophys. Res. 269 (2000) 451–456.
[311] C. Krebs, W.E. Broderick, T.F. Henshaw, J.B. Broderick, B.H. Huynh, J. Am. Chem. Soc. 124 (2002) 912–913.
[312] C. Krebs, T.F. Henshaw, J. Cheek, B.H. Huynh, J.B. Broderick, J. Am. Chem. Soc. 122 (2000) 12497–12506.
[313] G. Layer, J. Moser, D.W. Heinz, D. Jahn, W.D. Schubert, EMBO 22 (2003) 6214–6224.
[314] C.J. Walsby, W. Hong, W.E. Broderick, J. Cheek, D. Ortillo, J.B. Broderick, B.M. Hoffman, J. Am. Chem. Soc. 124 (2002) 3143–3151.
[315] F. Berkovitch, Y. Nicolet, J.T. Wan, J.T. Jarrett, C.L. Drennan, Science 303 (2004) 76–79.
[316] P. Hänzelmann, H. Schindelin, Proc. Natl. Acad. Sci. USA 101 (2004) 12870–12875.
[317] H. Conradt, M. Hohmann-Berger, H.-P. Hohmann, H.P. Blaschkowski, J. Knappe, Arch. Bioch. Biophys. 228 (1984) 133–142.
[318] J. Knappe, F.A. Neugebauer, H.P. Blaschkowski, M. Gänzler, Proc. Natl. Acad. Sci. USA 81 (1984) 1332–1335.
[319] A. Wagner, M. Frey, F.A. Neugebauer, W. Schäfer, J. Knappe, Proc. Natl. Acad. Sci. USA 89 (1992) 996–1000.
[320] P.A. Frey, A.D. Hegeman, F.J. Ruzicka, Crit. Rev. Biochem. Mol. 43 (2008) 63–88.
[321] S. Arragain, R. Garcia-Serres, G. Blondin, T. Douki, M. Clemancey, J.-M. Latour, F. Forouhar, H. Neely, G.T. Montelione, J.F. Hunt, J. Biol. Chem. 285 (2010) 5792–5801.
[322] M.M. Wuebbens, K. Rajagopalan, J. Biol. Chem. 270 (1995) 1082–1087.
[323] C. Rieder, W. Eisenreich, J. O'Brien, G. Richter, E. Götze, P. Boyle, S. Blanchard, A. Bacher, H. Simon, Eur. J. Biochem. 255 (1998) 24–36.
[324] M.M. Wuebbens, M.T. Liu, K. Rajagopalan, H. Schindelin, Structure 8 (2000) 709–718.
[325] N.S. Lees, P. Hänzelmann, H.L. Hernandez, S. Subramanian, H. Schindelin, M.K. Johnson, B.M. Hoffman, J. Am. Chem. Soc. 131 (2009) 9184–9185.
[326] M.C. Posewitz, P.W. King, S.L. Smolinski, L. Zhang, M. Seibert, M.L. Ghirardi, J. Biol. Chem. 279 (2004) 25711–25720.
[327] P.W. King, M.C. Posewitz, M.L. Ghirardi, M. Seibert, J. Bacteriol. 188 (2006) 2163–2172.
[328] S.E. McGlynn, S.S. Ruebush, A. Naumov, L.E. Nagy, A. Dubini, P.W. King, J. B. Broderick, M.C. Posewitz, J.W. Peters, J. Biol. Inorg. Chem. 12 (2007) 443–447.
[329] N.S. Sickerman, M.W. Ribbe, Y. Hu, Acc. Chem. Res. 50 (2017) 2834–2841.
[330] W. Lubitz, H. Ogata, O. Rüdiger, E. Reijerse, Chem. Rev. 114 (2014) 4081–4148.
[331] G. Berggren, A. Adamska, C. Lambertz, T. Simmons, J. Esselborn, M. Atta, S. Gambarelli, J.-M. Mouesca, E. Reijerse, W. Lubitz, Nature 499 (2013) 66.
[332] D. Schilter, J.M. Camara, M.T. Huynh, S. Hammes-Schiffer, T.B. Rauchfuss, Chem. Rev. 116 (2016) 8693–8749.
[333] J.M. Camara, T.B. Rauchfuss, Nature Chem. 4 (2012) 26–30.
[334] J.C. Lansing, J.M. Camara, D.E. Gray, T.B. Rauchfuss, Organometallics 33 (2014) 5897–5906.
[335] P.M. Vignais, B. Billoud, J. Meyer, F.E.M.S. Microbiol, Rev. 25 (2001) 455–501.
[336] V. Svetlitchnyi, C. Peschel, G. Acker, O. Meyer, J. Bacteriol. 183 (2001) 5134–5144.
[337] S.W. Ragsdale, M. Kumar, Chem. Rev. 96 (1996) 2515–2540.
[338] T.C. Harrop, P.K. Mascharak, Coord. Chem. Rev. 249 (2005) 3007–3024.
[339] C.L. Drennan, J. Heo, M.D. Sintchak, E. Schreiter, P.W. Ludden, Proc. Natl. Acad. Sci. USA 98 (2001) (1978) 11973–11981.
[340] H. Dobbek, V. Svetlitchnyi, L. Gremer, R. Huber, O. Meyer, Science 293 (2001) 1281–1285.
[341] C. Darnault, A. Volbeda, E.J. Kim, P. Legrand, X. Vernède, P.A. Lindahl, J.C. Fontecilla-Camps, Nat. Struct. Mol. Biol. 10 (2003) 271–279.
[342] Y. Kung, T.I. Doukov, J. Seravalli, S.W. Ragsdale, C.L. Drennan, Biochemistry 48 (2009) 7432–7440.

[343] Y. Kung, C.L. Drennan, Curr. Opin. Chem. Biol. 15 (2011) 276–283.
[344] R. Panda, C.P. Berlinguette, Y. Zhang, R.H. Holm, J. Am. Chem. Soc. 127 (2005) 11092–11101.
[345] J. Zhou, M.J. Scott, Z. Hu, G. Peng, E. Munck, R. Holm, J. Am. Chem. Soc. 114 (1992) 10843–10854.
[346] J. Sun, C. Tessier, R. Holm, Inorg. Chem. 46 (2007) 2691–2699.
[347] S. Ciurli, S.B. Yu, R. Holm, K. Srivastava, E. Munck, J. Am. Chem. Soc. 112 (1990) 8169–8171.
[348] S. Ciurli, P.K. Ross, M.J. Scott, S.B. Yu, R. Holm, J. Am. Chem. Soc. 114 (1992) 5415–5423.
[349] R.R. Eady, Chem. Rev. 96 (1996) 3013–3030.
[350] R.L. Robson, R.R. Eady, T.H. Richardson, R.W. Miller, M. Hawkins, J.R. Postgate, Nature 322 (1986) 388–390.
[351] B.J. Hales, E.E. Case, J.E. Morningstar, M.F. Dzeda, L.A. Mauterer, Biochemistry 25 (1986) 7251–7255.
[352] A. Müller, K. Schneider, K. Knüttel, W.R. Hagen, FEBS Lett. 303 (1992) 36–40.
[353] T. Lovell, R.A. Torres, W.-G. Han, T. Liu, D.A. Case, L. Noodleman, Inorg. Chem. 41 (2002) 5744–5753.
[354] L.C. Seefeldt, Z.-Y. Yang, D.A. Lukoyanov, D.F. Harris, D.R. Dean, S. Raugei, B.M. Hoffman, Chem. Rev. (2020).
[355] S.F. McWilliams, P.L. Holland, Acc. Chem. Res. 48 (2015) 2059–2065.
[356] J. Rittle, J.C. Peters, Proc. Natl. Acad. Sci. U.S.A. 110 (2013) 15898–15903.
[357] P.L. Holland, Acc. Chem. Res. 41 (2008) 905–914.
[358] J.S. Anderson, J. Rittle, J.C. Peters, Nature 501 (2013) 84–87.
[359] T.J. Del Castillo, N.B. Thompson, J.C. Peters, J. Am. Chem. Soc. 138 (2016) 5341–5350.
[360] N.B. Thompson, M.T. Green, J.C. Peters, J. Am. Chem. Soc. 139 (2017) 15312–15315.
[361] J. Kim, D. Rees, Science 257 (1992) 1677–1682.
[362] J. Kirn, D. Rees, Nature 360 (1992) 553–560.
[363] O. Einsle, F.A. Tezcan, S.L. Andrade, B. Schmid, M. Yoshida, J.B. Howard, D.C. Rees, Science 297 (2002) 1696–1700.
[364] T. Spatzal, M. Aksoyoglu, L. Zhang, S.L. Andrade, E. Schleicher, S. Weber, D.C. Rees, O. Einsle, Science 334 (2011) 940.
[365] J.A. Wiig, Y. Hu, C.C. Lee, M.W. Ribbe, Science 337 (2012) 1672–1675.
[366] D. Sippel, O. Einsle, Nat. Chem. Biol. 13 (2017) 956.
[367] T. Spatzal, K.A. Perez, O. Einsle, J.B. Howard, D.C. Rees, Science 345 (2014) 1620–1623.
[368] W. Kang, C.C. Lee, A.J. Jasniewski, M.W. Ribbe, Y. Hu, Science 368 (2020) 1381–1385.
[369] J. Bergmann, E. Oksanen, U. Ryde, J. Biol. Inorg. Chem. (2021) 1–13.
[370] B.K. Burgess, D.J. Lowe, Chem. Rev. 96 (1996) 2983–3012.
[371] J. Kim, D. Woo, D. Rees, Biochemistry 32 (1993) 7104–7115.
[372] F.A. Tezcan, J.T. Kaiser, D. Mustafi, M.Y. Walton, J.B. Howard, D.C. Rees, Science 309 (2005) 1377–1380.
[373] R.A. Torres, T. Lovell, L. Noodleman, D.A. Case, J. Am. Chem. Soc. 125 (2003) 1923–1936.
[374] P. Strop, P.M. Takahara, H.-J. Chiu, H.C. Angove, B.K. Burgess, D.C. Rees, Biochemistry 40 (2001) 651–656.
[375] R. Burris, J. Biol. Chem 266 (1991) 9339–9342.
[376] Y. Ohki, M. Imada, A. Murata, Y. Sunada, S. Ohta, M. Honda, T. Sasamori, N. Tokitoh, M. Katada, K. Tatsumi, J. Am. Chem. Soc. 131 (2009) 13168–13178.
[377] D.L. Gerlach, D. Coucouvanis, J. Kampf, N. Lehnert, Eur. J. Inorg. Chem. 2013 (2013) 5253–5264.
[378] F. Osterloh, Y. Sanakis, R.J. Staples, E. Münck, R.H. Holm, Angew. Chem. Int. Ed. 38 (1999) 2066–2070.
[379] Y. Zhang, J.-L. Zuo, H.-C. Zhou, R. Holm, J. Am. Chem. Soc. 124 (2002) 14292–14293.
[380] Y. Zhang, R. Holm, J. Am. Chem. Soc. 125 (2003) 3910–3920.
[381] H.L. Rutledge, J. Rittle, L.M. Williamson, W.A. Xu, D.M. Gagnon, F.A. Tezcan, J. Am. Chem. Soc. 141 (2019) 10091–10098.
[382] S. Duval, K. Danyal, S. Shaw, A.K. Lytle, D.R. Dean, B.M. Hoffman, E. Antony, L. C. Seefeldt, Proc. Natl. Acad. Sci. U.S.A. 110 (2013) 16414–16419.
[383] C.C. Lee, Y. Hu, M.W. Ribbe, Proc. Natl. Acad. Sci. U.S.A. 106 (2009) 9209–9214.
[384] S.J. Yoo, H.C. Angove, V. Papaefthymiou, B.K. Burgess, E. Münck, J. Am. Chem. Soc. 122 (2000) 4926–4936.
[385] S. Sun, S. Anders, H. Hamann, J. Thiele, J. Baglin, J. Am. Chem. Soc 124 (2002) 2884–2885.
[386] S.P. Cramer, W.O. Gillum, K.O. Hodgson, L.E. Mortenson, E.I. Stiefel, J.R. Chisnell, W.J. Brill, V.K. Shah, J. Am. Chem. Soc. 100 (1978) 3814–3819.
[387] B.M. Hoffman, J.E. Roberts, W. Orme-Johnson, J. Am. Chem. Soc. 104 (1982) 860–862.
[388] R.A. Venters, M.J. Nelson, P.A. McLean, A.E. True, M.A. Levy, B.M. Hoffman, W. H. Orme-Johnson, J. Am. Chem. Soc. 108 (1986) 3487–3498.
[389] A.E. True, P. McLean, M.J. Nelson, W. Orme-Johnson, B.M. Hoffman, J. Am. Chem. Soc. 112 (1990) 651–657.
[390] B. Hedman, P. Frank, S.F. Gheller, A.L. Roe, W.E. Newton, K.O. Hodgson, J. Am. Chem. Soc. 110 (1988) 3798–3805.
[391] R. Bjornsson, F. Neese, R.R. Schrock, O. Einsle, S. DeBeer, J. Biol. Inorg. Chem. 20 (2015) 447–460.
[392] T. Wolff, J. Berg, C. Warrick, K. Hodgson, R. Holm, R. Frankel, J. Am. Chem. Soc 100 (1978) 4630.
[393] T.E. Wolff, J.M. Berg, P.P. Power, K.O. Hodgson, R. Holm, Inorg. Chem. 19 (1980) 430–437.
[394] G. Christou, C.D. Garner, J. Chem. Soc. Dalton Trans. (1980) 2354–2362.
[395] W.H. Armstrong, R. Holm, J. Am. Chem. Soc. 103 (1981) 6246–6248.
[396] T.E. Wolff, J.M. Berg, R. Holm, Inorg. Chem. 20 (1981) 174–180.
[397] W. Armstrong, P. Mascharak, R. Holm, J. Am. Chem. Soc. 104 (1982) 4373–4383.
[398] P. Mascharak, W. Armstrong, Y. Mizobe, R. Holm, J. Am. Chem. Soc. 105 (1983) 475–483.
[399] K.D. Demadis, D. Coucouvanis, Inorg. Chem. 34 (1995) 436–448.
[400] M. Cook, M. Karplus, J. Am. Chem. Soc. 107 (1985) 257–259.
[401] M. Cook, M. Karplus, J. Chem. Phys. 83 (1985) 6344–6366.
[402] R. Bjornsson, F.A. Lima, T. Spatzal, T. Weyhermüller, P. Glatzel, E. Bill, O. Einsle, F. Neese, S. DeBeer, Chem. Sci. 5 (2014) 3096–3103.
[403] F.A. Lima, R. Bjornsson, T. Weyhermüller, P. Chandrasekaran, P. Glatzel, F. Neese, S. DeBeer, Phys. Chem. Chem. Phys. 15 (2013) 20911–20920.
[404] D.V. Fomitchev, C.C. McLauchlan, R. Holm, Inorg. Chem. 41 (2002) 958–966.
[405] D. Coucouvanis, Acc. Chem. Res. 14 (1981) 201–209.
[406] Z. Li, S. Du, X. Wu, Dalton Trans. (2004) 2438–2443.
[407] S. Ohta, Y. Ohki, T. Hashimoto, R.E. Cramer, K. Tatsumi, Inorg. Chem. 51 (2012) 11217–11219.
[408] Alex McSkimming, Daniel L.M. Suess, Dinitrogen binding and activation at a molybdenum–iron–sulfur cluster, Nat. Chem. 13 (2021) 666–670.
[409] Y. Ohki, Y. Ikagawa, K. Tatsumi, J. Am. Chem. Soc. 129 (2007) 10457–10465.
[410] I. Dance, Chem. Commun. (2003) 324–325.
[411] B. Hinnemann, J.K. Nørskov, J. Am. Chem. Soc. 125 (2003) 1466–1467.
[412] T. Lovell, T. Liu, D.A. Case, L. Noodleman, J. Am. Chem. Soc. 125 (2003) 8377–8383.
[413] V. Vrajmasu, E. Münck, E.L. Bominaar, Inorg. Chem. 42 (2003) 5974–5988.
[414] X.-D. Chen, J.S. Duncan, A.K. Verma, S.C. Lee, J. Am. Chem. Soc. 132 (2010) 15884–15886.
[415] X.-D. Chen, W. Zhang, J.S. Duncan, S.C. Lee, Inorg. Chem. 51 (2012) 12891–12904.
[416] G. Xu, Z. Wang, R. Ling, J. Zhou, X.-D. Chen, R.H. Holm, Proc. Natl. Acad. Sci. USA 115 (2018) 5089–5092.
[417] M.V. Bennett, S. Stoian, E.L. Bominaar, E. Münck, R.H. Holm, J. Am. Chem. Soc. 127 (2005) 12378–12386.
[418] M.V. Bennett, R. Holm, Angew. Chem. Int. Ed. 45 (2006) 5613–5616.
[419] T.M. Powers, A.R. Fout, S.-L. Zheng, T.A. Betley, J. Am. Chem. Soc. 133 (2011) 3336–3338.
[420] D.M. Ermert, J.B. Gordon, K.A. Abboud, L.J. Murray, Inorg. Chem. 54 (2015) 9282–9289.
[421] M. Tachikawa, E. Muetterties, Prog. Inorg. Chem. 28 (1981) 203–237.
[422] M. Tachikawa, A. Sievert, E. Muetterties, M. Thompson, C. Day, V. Day, J. Am. Chem. Soc. 102 (1980) 1725–1727.
[423] C. Joseph, S. Kuppuswamy, V.M. Lynch, M.J. Rose, Inorg. Chem. 57 (2018) 20–23.
[424] E.H. Braye, L.F. Dahl, W. Hubel, D.L. Wampler, J. Am. Chem. Soc. 84 (1962) 4633–4639.
[425] Y.V. Mironov, N.G. Naumov, S.G. Kozlova, S.J. Kim, V.E. Fedorov, Angew. Chem. Int. Ed. 44 (2005) 6867–6871.
[426] Y.M. Gayfulin, A.I. Smolentsev, S.G. Kozlova, V.V. Yanshole, Y.V. Mironov, Polyhedron 68 (2014) 334–339.
[427] Y.M. Gayfulin, M.R. Ryzhikov, D.G. Samsonenko, Y.V. Mironov, Polyhedron 151 (2018) 426–432.
[428] Y.M. Gayfulin, A.I. Smolentsev, S.G. Kozlova, I.N. Novozhilov, P.E. Plyusnin, N. B. Kompankov, Y.V. Mironov, Inorg. Chem. 56 (2017) 12389–12400.
[429] Y.V. Mironov, Y.M. Gayfulin, S.G. Kozlova, A.I. Smolentsev, M.S. Tarasenko, A. S. Nizovtsev, V.E. Fedorov, Inorg. Chem. 51 (2012) 4359–4367.
[430] M. Okazaki, T. Ohtani, H. Ogino, J. Am. Chem. Soc. 126 (2004) 4104–4105.
[431] M. Grabolle, H. Dau, Biochim. Biophys. Acta-Bioenerg. 1708 (2005) 209–218.
[432] F. Rappaport, M. Guergova-Kuras, P.J. Nixon, B.A. Diner, J. Lavergne, Biochemistry 41 (2002) 8518–8527.
[433] , Advances in Photosynthesis and Respiration 22 (2005) 139.
[434] Y. Umena, K. Kawakami, J.-R. Shen, N. Kamiya, Nature 473 (2011) 55–60.
[435] V. Klimov, A. Klevanik, V. Shuvalov, FEBS letters 82 (1977) 183–186.
[436] J.F. Allen, J. Bennett, K.E. Steinback, C.J. Arntzen, Nature 291 (1981) 25–29.
[437] C. Bengis, N. Nelson, J. Biol. Chem. 250 (1975) 2783–2788.
[438] J. Barber, Bioelectrochemistry 55 (2002) 135–138.
[439] C. Deng, D. Zhang, X. Pan, F. Chang, S. Wang, J. Photochem. Photobiol. B. Biol. 127 (2013) 1–7.
[440] H.D. Holland, Philos, Trans. Royal Soc. B Biol. Sci. 361 (2006) 903–915.
[441] H. Egneus, Physiolog. Plantarum 26 (1972) 81–91.
[442] R.J. Strasser, W.L. Butler, Plant Physiol. 58 (1976) 371–376.
[443] H. Egnéus, Physiolog. Plantarum 21 (1968) 602–614.
[444] O. Hayaishi, Molecular oxygen in biology: topics in molecular oxygen research, North-Holland Publishing Company, 1974..
[445] D.F. Ghanotakis, C.F. Yocum, Ann. Rev. Plant Biol. 41 (1990) 255–276.
[446] M. Aizawa, M. Hirano, S. Suzuki, Electrochim. Acta 24 (1979) 89–94.
[447] B. Kok, B. Forbush, M. McGloin, Photochem. Photobiol. 11 (1970) 457–475.
[448] E. Greenbaum, D.C. Mauzerall, Photochem. Photobiol. 23 (1976) 369–372.
[449] D. Mauzerall, Proc. Natl. Acad. Sci. USA 69 (1972) 1358–1362.
[450] G. Cheniae, I. Martin, Biochim. Biophys. Acta-Bioenerg. 197 (1970) 219–239.
[451] S. Yoshikawa, A. Shimada, Chem. Rev. 115 (2015) 1936–1989.
[452] V.C.-C. Wang, S. Maji, P.P.-Y. Chen, H.K. Lee, S.S.-F. Yu, S.I. Chan, Chem. Rev. 117 (2017) 8574–8621.
[453] A. Decker, E.I. Solomon, Curr. Opin. Chem. Biol. 9 (2005) 152–163.

[454] P. Beaune, in, Annales de Biologie Clinique (1996) 267.
[455] I. Matsunaga, A. Ueda, T. Sumimoto, K. Ichihara, M. Ayata, H. Ogura, Arch. Bioch. Biophys. 394 (2001) 45–53.
[456] D.F. Ghanotakis, G.T. Babcock, C.F. Yocum, FEBS Lett. 167 (1984) 127–130.
[457] K.-C. Han, S. Katoh, Plant Cell Physiol. 34 (1993) 585–593.
[458] P. Aedelroth, K. Lindberg, L. Andreasson, Biochemistry 34 (1995).
[459] S. Izawa, R. Heath, G. Hind, Biochim. Biophys. Acta-Bioenerg. 180 (1969) 388–398.
[460] H. Wincencjusz, H.J. van Gorkom, C.F. Yocum, Biochemistry 36 (1997) 3663–3670.
[461] H. Wincencjusz, C.F. Yocum, H.J. van Gorkom, Biochemistry 37 (1998) 8595–8604.
[462] K. Hasegawa, Y. Kimura, T.-A. Ono, Biochemistry 41 (2002) 13839–13850.
[463] K. Hasegawa, Y. Kimura, T.-A. Ono, Biophys. J. 86 (2004) 1042–1050.
[464] K. Lindberg, L.-E. Andréasson, Biochemistry 35 (1996) 14259–14267.
[465] A. Boussac, P. Setif, A. Rutherford, Biochemistry 31 (1992) 1224–1234.
[466] A. Boussac A.W. Rutherford in Biophysical Chemistry of Dioxygen Reactions in Respiration and Photosynthesis: Proceedings of the Nobel Conference Held at Fiskebäckskil 1988 Cambridge University Press 123..
[467] K.L. Westphal, N. Lydakis-Simantiris, R.I. Cukier, G.T. Babcock, Biochemistry 39 (2000) 16220–16229.
[468] J.M. Peloquin, K.A. Campbell, D.W. Randall, M.A. Evanchik, V.L. Pecoraro, W.H. Armstrong, R.D. Britt, J. Am. Chem. Soc. 122 (2000) 10926–10942.
[469] V.K. Yachandra, R. Guiles, A. McDermott, R.D. Britt, S. Dexheimer, K. Sauer, M. P. Klein, Biochim. Biophys. Acta-Bioenerg. 850 (1986) 324–332.
[470] V.K. Yachandra, V.J. DeRose, M.J. Latimer, I. Mukerji, K. Sauer, M.P. Klein, Science 260 (1993) 675–679.
[471] Y. Zhang, L. Jianmin, Z. Min, Q. Wang, X. Wu, H. Asada, M. Fuhiwara, T. Matsushita, K. Yoshizawa, T. Ohta, Science 260 (1993) 675.
[472] J. Barber, Inorg. Chem. 47 (2008) 1700–1710.
[473] M. Suga, F. Akita, K. Hirata, G. Ueno, H. Murakami, Y. Nakajima, T. Shimizu, K. Yamashita, M. Yamamoto, H. Ago, Nature 517 (2015) 99–103.
[474] G. Cheniae, I. Martin, Biochem. Biophys. Res. 28 (1967) 89–95.
[475] C. Yocum, C. Yerkes, R. Blankenship, R. Sharp, G. Babcock, Proc. Natl. Acad. Sci. USA 78 (1981) 7507–7511.
[476] C. Preston, C. Critchley, FEBS Lett. 184 (1985) 318–322.
[477] C. Cañada-Vilalta, J.C. Huffman, G. Christou, Polyhedron 20 (2001) 1785–1793.
[478] W. Ames, D.A. Pantazis, V. Krewald, N. Cox, J. Messinger, W. Lubitz, F. Neese, J. Am. Chem. Soc. 133 (2011) 19743–19757.
[479] P.E. Siegbahn, Chem-Eur. J. 14 (2008) 8290–8302.
[480] S. Luber, I. Rivalta, Y. Umena, K. Kawakami, J.-R. Shen, N. Kamiya, G.W. Brudvig, V.S. Batista, Biochemistry 50 (2011) 6308–6311.
[481] D.A. Pantazis, W. Ames, N. Cox, W. Lubitz, F. Neese, Angew. Chem. Int. Ed. 51 (2012) 9935–9940.
[482] R. Pokhrel, G.W. Brudvig, Phys. Chem. Chem. Phys. 16 (2014) (1821) 11812–11821.
[483] G. Yin, J.M. McCormick, M. Buchalova, A.M. Danby, K. Rodgers, V.W. Day, K. Smith, C.M. Perkins, D. Kitko, J.D. Carter, Inorg. Chem. 45 (2006) 8052–8061.
[484] J. Yano, J. Kern, K. Sauer, M.J. Latimer, Y. Pushkar, J. Biesiadka, B. Loll, W. Saenger, J. Messinger, A. Zouni, Science 314 (2006) 821–825.
[485] P. Plaksin, R. Stoufer, M. Mathew, G. Palenik, J. Am. Chem. Soc. 94 (1972) 2121–2122.
[486] K. Weighardt, Angew. Chem. Int. Ed. Engl. 95 (1983).
[487] J.S. Bashkin, H.R. Chang, W.E. Streib, J.C. Huffman, D.N. Hendrickson, G. Christou, J. Am. Chem. Soc. 109 (1987) 6502–6504.
[488] M.K. Chan, W.H. Armstrong, J. Am. Chem. Soc. 113 (1991) 5055–5057.
[489] C. Philouze, G. Blondin, J.-J. Girerd, J. Guilhem, C. Pascard, D. Lexa, J. Am. Chem. Soc. 116 (1994) 8557–8565.
[490] J. Limburg, J.S. Vrettos, L.M. Liable-Sands, A.L. Rheingold, R.H. Crabtree, G.W. Brudvig, Science 283 (1999) 1524–1527.
[491] H. Chen, J. Faller, R.H. Crabtree, G.W. Brudvig, J. Am. Chem. Soc. 126 (2004) 7345–7349.
[492] I.J. Hewitt, J.-K. Tang, N. Madhu, R. Clérac, G. Buth, C.E. Anson, A.K. Powell, Chem. Commun. (2006) 2650–2652.
[493] S. Mukherjee, J.A. Stull, J. Yano, T.C. Stamatatos, K. Pringouri, T.A. Stich, K.A. Abboud, R.D. Britt, V.K. Yachandra, G. Christou, Proc. Natl. Acad. Sci. USA 109 (2012) 2257–2262.
[494] G.W. Brudvig, R.H. Crabtree, Proc. Natl. Acad. Sci. USA 83 (1986) 4586–4588.
[495] K. Wieghardt, U. Bossek, W. Gebert, Angew. Chem., 22 (1983) 328–329. https://doi.org/10.1002/anie.198303281..
[496] S. Mukhopadhyay, H.J. Mok, R.J. Staples, W.H. Armstrong, J. Am. Chem. Soc. 126 (2004) 9202–9204.
[497] W.F. Ruettinger, D.M. Ho, G.C. Dismukes, Inorg. Chem. 38 (1999) 1036–1037.
[498] Y. Masayuki, K. Wolf, P. Baesjou, S. Bernasek, G. Dismukes, Angew Chem. Int Ed 40 (2001) 2925–2928.
[499] T.G. Carrell, E. Bourles, M. Lin, G.C. Dismukes, Inorg. Chem. 42 (2003) 2849–2858.
[500] E. Libby, K. Folting, G. Christou, J. McCusker, E. Schmitt, D. Hendrickson, Inorg. Chem. 30 (1991) 3486–3495.
[501] J.K. McCusker, J.B. Vincent, E.A. Schmitt, M.L. Mino, K. Shin, D.K. Coggin, P.M. Hagen, J.C. Huffman, G. Christou, D.N. Hendrickson, J. Am. Chem. Soc. 113 (1991) 3012–3021.
[502] R. Brimblecombe, G.F. Swiegers, G.C. Dismukes, L. Spiccia, Angew. Chem. 120 (2008) 7445–7448.
[503] R. Brimblecombe, D.R. Kolling, A.M. Bond, G.C. Dismukes, G.F. Swiegers, L. Spiccia, Inorg. Chem. 48 (2009) 7269–7279.
[504] B. Cheng, F. Cukiernik, P.H. Fries, J.-C. Marchon, W.R. Scheidt, Inorg. Chem. 34 (1995) 4627–4639.
[505] S. Pal, M.K. Chan, W.H. Armstrong, J. Am. Chem. Soc. 114 (1992) 6398–6406.
[506] K. Wieghardt, U. Bossek, B. Nuber, J. Weiss, J. Bonvoisin, M. Corbella, S. Vitols, J. Girerd, J. Am. Chem. Soc. 110 (1988) 7398–7411.
[507] R. Terrett, S. Petrie, R.J. Pace, R. Stranger, Chem. Commun. 50 (2014) 3187–3190.
[508] W.F. Ruettinger, G.C. Dismukes, Inorg. Chem. 39 (2000) 4186.
[509] M.R. Gau, C.R. Hamilton, M.J. Zdilla, Chem. Commun. 50 (2014) 7780–7782.
[510] D.N. Hendrickson, G. Christou, E.A. Schmitt, E. Libby, J.S. Bashkin, S. Wang, H. L. Tsai, J.B. Vincent, P.D. Boyd, J. Am. Chem. Soc. 114 (1992) 2455–2471.
[511] S. Wang, H.-L. Tsai, E. Libby, K. Folting, W.E. Streib, D.N. Hendrickson, G. Christou, Inorg. Chem. 35 (1996) 7578–7589.
[512] G. Blondin, R. Davydov, C. Philouze, M.-F. Charlot, B. Åkermark, J.-J. Girerd, A. Boussac, J. Chem. Soc. Dalton Trans. (1997) 4069–4074.
[513] B. Nepal, S. Das, Angew. Chem. 125 (2013) 7365–7368.
[514] S.H. Kim, W. Gregor, J.M. Peloquin, M. Brynda, R.D. Britt, J. Am. Chem. Soc. 126 (2004) 7228–7237.
[515] P.E. Siegbahn, Inorg. Chem. 39 (2000) 2923–2935.
[516] K.N. Ferreira, T.M. Iverson, K. Maghlaoui, J. Barber, S. Iwata, Science 303 (2004) 1831–1838.
[517] C. Kupitz, S. Basu, I. Grotjohann, R. Fromme, N.A. Zatsepin, K.N. Rendek, M.S. Hunter, R.L. Shoeman, T.A. White, D. Wang, Nature 513 (2014) 261–265.
[518] S. Iwata, J. Barber, Curr. Opin. Struct. Biol. 14 (2004) 447–453.
[519] P.E. Siegbahn, Acc. Chem. Res. 42 (2009) 1871–1880.
[520] J. Yano, J. Kern, K.-D. Irrgang, M.J. Latimer, U. Bergmann, P. Glatzel, Y. Pushkar, J. Biesiadka, B. Loll, K. Sauer, Proc. Natl. Acad. Sci. USA 102 (2005) 12047–12052.
[521] B. Loll, J. Kern, W. Saenger, A. Zouni, J. Biesiadka, Nature 438 (2005) 1040–1044.
[522] J. Yano, Y. Pushkar, P. Glatzel, A. Lewis, K. Sauer, J. Messinger, U. Bergmann, V. Yachandra, J. Am. Chem. Soc. 127 (2005) 14974–14975.
[523] J.P. McEvoy, G.W. Brudvig, Chem. Rev. 106 (2006) 4455–4483.
[524] E.M. Sproviero, J.A. Gascón, J.P. McEvoy, G.W. Brudvig, V.S. Batista, J. Am. Chem. Soc. 130 (2008) 3428–3442.
[525] D.J. MacLachlan, B.J. Hallahan, S.V. Ruffle, J.H. Nugent, M.C. Evans, R.W. Strange, S.S. Hasnain, Biochem. J. 285 (1992) 569–576.
[526] M. Haumann, C. Müller, P. Liebisch, L. Iuzzolino, J. Dittmer, M. Grabolle, T. Neisius, W. Meyer-Klaucke, H. Dau, Biochemistry 44 (2005) 1894–1908.
[527] M.J. Latimer, V.J. DeRose, V.K. Yachandra, K. Sauer, M.P. Klein, J. Phys. Chem. B 102 (1998) 8257–8265.
[528] B. Brena, P.E. Siegbahn, H. Ågren, J. Am. Chem. Soc. 134 (2012) 17157–17167.
[529] C. Glöckner, J. Kern, M. Broser, A. Zouni, V. Yachandra, J. Yano, J. Biol. Chem. 288 (2013) 22607–22620.
[530] A. Galstyan, A. Robertazzi, E.W. Knapp, J. Am. Chem. Soc. 134 (2012) 7442–7449.
[531] P.E. Siegbahn, Biochim. Biophys. Acta-Bioenerg. 1827 (2013) 1003–1019.
[532] S. Petrie, R.J. Pace, R. Stranger, Angew. Chem. Int. Ed. 54 (2015) 7120–7124.
[533] H. Chen, D.A. Case, G.C. Dismukes, J. Phys. Chem. B 122 (2018) (1882) 11868–11871.
[534] R.J. Pace, L. Jin, R. Stranger, Dalton Trans. 41 (2012) 11145–11160.
[535] H. Chen, G.C. Dismukes, D.A. Case, J. Phys. Chem. B 122 (2018) 8654–8664.
[536] M. Zheng, G.C. Dismukes, Inorg. Chem. 35 (1996) 3307–3319.
[537] L. Zaltsman, G.M. Ananyev, E. Bruntrager, G.C. Dismukes, Biochemistry 36 (1997) 8914–8922.
[538] D.R. Kolling, N. Cox, G.M. Ananyev, R.J. Pace, G.C. Dismukes, Biophys. J. 103 (2012) 313–322.
[539] W. Hillier, T. Wydrzynski, Biochim. Biophys. Acta-Bioenerg. 1503 (2001) 197–209.
[540] M. Askerka, J. Wang, G.W. Brudvig, V.S. Batista, Biochemistry 53 (2014) 6860–6862.
[541] M. Suga, F. Akita, M. Sugahara, M. Kubo, Y. Nakajima, T. Nakane, K. Yamashita, Y. Umena, M. Nakabayashi, T. Yamane, Nature 543 (2017) 131–135.
[542] J. Kern, R. Chatterjee, I.D. Young, F.D. Fuller, L. Lassalle, M. Ibrahim, S. Gul, T. Fransson, A.S. Brewster, R. Alonso-Mori, Nature 563 (2018) 421–425.
[543] P.E. Siegbahn, ChemPhysChem 12 (2011) 3274–3280.
[544] I.D. Young, M. Ibrahim, R. Chatterjee, S. Gul, F.D. Fuller, S. Koroidov, A.S. Brewster, R. Tran, R. Alonso-Mori, T. Kroll, Nature 540 (2016) 453–457.
[545] P.E. Siegbahn, Chem. Phys. Lett. 690 (2017) 172–176.
[546] S.P. Hau-Riege, B.J. Bennion, Phys. Rev. E 91 (2015) 022705.
[547] J. Wang, Protein Sci. 25 (2016) 1407–1419.
[548] J. Wang, Protein Sci. 25 (2016) 1797–1802.
[549] M. Askerka, D.J. Vinyard, J. Wang, G.W. Brudvig, V.S. Batista, Biochemistry 54 (2015) 1713–1716.
[550] A. Tanaka, Y. Fukushima, N. Kamiya, J. Am. Chem. Soc. 139 (2017) 1718–1721.
[551] J. Wang, M. Askerka, G.W. Brudvig, V.S. Batista, A.C.S. Energ, Lett. 2 (2017) 397–407.
[552] R.J. Debus, M.A. Strickler, L.M. Walker, W. Hillier, Biochemistry 44 (2005) 1367–1374.
[553] M.A. Strickler, W. Hillier, R.J. Debus, Biochemistry 45 (2006) 8801–8811.
[554] R.M. Cinco, K.L. McFarlane Holman, J.H. Robblee, J. Yano, S.A. Pizarro, E. Bellacchio, K. Sauer, V.K. Yachandra, Biochemistry 41 (2002) 12928–12933.
[555] M. Kusunoki, J. Photochem. Photobiol. B. Biol. 104 (2011) 100–110.

[556] K.A. Campbell, J.M. Peloquin, D.P. Pham, R.J. Debus, R.D. Britt, J. Am. Chem. Soc. 120 (1998) 447–448.
[557] P.E. Siegbahn, R.H. Crabtree, J. Am. Chem. Soc. 121 (1999) 117–127.
[558] M. Ibrahim, T. Fransson, R. Chatterjee, M.H. Cheah, R. Hussein, L. Lassalle, K.D. Sutherlin, I.D. Young, F.D. Fuller, S. Gul, Proc. Natl. Acad. Sci. USA 117 (2020) 12624–12635.
[559] T. Lohmiller, V. Krewald, M.P. Navarro, M. Retegan, L. Rapatskiy, M.M. Nowaczyk, A. Boussac, F. Neese, W. Lubitz, D.A. Pantazis, Phys. Chem. Chem. Phys. 16 (2014) (1892) 11877–11881.
[560] M.P. Navarro, W.M. Ames, H. Nilsson, T. Lohmiller, D.A. Pantazis, L. Rapatskiy, M.M. Nowaczyk, F. Neese, A. Boussac, J. Messinger, Proc. Natl. Acad. Sci. USA 110 (2013) 15561–15566.
[561] P.H. Oyala, T.A. Stich, R.J. Debus, R.D. Britt, J. Am. Chem. Soc. 137 (2015) 8829–8837.
[562] J. Schraut, M. Kaupp, Chem-Eur. J. 20 (2014) 7300–7308.
[563] M. Retegan, D.A. Pantazis, Chem. Sci. 7 (2016) 6463–6476.
[564] M. Asada, H. Mino, J. Phys. Chem. B 119 (2015) 10139–10144.
[565] K. Becker, K.U. Cormann, M.M. Nowaczyk, J. Photochem. Photobiol. B. Biol. 104 (2011) 204–211.
[566] J. Dasgupta, G.M. Ananyev, G.C. Dismukes, Coord. Chem. Rev. 252 (2008) 347–360.
[567] C.F. Yocum, Coord. Chem. Rev. 252 (2008) 296–305.
[568] M.M. Najafpour, J. Photochem. Photobiol. B. Biol. 104 (2011) 111–117.
[569] M.M. Najafpour, T. Ehrenberg, M. Wiechen, P. Kurz, Angew. Chem. Int. Ed. 49 (2010) 2233–2237.
[570] R.M. Cinco, J.H. Robblee, J. Messinger, C. Fernandez, K.L.M. Holman, K. Sauer, V.K. Yachandra, Biochemistry 43 (2004) 13271–13282.
[571] N. Cox, L. Rapatskiy, J.-H. Su, D.A. Pantazis, M. Sugiura, L. Kulik, P. Dorlet, A.W. Rutherford, F. Neese, A. Boussac, J. Am. Chem. Soc. 133 (2011) 3635–3648.
[572] A. Boussac, F. Rappaport, P. Carrier, J.-M. Verbavatz, R. Gobin, D. Kirilovsky, A. W. Rutherford, M. Sugiura, J. Biol. Chem. 279 (2004) 22809–22819.
[573] B. Gerey, M. Gennari, E. Gouré, J. Pécaut, A. Blackman, D.A. Pantazis, F. Neese, F. Molton, J. Fortage, C. Duboc, Dalton Trans. 44 (2015) 12757–12770.
[574] J.S. Kanady, P.-H. Lin, K.M. Carsch, R.J. Nielsen, M.K. Takase, W.A. Goddard III, T. Agapie, J. Am. Chem. Soc. 136 (2014) 14373–14376.
[575] J.S. Kanady, Nature Mater. 9 (2010) 989.
[576] C. Chen, C. Zhang, H. Dong, J. Zhao, Chem. Commun. 50 (2014) 9263–9265.
[577] Z. Han, K.T. Horak, H.B. Lee, T. Agapie, J. Am. Chem. Soc. 139 (2017) 9108–9111.
[578] N. Cox, M. Retegan, F. Neese, D.A. Pantazis, A. Boussac, W. Lubitz, Science 345 (2014) 804–808.
[579] J.P. McEvoy, G.W. Brudvig, Phys. Chem. Chem. Phys. 6 (2004) 4754–4763.
[580] J.D. Blakemore, R.H. Crabtree, G.W. Brudvig, Chem. Rev. 115 (2015) 12974–13005.
[581] M.D. Karkas, O. Verho, E.V. Johnston, B.r. Åkermark, Chem. Rev. 114 (2014) 11863–12001.
[582] C. Zhang, C. Chen, H. Dong, J.-R. Shen, H. Dau, J. Zhao, Science 348 (2015) 690–693.
[583] C.W. Cady, G. Gardner, Z.O. Maron, M. Retuerto, Y.B. Go, S. Segan, M. Greenblatt, G.C. Dismukes, ACS Catal. 5 (2015) 3403–3410.
[584] D.G. Nocera, Acc. Chem. Res. 45 (2012) 767–776.
[585] J.G. McAlpin, T.A. Stich, C.A. Ohlin, Y. Surendranath, D.G. Nocera, W.H. Casey, R.D. Britt, J. Am. Chem. Soc. 133 (2011) 15444–15452.
[586] X. Li, P.E. Siegbahn, J. Am. Chem. Soc. 135 (2013) 13804–13813.
[587] S. Mukhopadhyay, S.K. Mandal, S. Bhaduri, W.H. Armstrong, Chem. Rev. 104 (2004) 3981–4026.
[588] C.W. Hoganson, G.T. Babcock, Science 277 (1997) 1953–1956.
[589] S. Fukuzumi, Y.-M. Lee, W. Nam, Dalton Trans. 48 (2019) 779–798.
[590] H. Isobe, M. Shoji, J.-R. Shen, K. Yamaguchi, Inorg. Chem. 55 (2016) 502–511.
[591] E.M. Sproviero, J.P. McEvoy, J.A. Gascón, G.W. Brudvig, V.S. Batista, Photosynth. Res. 97 (2008) 91–114.
[592] N. Cox, D.A. Pantazis, F. Neese, W. Lubitz, Acc. Chem. Res. 46 (2013) 1588–1596.
[593] D.J. Weber, A.M. Libson, A.G. Gittis, M.S. Lebowitz, A.S. Mildvan, Biochemistry 33 (1994) 8017–8028.
[594] X.-J. Su, C. Zheng, Q.-Q. Hu, H.-Y. Du, R.-Z. Liao, M.-T. Zhang, Dalton Trans. 47 (2018) 8670–8675.
[595] F. Acuña-Parés, M. Costas, J.M. Luis, J. Lloret-Fillol, Inorg. Chem. 53 (2014) 5474–5485.
[596] C. Panda, J. Debgupta, D. Díaz Díaz, K.K. Singh, S. Sen Gupta, B.B. Dhar, J. Am. Chem. Soc. 136 (2014) 12273–12282.
[597] M. Schulze, V. Kunz, P.D. Frischmann, F. Würthner, Nature Chem. 8 (2016) 576–583.
[598] D. Lebedev, Y. Pineda-Galvan, Y. Tokimaru, A. Fedorov, N. Kaeffer, C. Copéret, Y. Pushkar, J. Am. Chem. Soc. 140 (2018) 451–458.
[599] W.F. Xie, L.Y. Guo, J.H. Xu, M. Jagodič, Z. Jagličić, W.G. Wang, G.L. Zhuang, Z. Wang, C.H. Tung, D. Sun, Eur. J. Inorg. Chem. 2016 (2016) 3253–3261.
[600] Y. Gao, T.r. Åkermark, J. Liu, L. Sun, B.r. Åkermark, J. Am. Chem. Soc. 131 (2009) 8726–8727.
[601] E.A. Mohamed, Z.N. Zahran, Y. Naruta, J. Catal. 352 (2017) 293–299.
[602] E.A. Karlsson, B.L. Lee, T. Åkermark, E.V. Johnston, M.D. Kärkäs, J. Sun, Ö. Hansson, J.E. Bäckvall, B. Åkermark, Angew. Chem. Int. Ed. 50 (2011) 11715–11718.
[603] P.E. Siegbahn, Proc. Natl. Acad. Sci. USA 114 (2017) 4966–4968.
[604] R. Gupta, T. Taguchi, B. Lassalle-Kaiser, E.L. Bominaar, J. Yano, M.P. Hendrich, A. Borovik, Proc. Natl. Acad. Sci. USA 112 (2015) 5319–5324.
[605] H. Nilsson, F. Rappaport, A. Boussac, J. Messinger, Nature Commun. 5 (2014) 4305.
[606] V. Krewald, M. Retegan, N. Cox, J. Messinger, W. Lubitz, S. DeBeer, F. Neese, D. A. Pantazis, Chem. Sci. 6 (2015) 1676–1695.
[607] M. Lundberg, M.R. Blomberg, P.E. Siegbahn, Inorg. Chem. 43 (2004) 264–274.
[608] X. Li, P.E. Siegbahn, Phys. Chem. Chem. Phys. 17 (2015) 12168–12174.
[609] P.E. Siegbahn, Chem-Eur. J. 12 (2006) 9217–9227.
[610] L. Rapatskiy, N. Cox, A. Savitsky, W.M. Ames, J. Sander, M.M. Nowaczyk, M. Rögner, A. Boussac, F. Neese, J. Messinger, J. Am. Chem. Soc. 134 (2012) 16619–16634.
[611] S. Yamanaka, H. Isobe, K. Kanda, T. Saito, Y. Umena, K. Kawakami, J.-R. Shen, N. Kamiya, M. Okumura, H. Nakamura, Chem. Phys. Lett. 511 (2011) 138–145.
[612] Y. Guo, L.-L. He, D.-X. Zhao, L.-D. Gong, C. Liu, Z.-Z. Yang, Phys. Chem. Chem. Phys. 18 (2016) 31551–31565.
[613] T. Lohmiller, N. Cox, J.-H. Su, J. Messinger, W. Lubitz, J. Biol. Chem. 287 (2012) 24721–24733.
[614] J.-H. Su, N. Cox, W. Ames, D.A. Pantazis, L. Rapatskiy, T. Lohmiller, L.V. Kulik, P. Dorlet, A.W. Rutherford, F. Neese, A. Boussac, W. Lubitz, J. Messinger, Biochim. Biophys. Acta-Bioenerg. 1807 (2011) 829–840.
[615] D.J. Vinyard, M. Askerka, R.J. Debus, V.S. Batista, G.W. Brudvig, Biochemistry 55 (2016) 4432–4436.
[616] H. Dau, J.C. Andrews, T.A. Roelofs, M.J. Latimer, W. Liang, V.K. Yachandra, K. Sauer, M.P. Klein, Biochemistry 34 (1995) 5274–5287.
[617] R. Pokhrel, R.J. Service, R.J. Debus, G.W. Brudvig, Biochemistry 52 (2013) 4758–4773.
[618] H.-A. Chu, Y.-W. Feng, C.-M. Wang, K.-A. Chiang, S.-C. Ke, Biochemistry 43 (2004) 10877–10885.
[619] D.J. Vinyard, G.W. Brudvig, Biochemistry 54 (2015) 622–628.
[620] J. Messinger, Phys. Chem. Chem. Phys. 6 (2004) 4764–4771.
[621] N. Cox, J. Messinger, Biochim. Biophys. Acta-Bioenerg. 1827 (2013) 1020–1030.
[622] J. Messinger, G. Renger, Primary processes of photosynthesis, The Royal Society of Chemistry, 2008, pp. 291–351.
[623] P. Geijer, F. Morvaridi, S. Styring, Biochemistry 40 (2001) 10881–10891.
[624] G. Renger, Biochim. Biophys. Acta-Bioenerg. 1817 (2012) 1164–1176.
[625] M. Haumann, O. Bögershausen, D. Cherepanov, R. Ahlbrink, W. Junge, Photosynth. Res. 51 (1997) 193–208.
[626] F. Rappaport, M. Blanchard-Desce, J. Lavergne, Biochim. Biophys. Acta-Bioenerg. 1184 (1994) 178–192.
[627] T. Noguchi, H. Suzuki, M. Tsuno, M. Sugiura, C. Kato, Biochemistry 51 (2012) 3205–3214.
[628] K.M. Davis, B.T. Sullivan, M.C. Palenik, L. Yan, V. Purohit, G. Robison, I. Kosheleva, R.W. Henning, G.T. Seidler, Y. Pushkar, Phys. Rev. X 8 (2018) 041014.
[629] S.C. Jensen, K.M. Davis, B. Sullivan, D.A. Hartzler, G.T. Seidler, D.M. Casa, E. Kasman, H.E. Colmer, A.A. Massie, T.A. Jackson, J. Phys. Chem. Lett. 8 (2017) 2584–2589.
[630] K. Saito, A.W. Rutherford, H. Ishikita, Nature Commun. 6 (2015) 1–10.
[631] Z. Guo, B.A. Barry, J. Phys. Chem. B 121 (2017) 3987–3996.
[632] L.V. Kulik, B. Epel, W. Lubitz, J. Messinger, J. Am. Chem. Soc. 129 (2007) 13421–13435.
[633] D.J. Vinyard, S. Khan, M. Askerka, V.S. Batista, G.W. Brudvig, J. Phys. Chem. B 121 (2017) 1020–1025.
[634] P.H. Oyala, T.A. Stich, J.A. Stull, F. Yu, V.L. Pecoraro, R.D. Britt, Biochemistry 53 (2014) 7914–7928.
[635] A. Boussac, J.L. Zimmermann, A.W. Rutherford, Biochemistry 28 (1989) 8984–8989.
[636] B.J. Hallahan, J.H. Nugent, J.T. Warden, M.C. Evans, Biochemistry 31 (1992) 4562–4573.
[637] J.M. Peloquin, K.A. Campbell, R.D. Britt, J. Am. Chem. Soc. 120 (1998) 6840–6841.
[638] M.L. Gilchrist, J.A. Ball, D.W. Randall, R.D. Britt, Proc. Natl. Acad. Sci. USA 92 (1995) 9545–9549.
[639] M. Askerka, D.J. Vinyard, G.W. Brudvig, V.S. Batista, Biochemistry 54 (2015) 5783–5786.
[640] A.W. Rutherford, A. Osyczka, F. Rappaport, FEBS Lett. 586 (2012) 603–616.
[641] L.V. Kulik, B. Epel, W. Lubitz, J. Messinger, J. Am. Chem. Soc. 127 (2005) 2392–2393.
[642] L. Jin, P. Smith, C.J. Noble, R. Stranger, G.R. Hanson, R.J. Pace, Phys. Chem. Chem. Phys. 16 (2014) 7799–7812.
[643] V. Krewald, F. Neese, D.A. Pantazis, Israel J. Chem. 55 (2015) 1219–1232.
[644] M. Askerka, G.W. Brudvig, V.S. Batista, Acc. Chem. Res. 50 (2017) 41–48.
[645] M. Shoji, H. Isobe, S. Yamanaka, M. Suga, F. Akita, J.-R. Shen, K. Yamaguchi, Chem. Phys. Lett. 623 (2015) 1–7.
[646] J.M. Peloquin, R.D. Britt, Biochim. Biophys. Acta-Bioenerg. 1503 (2001) 96–111.
[647] S. Nakamura, T. Noguchi, Proc. Natl. Acad. Sci. USA 113 (2016) 12727–12732.
[648] L. Kulik, W. Lubitz, J. Messinger, Biochemistry 44 (2005) 9368–9374.
[649] T. Noguchi, M. Sugiura, Biochemistry 41 (2002) 2322–2330.
[650] H.-A. Chu, W. Hillier, R.J. Debus, Biochemistry 43 (2004) 3152–3166.